NON-STEADY BEHAVIOR OF A FLAME SPREADING FROM A POINT IN A TWO-DIMENSIONAL DUCT

Thesis by

Malladi Venkata Subbaiah

In Partial Fulfillment of the Requirements

for the Degree of

Doctor of Philosophy

California Institute of Technology

Pasadena, California

1980

(Submitted May 19, 1980)

ACKNOWLEDGEMENTS

I am deeply grateful to Professor Frank E. Marble for his scholarly guidance and generous support during the course of my graduate study at Caltech. His patience and encouragement have been invaluable.

I am very thankful to my dear wife, Shyamala, for all her love and affection. Her enthusiastic assistance in the preparation of this thesis is greatly appreciated.

I wish to thank my parents for their continued support and encouragement throughout my education.

I thank Mr. Victor Jaramillo for his help with the figures. Finally, I would like to acknowledge the willing cooperation by the staff of the Computing Center.

This work was supported in part by the U.S. Department of Energy, Grant EX-76-G-03-1305.

ABSTRACT

Non-steady behavior of a flame stabilized in a two-dimensional duct is studied in this thesis. The problem is formulated by an integral technique in which the governing equations are integrated across the duct to obtain integral relations for the mean flow variables. The flow fields on either side of the flame sheet are matched by appropriate matching conditions. Fluid flow through the flame surface causes the integral relations to explicitly involve the fluid velocities at the flame. An independent description of the flame shape and the irrotational flow field upstream of the flame is provided by a source distribution on the duct axis.

The integral relations are analyzed by a perturbation technique, in which the dominant order solution represents the steady flame development. The steady flame configuration is perturbed by an acoustic wave incident on the compact flame region. The time dependent counterpart of the integral relations describes the ensuing non-steady flow fields. The flame perturbation exhibits a travelling wave pattern with considerable amplification along the flame zone. A simple model to describe the growth of the flame perturbation is put forth, by considering the flame surface as an unstable shear layer.

Acoustic reflection and transmission coefficients of the flame region are obtained utilizing the time-dependent flame calculations. The response spectra exhibit active responses at certain well defined frequencies. The non-steady flame model is incorporated in a rudimentary afterburner configuration to investigate the low frequency behaviour of the afterburner. The results suggest a possible mechanism of low frequency instability in a combustion system.

CONTENTS

1. INTRODUCTION

Combustion systems of practical interest frequently exhibit oscillations of objectionable levels, even leading to instability in some instances. Response of the combustion processes to local pressure and velocity fluctuations is an important factor that feeds considerable energy into the system to sustain the oscillations. When the frequencies of interest are, say, less than 100Hz, the chemical reaction times are less important and the fluid mechanical adjustments in the flame region play an important role on the detailed response of the system.

As a result of fast chemical kinetics, laminar flame fronts are usually very thin compared to length scales associated with combustion devices of practical interest. Therefore, in problems where detailed calculations of flame structure are not important, one often considers the flame front as a surface of discontinuity separating the cold fuel oxidizer mixture and hot combustion products. Matching conditions analogous to the shock conditions in compressible flows are used to match the flow fields on either side of the flame sheet.

Instantaneous pictures of turbulent flames [see for example, Williams, Hottel and Scurlock[20] (1949), Wright and Zukoski[22] (1960) and Lewis and von Elbe[10] (1961)] suggest that flame sheet modelling of turbulent flames is of restricted scope. Also, even with time averaged description of turbulent flames, one is left to deal with the considerably thick visible flame region, rendering it difficult to have an unique representation of flame surface. Scurlock[14] (1948), Karlovitz et al[8] (1951) and Wohl et al[21] (1953) used widely different criterion in their descriptions of flame

sheets. Any such representation will be strictly applicable only for large-scale turbulent flows with the turbulent scales much larger than the flame thickness [Williams[19] (1974)]. Stability analyses utilizing such a flame sheet description will have to be restricted to correspondingly large disturbance wave lengths.

Steady behaviour of confined pre-mixed flames stabilized by bluff body flame holders attracted the attention of several early research workers.[3] Scurlock[14] (1948), Tsien[18] (1951), Ball[1] (1951) Fabri et al[4] (1953) and Iida[6] (1956) studied the problem analytically, while Williams et al[20] (1949), Thurston[17] (1958) and Wright and Zukoski[22] (1960) investigated experimentally. Scurlock's calculations were done primarily to obtain average flame speed from measured values of flame spreading [Williams, Hottel and Scurlock[20] (1949)]. Several other researchers emphasized on the measurement and calculation of flame speed for turbulent flames. Spalding[15] (1958) postulated that the turbulent flame development is controlled by the rate of entrainment of cold gas by hot gas and utilized a two-dimensional turbulent jet mixing model to calculate the entrainment rates. Wright and Zukoski[22] (1960) experimentally showed that turbulent flame speed was proportional to the flow velocity and was independent of laminar flame speed. Wohl et al[21] (1953) studied the effect of turbulence on turbulent flame speed. With the recent developments in turbulent flames, the concept of a turbulent flame speed in the conventional sense does not seem to be very useful.

Scurlock[14] (1948) was the first to investigate steady flow field and flame spreading from idealized point flame holders in a two-dimensional duct. He obtained a numerical solution for the flame shape and velocity

profile in the region downstream of the flame. Incompressible flow with uniform velocity profile in the unburned region and uniform static pressure across any cross section were assumed. Tsien[18] (1951) provided a simpler treatment of the above problem with assumed uniform velocity in the cold region and linear velocity distribution in the hot region, as suggested by Scurlock's results. He further extended his calculations to include compressibility effects and found that for large approach Mach number or heat release, the flame did not reach the channel wall and the input fuel mixture was not completely burned. This is due to the 'choked' flow condition created by flow acceleration in the unburned region. Tsien also calculated vorticity produced by the flame in terms of fluid velocity and streamline curvature immediately upstream of the flame. Zukoski[23] (1978) showed that the flame shape is relatively insensitive to the assumed velocity profile in the burned region. But, the maximum velocity in the hot region will obviously depend on the assumed profile. Fabri et al[4] (1953) and Iida[6] (1956) linearized the equations of motion for small flame speeds and obtained an integral equation for stream function, which was solved by successive integration. The assumption of uniform velocity in the unburned region does not provide accurate initial conditions for these calculations. Iida also investigated the problem experimentally. The measured values of flame shape and velocity profiles for free stream turbulence levels below 1.65% were in good agreement with the calculated results.

In the above calculations momentum transfer in the direction normal to the duct walls was ignored. Validity of such calculations are restricted to very low flame speeds in comparison to the approach fluid

velocity. Also, in the above quasi-one-dimensional approaches, flame shape and flow field as a function of the downstream distance from the flame holder are not readily available. Additional approximation on the velocity component at the flame, in a direction perpendicular to the channel axis, has to be made for an accurate description of the flame shape. Ball[1] (1951) [See also Gue'noche[5] (1964)] made a two-dimensional calculation for the steady flame shape and flow field in a two-dimensional duct by solving incompressible, inviscid, laminar flow equations of motion by a relaxation method. Such a calculation is not restricted to very low flame speeds and shows the effect of pressure field set up by the flame.

Another approach in recent years is to numerically solve the time averaged equations of motion for turbulent flows, incorporating a suitable closure hypothesis and description of chemical reaction rates in the flame region [Spalding[16] (1976)]. These models, at present, relying heavily on certain emperical correlations arrived from experiments, are of limited scope.

Though the steady flame spreading and flow field of stabilized two-dimensional flames were under investigation for a considerable period, the non-steady behaviour of such flames did not receive the same attention. The analogous problem of stability of plane flames, known as Landau instability was extensively studied. Landau[9] (1944) showed that laminar plane flames with constant flame speed were unstable to disturbances of all wave lengths and interpreted the result as the onset of flame generated turbulence. Subsequent analyses by Markstein[12] (1951) and Istratov and Librovich[7] (1969) and experiments by Petersen and Emmons[13]

(1961) were aimed at explaining the experimentally observed stable laminar flames, by incorporating the effects of flame curvature, heat conduction and viscosity on the flame propagation. But the basic two-dimensional nature of the stability of stabilized flames was not recognized. Blackshear[2] (1956) studied the temporal instability of the stabilized flame subjected to transverse velocity disturbance. The flame is modelled as an impermeable interface separating two parallel streams (burned and unburned regions) with local velocity profiles as assumed by Tsien. The results indicate that the interface is neutrally stable to symmetric disturbance and unstable to antisymmetric disturbance, when the velocity profile is uniform in the unburned region and triangular in the burned region.

Marble and Candel[11] (1978) were the first to identify the non-steady fluid mechanical response of stabilized flames as a possible source of the low frequency oscillations observed in large combustors like the utility boilers and aircraft afterburners. They studied analytically the non-steady behaviour of a flame stabilized by a flame holder of finite size in a two-dimensional duct, subjected to external acoustic disturbances. The present investigation is a continuation of the work initiated by Marble and Candel.

Non-steady behaviour of a flame stabilized in a two-dimensional duct is analyzed in this thesis. The problem is formulated in chapter 2 by an integral technique in which the governing equations are integrated across the duct to obtain certain integral relations for the averaged flow variables. The flow fields on either side of the flame sheet are matched by appropriate matching conditions. Fluid flow through the

flame surface causes the integral relations to explicitly involve the fluid velocities at the flame. This necessitates an independent description of the irrotational flow field upstream of the flame in chapter 3. The integral relations developed in chapter 2 are analyzed by a perturbation technique, in which the dominant order solution represents the steady flame development.

The steady problem, discussed in chapter 3, provides the steady flow field for the time-dependent flame calculations of chapter 4. The steady flame configuration is perturbed by an acoustic wave incident on the compact flame region. The time dependent counterpart of the integral relations describes the ensuing non-steady flow fields. The flame perturbation exhibits a travelling wave pattern with considerable amplification along the flame zone. A simple model to describe the growth of the flame perturbation is put forth, by considering the flame surface as an unstable shear layer.

Acoustic reflection and transmission coefficients of the flame region are obtained utilizing the time-dependent flame calculations. The response spectra exhibit active responses at certain well defined frequencies. In the final chapter, the above non-steady flame model is incorporated in a rudimentary afterburner configuration to investigate the low frequency behaviour of the afterburner. The analysis utilizing the basic non-steady flame model can be extended to more complex systems. The results suggest a possible mechanism of low frequency instability in a combustion system.

1.1 REFERENCES:

[1] Ball, G.A., "Combustion Aerodynamics. A Study of a Two-Dimensional Flame",Department of Engineering Science and Applied Physics, Harvard University, July, 1951.

[2] Blackshear Jr., P.L., "Growth of Disturbances in a Flame Generated Shear Region", NACA 3830, 1956.

[3] Emmons, H W.(Ed), Fundamentals of Gas Dynamics, High Speed Aerodynamics and Jet Propulsion, Volume III, Princeton University Press, 1958, pp 611 ff.

[4] Fabri, J., Siestrunck, R. and Foure, C., "On the Aerodynamic Field of Stabilized Flames", Fourth Symposium (International) on Combustion, 1953, pp. 443-450.

[5] Gue'noche, H., "Flame Propagation in Tubes and Closed Vessels", p. 148, in NON-STEADY FLAME PROPAGATION, AGARDograph Number 75, (Edited by Markstein, G.H.) 1964, The Macmillan Company, New York.

[6] Iida, H., "Combustion in Turbulent Gas Streams", Sixth Symposium(International) on Combustion, 1956, pp. 341-350.

[7] Istratov, A.G. and Librovich, V.V., "STABILITY OF FLAMES", 1969, Army Foreign Science and Technology Center, Washington D.C., FSTC-23-952-68.

[8] Karlovitz, B., Denniston, D.W. and Wells, F.E., "Investigation of Turbulent Flames", Journal of Chemical Physics, Volume 19, 1951, pp. 541-548.

[9] Landau, L., "On the Theory of Slow Combustion", Acta Physicochimicca U.R.S.S., L., Volume XIX, Number 1, 1944, pp. 77-85.

[10] Lewis, B. and von Elbe, G., "COMBUSTION, FLAMES AND EXPLOSIONS OF GASES", Academic Press Inc., Second Edition, 1961, Chaper VI, pp. 401-407.

[11] Marble, F.E. and Candel, S.M., "An Analytical Study of the Non-Steady Behaviour of Large Combustors", Seventeenth Symposium (International) on Combustion, August 1978, pp. 761-769 .

[12] Markstein, G.H., "Experimental and Theoretical Studies of Flame-front Stability", J. Aeronaut. Sci., Volume 18, 1951, pp. 199-209.

[13] Petersen, R.E., and Emmons, H.W., "Stability of Laminar Flames", Physics of Fluids, Volume 4, Number 4, 1961, pp. 456-464.

[14] Scurlock, A. C., "Flame Stabilization and Propagation in High-Velocity Gas Streams", Meteor Report No. 19, Massachusetts of Institute of Technology, 1948.

[15] Spalding, D.B., "Theory of Rate of Spread of Confined Turbulent Pre-mixed Flames", Seventh Symposium (International) on Combustion, 1959, pp. 595-603.

[16] Spalding, D.B., "Mathematical Models of Turbulent Flames; A Review", Combustion Science and Technology, Volume 13, 1976, pp. 3-25.

[17] Thurston, D.W., "An Experimental Investigation of Flame Spreading from Bluff Body Flameholders", Engineer's Thesis, California

Institute of Technology, Pasadena, California, 1958.

[18] Tsien, H. S., "Influence of Flame Front on the Flow Field", Journal of Applied Mechanics, June 1951, pp. 188-194.

[19] Williams, F.A., "A Review of Some Theoretical Considerations of Turbulent Flame Structures", AGARD-CP-164, 1974, Section II-1.

[20] Williams, G.C., Hottel, H.C., and Scurlock, A.C., "Flame Stabilization and Propagation in High Velocity Gas Streams", Third Symposium on Combustion and Flame and Explosion Phenomena, Williams and Wilkins Company, Baltimore, Maryland, 1949, p. 21-40.

[21] Wohl, K., Shore, L., Von Rosenberg, H., and Weil, C. W., "The Burning Velocity of Turbulent Flames", Fourth Symposium (International) on Combustion, 1953, p. 620-635.

[22] Wright, F.H. and Zukoski, E.E., "Flame Spreading from Bluff Body Flame Holders", Proceedings, Eighth Symposium (International) on Combustion, 1960, pp. 933-943.

[23] Zukoski, E., "AFTERBURNERS", The Aerothermodynamics of Aircraft Gas Turbine Engines, Edited by Oates, G. C., AFAPL-TR-78-52, Chapter 21, 1978.

2. GENERAL FORMULATION OF A STABILIZED-FLAME

In this chapter, the governing equations to describe the non-steady behaviour of a stabilized flame in a two-dimensionl duct of constant cross section are presented. The approach is similar to that of Marble and Candel[1] (1978). Integral relations describing mass and momentum conservations in the unburned and burned regions of the flame zone and matching conditions across the flame are developed. The steady and time-dependent problems are discussed in detail in the succeeding three chapters.

2.1 ANALYTICAL DESCRIPTION OF A NON-STEADY STABILIZED FLAME:

We consider a flame, stabilized by a flame holder of half-width η_0, in a two-dimensional parallel duct of width 2ℓ, as shown in figure 2.1. The flame region is modelled as a surface of discontinuity separating the cold fuel-oxidizer mixture, region 1 and hot combustion products, region 2. $\eta(x,t)$ is the distance of the flame sheet from the centerline of the duct, the x-axis. A combustible mixture of fuel and oxidizer approaches the flame region with an uniform velocity U_o at the far upstream. Let $p(x,y,t)$ and $\rho(x,y,t)$ be the pressure and density and $u(x,y,t)$ and $v(x,y,t)$ be the velocity components parallel and normal to the duct axis. The variables are indicated by subscript 1 in region 1, upstream of the flame and by subscript 2 in region 2, downstream of the flame.

Neglecting gravitational and viscous effects, the flow fields in regions 1 and 2 are governed by the following equations:

In region 1,

Continuity equation

$$\frac{\partial \rho_1}{\partial t} + \frac{\partial}{\partial x}(\rho_1 u_1) + \frac{\partial}{\partial y}(\rho_1 v_1) = 0 \tag{2.1}$$

Momentum equations

$$\frac{\partial}{\partial t}(\rho_1 u_1) + \frac{\partial}{\partial x}(\rho_1 u_1^2) + \frac{\partial}{\partial y}(\rho_1 u_1 v_1) = -\frac{\partial p_1}{\partial x} \tag{2.2}$$

$$\frac{\partial}{\partial t}(\rho_1 v_1) + \frac{\partial}{\partial x}(\rho_1 u_1 v_1) + \frac{\partial}{\partial y}(\rho_1 v_1^2) = -\frac{\partial p_1}{\partial y} \tag{2.3}$$

Neglecting heat conduction also, energy equation can be written in the form,

$$\frac{1}{p_1}\frac{D_1 p_1}{Dt} - \frac{\gamma}{\rho_1}\frac{D_1 \rho_1}{Dt} = \frac{1}{C_v}\frac{D_1 s_1}{Dt} = 0 \tag{2.4}$$

where γ is the ratio of specific heats, C_p/C_v and

s_1 is the specific entropy

and $$\frac{D_1}{Dt} \equiv \frac{\partial}{\partial t} + u_1\frac{\partial}{\partial x} + v_1\frac{\partial}{\partial y}$$

The above equation states that the entropy remains constant, following the fluid. We assume the flow field far upstream to be irrotational with uniform velocity U_o and of uniform entropy. Consequently, flow in region 1 can be considered as irrotational and hence isentropic.

A similar set of equations in region 2 can be written as follows:

Continuity equation

$$\frac{\partial \rho_2}{\partial t} + \frac{\partial}{\partial x}(\rho_2 u_2) + \frac{\partial}{\partial y}(\rho_2 v_2) = 0 \tag{2.5}$$

Momentum equations

$$\frac{\partial}{\partial t}(\rho_2 u_2) + \frac{\partial}{\partial x}(\rho_2 u_2^2) + \frac{\partial}{\partial y}(\rho_2 u_2 v_2) = -\frac{\partial p_2}{\partial x} \tag{2.6}$$

$$\frac{\partial}{\partial t}(\rho_2 v_2) + \frac{\partial}{\partial x}(\rho_2 u_2 v_2) + \frac{\partial}{\partial y}(\rho_2 v_2^2) = -\frac{\partial p_2}{\partial y} \tag{2.7}$$

Energy equation

$$\frac{1}{p_2}\frac{D_2 p_2}{Dt} - \frac{\gamma}{\rho_2}\frac{D_2 \rho_2}{Dt} = \frac{1}{C_v}\frac{D_2 S_2}{Dt} = 0 \tag{2.8}$$

where

$$\frac{D_2}{Dt} = \frac{\partial}{\partial t} + u_2\frac{\partial}{\partial x} + v_2\frac{\partial}{\partial y}$$

However, the flow field in region 2 is, in general, rotational as a result of the entropy produced by the flame. This aspect of vorticity production by the flame will be considered later in detail.

The above flow fields in regions 1 and 2 are matched across the flame sheet by mass and momentum conservation relations, analogous to the jump conditions across shock discontinuities in compressible flows. To arrive at the appropriate matching conditions at the flame surface, let us adapt a coordinate system with axes m and n, tangential and normal

to the flame respectively (Fig. 2.2). Let u_m and u_n be the corresponding velocity components. We write the mass and momentum conservation equations for the control volume shown in figure 2.2:

Conservation of mass gives,

$$\frac{\partial}{\partial t}\int_{n_1}^{n_2}\rho\,dn + \left[\rho u_n\right]_{n_1}^{n_2} + \frac{\partial}{\partial m}\int_{n_1}^{n_2}\rho u_m\,dn = 0 \qquad (2.9)$$

Normal momentum equation is

$$\frac{\partial}{\partial t}\int_{n_1}^{n_2}\rho u_n\,dn + \left[\rho u_n^2\right]_{n_1}^{n_2} + \frac{\partial}{\partial m}\int_{n_1}^{n_2}\rho u_m u_n\,dn + \left[p\right]_{n_1}^{n_2} = 0 \qquad (2.10)$$

Tangential momentum equation can be written as

$$\frac{\partial}{\partial t}\int_{n_1}^{n_2}\rho u_m\,dn + \left[\rho u_m u_n\right]_{n_1}^{n_2} + \frac{\partial}{\partial m}\int_{n_1}^{n_2}\rho u_m^2\,dn + \frac{\partial}{\partial m}\int_{n_1}^{n_2}p\,dn = 0 \qquad (2.11)$$

We consider the limiting case, $n_1 \longrightarrow 0^-$ and $n_2 \longrightarrow 0^+$, and obtain the conservation relations valid at $y = \eta(x,t)$ as follows:

(2.9) gives

$$\left[\rho u_n\right]_{0^-}^{0^+} = 0$$

i.e.

$$\rho_1 w_1 = \rho_2 w_2 \qquad (2.12)$$

where w_1 and w_2 are the flame speeds. w_1/U_0 and w_2/U_0 are assumed to be constant.

(2.10) gives

$$P_1 + \rho_1 W_1^2 = P_2 + \rho_2 W_2^2 \tag{2.13}$$

Finally, (2.11) can be written as

$$\left[\rho u_m u_n\right]_{o^-}^{o^+} = 0$$

which gives (Fig. 2)

$$u_1 \cos\vartheta + \left(V_1 - \frac{\partial \eta}{\partial t}\right) \sin\vartheta = u_2 \cos\vartheta + \left(V_2 - \frac{\partial \eta}{\partial t}\right) \sin\vartheta \tag{2.14}$$

The above equation shows that conservation of tagential momentum implies that the tangential velocity is continuous across the flame.

Also, we must have the flame sheet and flow fields deform in a consistent manner. To ensure this, we develop kinematic conditions which are similar to the ones commonly used to describe waves at a fluid interface. In the present context, we have fixed propagation speeds normal to the flame and the kinematic conditions imply that the normal velocity of the fluid, relative to the flame surface is equal to the corresponding flame speed. These relations are (Fig. 2.2):

$$\frac{\partial \eta}{\partial t} \cos\vartheta + u_1 \sin\vartheta - V_1 \cos\vartheta = W_1 \tag{2.15}$$

$$\frac{\partial \eta}{\partial t} \cos\vartheta + u_2 \sin\vartheta - V_2 \cos\vartheta = W_2 \tag{2.16}$$

Let $H = C_p T + \Sigma + \frac{1}{2} q^2$ be the stagnation enthalpy, where Σ is the energy of formation and q is the total fluid velocity with respect to the flame. The energy equation can then be written as

$$\frac{\partial}{\partial t}\int_{n_1}^{n_2} \rho H \, dn + \left[\rho u_n H\right]_{n_1}^{n_2} + \frac{\partial}{\partial m}\int_{n_1}^{n_2}\left[\rho u_m H\right] dn = \frac{\partial}{\partial t}\int_{n_1}^{n_2} p \, dn$$

Assuming specific heat to be constant, we obtain in the quasi-steady approximation,

$$\rho_1 W_1\left[C_p T_1 + \frac{1}{2}\left[W_1^2 + \left(u_1 \cos\vartheta + v_1 \sin\vartheta - \frac{\partial \eta}{\partial t}\sin\vartheta\right)^2\right] + \Sigma_1\right]$$
$$= \rho_2 W_2\left[C_p T_2 + \frac{1}{2}\left[W_2^2 + \left(u_2 \cos\vartheta + v_2 \sin\vartheta - \frac{\partial \eta}{\partial t}\sin\vartheta\right)^2\right] + \Sigma_2\right] \qquad (2.17)$$

where Σ_1 and Σ_2 are the energies of formation per unit mass for the gas in regions 1 and 2 respectively. For combustion processes of practical interest, increase in sensible enthalpy, $(\Sigma_1 - \Sigma_2)$, is much larger than the changes in kinetic energy. Therefore, we can approximate equation (2.17) by

$$C_p T_1 + \Sigma_1 \approx C_p T_2 + \Sigma_2 \qquad (2.18)$$

From equation (2.13)

$$\frac{p_2}{p_1} = 1 - \gamma\left(\frac{W_1}{c_1}\right)^2\left(\frac{\rho_1}{\rho_2} - 1\right)$$

and depends on the square of the Mach number based upon the flame speed, which is considered to be small. Consequently, in equation (2.18) we can approximate using equation (2.12),

$$\frac{T_2}{T_1} \approx \frac{\rho_1}{\rho_2} \approx 1 + \frac{(\Sigma_1 - \Sigma_2)}{C_p T_1} \tag{2.19}$$

But, it is very important to consider the pressure change across the flame in the momentum balance and in determining the flame shape.

2.2 DEVELOPMENT OF THE INTEGRAL RELATIONS:

We wish to investigate the non-steady behaviour of the stabilized flame when subjected to external acoustic disturbances. We assume the imposed disturbance to be of a wavelength large compared to the length of the flame region. Consequently, we consider the flame zone to be compact and ignore any phase variation of the acoustic wave in the flame region. Also, consistent with the approximation in equation (2.19) and the assumed compactness of the flame zone, we can consider the flow fields in the regions 1 and 2 as incompressible. There is, of course, a large density change across the flame as given by (2.19). The pressure changes associated with the acoustic disturbance and the changes in the gas velocities are so small that they do not influence the combustion process significantly.

We now describe the flow fields in the regions 1 and 2 by an integral technique. Continuity and momentum equations are integrated with respect to y, between the flame and the channel wall. In region 1, upstream of the flame, the integration is carried out from $y = \eta(x,t)$ to

$y=\ell$, as shown below.

With the incompressible flow approximation discussed earlier, equation (2.1) becomes,

$$\int_{\eta(x,t)}^{\ell} \frac{\partial u_1}{\partial x}\, dy + \int_{\eta(x,t)}^{\ell} \frac{\partial v_1}{\partial y}\, dy = 0$$

We use the boundary condition at the solid wall,

$$V_1(x,\ell,t) = 0$$

and obtain

$$\frac{\partial}{\partial x}\int_{\eta}^{\ell} u_1\, dy + u_1(x,\eta,t)\frac{\partial \eta}{\partial x} - V_1(x,\eta,t) = 0 \qquad (2.20)$$

We define a mean axial velocity,

$$\bar{u}_1(x,t) = \frac{1}{[\ell-\eta(x,t)]}\int_{\eta(x,t)}^{\ell} u_1\, dy$$

Using the kinematic condition (2.15), we get from (2.20)

$$\frac{\partial}{\partial t}(\ell-\eta) + \frac{\partial}{\partial x}\left[(\ell-\eta)\bar{u}_1\right] + W_1 \sec\vartheta = 0 \qquad (2.21)$$

X-momentum equation (2.2) in region 1 gives,

$$\frac{\partial}{\partial t}\left[(\ell-\eta)\bar{u}_1\right] + u_1(x,\eta,t)\frac{\partial \eta}{\partial x} + \frac{\partial}{\partial x}\int_{\eta}^{\ell} u_1^2\, dy$$

$$+ u_1^2(x,\eta,t)\frac{\partial \eta}{\partial x} - u_1(x,\eta,t)\, v_1(x,\eta,t)$$

$$= -\frac{1}{\rho_1}\frac{\partial}{\partial x}\left[(\ell-\eta)\bar{P}_1\right] - \frac{1}{\rho_1} P_1(x,\eta,t)\frac{\partial \eta}{\partial x}$$

which can be written, using (2.15) as

$$\frac{\partial}{\partial t}\left[(\ell-\eta)\bar{u}_1\right] + \frac{\partial}{\partial x}\left[(\ell-\eta)\bar{u}_1^2\right] + \frac{\partial}{\partial x}\int_{\eta}^{\ell}(u_1-\bar{u}_1)^2\, dy$$

$$+ u_1(x,\eta,t)\, w_1 \sec\vartheta + \frac{\ell-\eta}{\rho_1}\frac{\partial \bar{P}_1}{\partial x}$$

$$+ \frac{1}{\rho_1}\left[P_1(x,\eta,t) - \bar{P}_1(x,t)\right]\frac{\partial \eta}{\partial x} = 0 \qquad (2.22)$$

Similarly, integrated equation of motion in the y-direction in region 1 takes the form,

$$\frac{\partial}{\partial t}\left[(\ell-\eta)\bar{v}_1\right] + \frac{\partial}{\partial x}\int_{\eta}^{\ell} u_1 v_1\, dy + v_1(x,\eta,t)\, w_1 \sec\vartheta$$

$$+ \frac{1}{\rho_1}\left[P_1(x,\ell,t) - P_1(x,\eta,t)\right] = 0 \qquad (2.23)$$

A similar integration from $y=0$ to $y=\eta(x,t)$ of the continuity and momentum equations (2.5-2.7) in region 2 gives the following equations

Continuity

$$\frac{\partial \eta}{\partial t} + \frac{\partial}{\partial x}(\eta \bar{u}_2) - w_2 \sec\vartheta = 0 \qquad (2.24)$$

X-momentum equation

$$\frac{\partial}{\partial t}(\eta \bar{u}_2) + \frac{\partial}{\partial x}(\eta \bar{u}_2^2) + \frac{\eta}{\rho_2}\frac{\partial \bar{p}_2}{\partial x} - u_2(x,\eta,t)\, w_2 \sec\vartheta + \frac{\partial}{\partial x}\int_0^{\eta}(u_2-\bar{u}_2)^2\, dy + \frac{1}{\rho_2}\left[\bar{p}_2 - p_2(x,\eta,t)\right]\frac{\partial \eta}{\partial x} = 0 \tag{2.25}$$

Y-momentum equation

$$\frac{\partial}{\partial t}(\eta \bar{v}_2) + \frac{\partial}{\partial x}\int_0^{\eta} u_2 v_2\, dy - v_2(x,\eta,t)\, w_2 \sec\vartheta + \frac{1}{\rho_2}\left[p_2(x,\eta,t) - p_2(x,0,t)\right] = 0 \tag{2.26}$$

We assume in equations (2.21-2.26),

$$p_1(x,\eta,t) = \bar{p}_1(x,t) \tag{2.27}$$

$$\int_{\eta}^{\ell}(u_1-\bar{u}_1)^2\, dy = 0 \tag{2.28}$$

and

$$p_2(x,\eta,t) = \bar{p}_2(x,t) \tag{2.29}$$

$$\int_0^{\eta}(u_2-\bar{u}_2)^2\, dy = 0 \tag{2.30}$$

These approximations are similar to the ones usually made for shallow water wave calculations, wherein the normal acceleration of the fluid is

neglected. In the present context, these assumptions are strictly valid only for the case of slender flames (i.e. $\left|\frac{d\eta^{(o)}}{dx}\right| << 1$), subjected to low frequency disturbances. Stabilized flames observed in the laboratory (Williams, Hottel and Scurlock[2], 1949 and Wright and Zukoski[3], 1960) and in typical technological applications like afterburners (Zukoski[4], 1978) usually meet this criterion.

To summarize, the non-steady response of a stabilized flame in a two-dimensional channel is governed by the integral relations

$$\frac{\partial(\ell-\eta)}{\partial t} + \frac{\partial}{\partial x}\left[(\ell-\eta)\bar{u}_1\right] + w_1 \sec\vartheta = 0 \tag{2.31}$$

$$\frac{\partial}{\partial t}\left[(\ell-\eta)\bar{u}_1\right] + \frac{\partial}{\partial x}\left[(\ell-\eta)\bar{u}_1^2\right] + \frac{(\ell-\eta)}{\rho_1}\frac{\partial \bar{P}_1}{\partial x} + u_1(x,\eta,t)\, w_1 \sec\vartheta = 0 \tag{2.32}$$

$$\frac{\partial \eta}{\partial t} + \frac{\partial}{\partial x}(\eta \bar{u}_2) - w_2 \sec\vartheta = 0 \tag{2.33}$$

$$\frac{\partial}{\partial t}(\eta\bar{u}_2) + \frac{\partial}{\partial x}(\eta\bar{u}_2^2) + \frac{\eta}{\rho_2}\frac{\partial \bar{P}_2}{\partial x} - u_2(x,\eta,t)\, w_2 \sec\vartheta = 0 \tag{2.34}$$

together with the matching conditions

$$\rho_1 w_1 = \rho_2 w_2 \tag{2.12}$$

$$p_1 + \rho_1 w_1^2 = p_2 + \rho_2 w_2^2 \tag{2.13}$$

equations (2.14 - 2.16) can be written as

$$u_1(x,\eta,t) + v_1(x,\eta,t)\frac{\partial \eta}{\partial x} = u_2(x,\eta,t) + v_2(x,\eta,t)\frac{\partial \eta}{\partial x} \tag{2.35}$$

$$\frac{\partial \eta}{\partial t} + u_1(x,\eta,t)\frac{\partial \eta}{\partial x} = v_1(x,\eta,t) + w_1 \sec\vartheta \tag{2.36}$$

$$\frac{\partial \eta}{\partial t} + u_2(x,\eta,t)\frac{\partial \eta}{\partial x} = v_2(x,\eta,t) + w_2 \sec\vartheta \tag{2.37}$$

From equations 2.35-2.37, we obtain

$$u_2(x,\eta,t) = u_1(x,\eta,t) + w_1(\lambda-1)\sin\vartheta \tag{2.38}$$

We notice that the above integral relations and matching conditions explicitly involve the local fluid velocities at the flame surface in both the regions. To complete the formulation, we have to independently estimate at least one velocity component at $y = \eta(x,t)$. This is to be expected since we have fluid propagation through the flame and the local momentum transfer at the flame should play an important role in the flame development. An exact solution for the upstream irrotational flow

field of the flame region is presented in chapter 3. An approximation for $u_1(x,\eta,t)$ will be developed from this exact solution.

The above system of equations is studied in the subsequent chapters using a perturbation technique. The zeroth order solution, representing the steady flame development, is perturbed by an acoustic wave incident on the flame region.

2.3 REFERENCES:

[1] Marble, F.E. and Candel, S.M., "An Analytical Study of the Non-Steady Behaviour of Large Combustors", Seventeenth Symposium (International) on Combustion, August 1978, pp. 761-769 .

[2] Williams, G.C., Hottel, H.C., and Scurlock, A.C., "Flame Stabilization and Propagation in High Velocity Gas Streams", Third Symposium on Combustion and Flame and Explosion Phenomena, Williams and Wilkins Company, Baltimore, Maryland, 1949, p. 21-40.

[3] Wright, F.H. and Zukoski, E.E., "Flame Spreading from Bluff Body Flame Holders", Proceedings, Eighth Symposium (International) on Combustion, 1960, pp. 933-943.

[4] Zukoski, E., "AFTERBURNERS", The Aerothermodynamics of Aircraft Gas Turbine Engines, Edited by Oates, G. C., AFAPL-TR-78-52, Chapter 21, 1978.

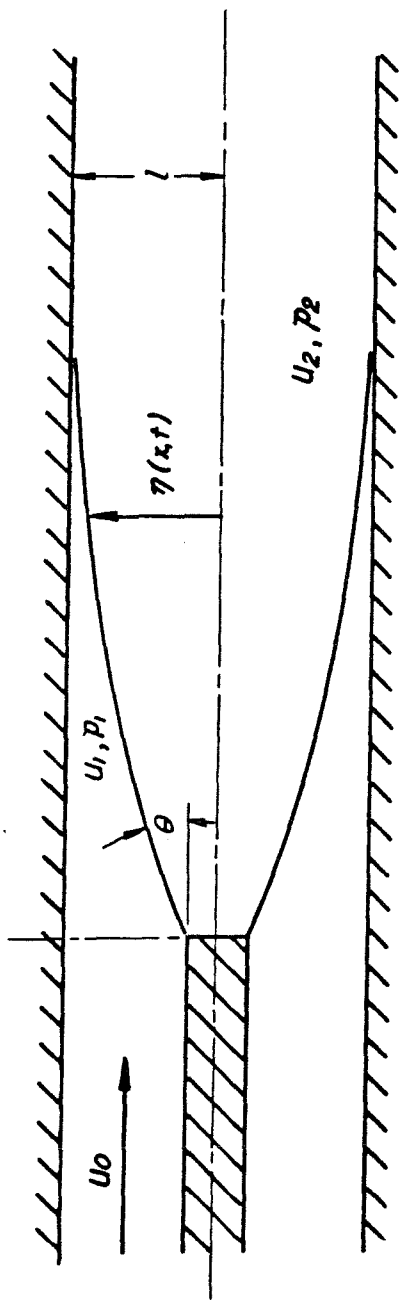

FIGURE 2.1 STABILIZED FLAME IN A DUCT

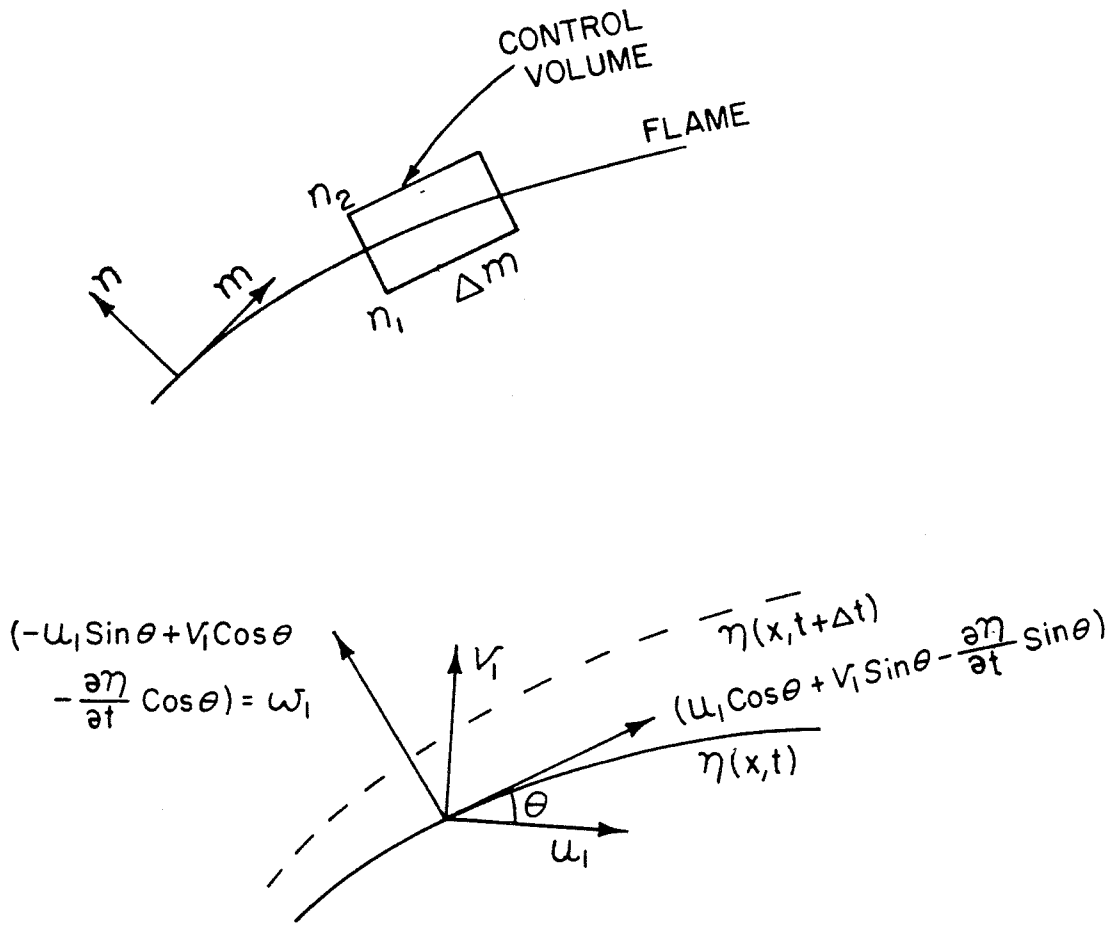

FIGURE 2.2 NOTATION FOR MATCHING CONDITIONS ACROSS THE FLAME

3. STEADY STATE FLAME CALCULATIONS

We develop, in the first section, an approximate analysis for the steady state stabilized flame in a two-dimensional duct. In the second section, an exact solution for the irrotational flow field upstream of the flame is presented. The third section deals with the numerical solution of steady-state equations arrived from the detailed formulation of chapter 2.

3.1 APROXIMATE ANALYSIS FOR THE STEADY-STATE FLAME DEVELOPMENT:

An approximate analysis, valid for low flame speeds, for the description of the steady stabilized flame, represented by $y = \eta^{(o)}(x)$ is presented below. Let the mean axial velocity, pressure and density be denoted by $\bar{u}_1^{(o)}(x)$, $\bar{p}_1^{(o)}(x)$ and ρ_1 in region 1 and by $\bar{u}_2^{(o)}(x)$, $\bar{p}_2^{(o)}(x)$ and ρ_2 in region 2. Let w_1 and w_2 be the fixed burning velocities, as in chapter 2.

Let

$$\left| \frac{d\eta^{(o)}}{dx} \right| << 1 \tag{3.1}$$

In region 1, mass conservation gives,

$$\frac{d}{dx}\left[(\ell - \eta^{(o)})\, \bar{u}_1^{(o)}\right] = - w_1 \tag{3.2}$$

With the assumed uniform approach velocity U_o far upstream, flow field in region 1 is irrotational and we use Bernoulli equation upstream of the flame and write,

$$\frac{1}{2}\left(\bar{u}_1^{(0)}\right)^2 + \frac{\bar{p}_1^{(0)}}{\rho_1} = \text{constant} = \frac{1}{2}U_0^2 + \frac{p_0}{\rho_1}$$

or

$$\frac{\bar{p}_1^{(0)}}{\rho_1 U_0^2} + \frac{1}{2}\left(\frac{\bar{u}_1^{(0)}}{U_0}\right)^2 = \frac{1}{\gamma M_0^2} + \frac{1}{2} \tag{3.3}$$

where p_0 is the static pressure at far upstream,

and $\gamma = c_p/c_v$ and M_0 is the approach Mach number.

In region 2, mass conservation gives,

$$\frac{d}{dx}\left(\eta^{(0)}\bar{u}_2^{(0)}\right) = w_2 \tag{3.4}$$

Next, we utilize the overall momentum conservation equation to get

$$\begin{aligned}\rho_1 U_0^2 \ell + p_0 \ell = {} & \rho_1\left(\bar{u}_1^{(0)}\right)^2\left(\ell - \eta^{(0)}\right) + \bar{p}_1^{(0)}\left(\ell - \eta^{(0)}\right) \\ & + \rho_2\left(\bar{u}_2^{(0)}\right)^2 \eta^{(0)} + \bar{p}_2^{(0)}\eta^{(0)}\end{aligned} \tag{3.5}$$

Consistent with the approximation (3.1), we assume that the streamlines are nearly parallel to the duct axis and treat the static pressure to be uniform in regions 1 and 2. But, normal momentum balance across the flame (equation 2.13) gives

$$\bar{p}_1^{(0)} - \bar{p}_2^{(0)} = (\lambda - 1)\,\rho_1 w_1^2$$

Integrating equation (3.2), and defining

$$\chi = \left(\frac{x}{\ell}\right)\left(\frac{w}{U_0}\right)$$

we get

$$\frac{\bar{u}_1^{(o)}}{U_o} = \frac{A - \chi}{(1 - \eta^{(o)}/\ell)} \qquad (3.8)$$

Similarly equation (3.4) gives

$$\frac{\bar{u}_2^{(o)}}{U_o} = \frac{B + \lambda\chi}{(\eta^{(o)}/\ell)} \qquad (3.9)$$

where $\lambda = \rho_1/\rho_2$

and A and B are constants of integration.

At the flame holder of half width η_o at $\chi = 0$, we assume the mean axial velocities in the two streams to be equal and write mass conservation equation to get

$$\frac{\bar{u}_1^{(o)}(0)}{U_o} = \frac{\bar{u}_2^{(o)}(0)}{U_o} = \frac{1}{1 - \eta_o/\ell + \frac{1}{\lambda}\eta_o/\ell}$$

Calculations were also done with different values (e.g. $\bar{u}_2^{(o)}(o) = 0$) for the mean axial velocity in region 2 at the flame holder. The results indicate that the effect is very localized near the flame holder and the overall flame development is not appreciably altered. The above choice gives a flame shape with a positive slope at the flame holder.

Hence, in equations (3.8) and (3.9),

$$A = (1 - \eta_o/\ell)\left(\frac{1}{1 - \eta_o/\ell + \frac{1}{\lambda}\eta_o/\ell}\right) \qquad (3.10)$$

$$B = \eta_0/\ell \left(\frac{1}{1 - \eta_0/\ell + \frac{1}{\lambda}\,\eta_0/\ell} \right) \tag{3.11}$$

We substitute $\bar{u}_1^{(0)}$, $\bar{u}_2^{(0)}$ and $\bar{p}_1^{(0)}$ into the overall momentum conservation equation (3.5) and obtain

$$\left(\frac{1}{2} - \eta^{(0)}/\ell\right)\left(\frac{A-\chi}{1-\eta^{(0)}/\ell}\right)^2 + \frac{1}{\lambda}\left(\eta^{(0)}/\ell\right)\left(\frac{B+\lambda\chi}{\eta^{(0)}/\ell}\right)^2$$
$$-(\lambda-1)\left(w_1/U_0\right)^2 \eta^{(0)}/\ell = \frac{1}{2} \tag{3.12}$$

which is cubic in $\eta^{(0)}$ and quadratic in χ .

3.1.1 RESULTS AND DISCUSSION: For simplicity, equation 3.12 is solved for $\chi(\eta^{(0)})$ to obtain the flame shape $\eta^{(0)}(x)$ implicitly. A typical flame shape for $\lambda = \rho_1/\rho_2 = 4.5$ is shown in figure 3.1.

Mean axial velocities and pressure are obtained from equations (3.8), (3.9) and (3.3). Distribution of $\bar{u}_1^{(0)}$ and $\bar{u}_2^{(0)}$ for the above flame configuration are shown in figure 3.2 and exhibit an approximately linear increase with the axial distance from the flame holder. Fig. 3.3 represents the corresponding mean pressure profile.

It can at once be observed from the equations (3.12), (3.3), (3.8) and (3.9) that the flame shape and flow variables exhibit a similarity representation for all flame speeds $w_1/U_0 \ll 1$, with $\chi = \frac{x}{\ell}\,\frac{w}{U_0}$ as the similarity variable.

3.2 AN EXACT REPRESENTATION FOR THE STEADY STATE FLOW FIELD UPSTREAM OF A STABILIZED FLAME:

As was discussed in chapter 2, flow field upstream of the flame is irrotational and can also be approximated as incompressible. Consequently, there exists a unique scalar potential $\varphi(x,y)$ such that

$$\frac{\partial^2\varphi}{\partial x^2} + \frac{\partial^2\varphi}{\partial y^2} = 0$$

and

$$u_1^{(o)}(x,y) = \frac{\partial\varphi}{\partial x}$$

$$v_1^{(o)}(x,y) = \frac{\partial\varphi}{\partial y} \qquad (3.13)$$

For the present calculation, let us consider the flame $\eta^{(o)}(x)$ to be stabilized by an idealized flame holder of negligible thickness, located at $x=0$. The kinematic condition (equation 2.15) at the flame surface in region 1, specialized to steady flow, can be written as

$$u_1^{(o)}(x,\eta^{(o)})\,\frac{d\eta^{(o)}}{dx} = v_1^{(o)}(x,\eta^{(o)}) + w_1 \sec\vartheta^{(o)} \qquad (3.14)$$

Substituting for $u_1^{(o)}(x,\eta^{(o)})$ and $v_1^{(o)}(x,\eta^{(o)})$ from (3.13) and noting that

$$\sec\vartheta^{(o)} = \left[1+\left(\frac{d\eta^{(o)}}{dx}\right)^2\right]^{1/2}$$

equation (3.14) can be written as

$$\left\{\left[\frac{\partial\varphi}{\partial x}(x,\eta^{(0)})\right]^2 - w_1^2\right\}\left(\frac{d\eta^{(0)}}{dx}\right)^2 - 2\frac{\partial\varphi}{\partial x}(x,\eta^{(0)})\frac{\partial\varphi}{\partial y}(x,\eta^{(0)})\frac{d\eta^{(0)}}{dx}$$

$$+\left[\frac{\partial\varphi}{\partial y}(x,\eta^{(0)})\right]^2 - w_1^2 = 0 \qquad (3.15)$$

Once we know the potential $\varphi(x,y)$, we can calculate from equation (3.15),

$$\frac{d\eta^{(0)}}{dx} = \frac{d\eta^{(0)}}{dx}\left[\frac{\partial\varphi}{\partial x}(x,\eta^{(0)}), \frac{\partial\varphi}{\partial y}(x,\eta^{(0)}), w_1\right] \qquad (3.16)$$

The first order, ordinary differential equation (3.16) can be integrated numerically as an initial value problem with the initial condition $\eta^{(0)}=0$ at $x=x_0$, where x_0 is obtained from the equation

$$u_1^{(0)}(x_0,0) = \frac{\partial\varphi}{\partial x}(x_0,0) = w_1$$

The flame shape obtained from the approximate calculation of the previous section and the results of Ball[1] (1951), lead us to model the flow field, upstream of the flame, by a source distribution located on the axis of the duct in the flame region.

The complex potential $W_1(x+iy)$ due to a source of strength m_1, located at $x=\xi$ in a two-dimensional channel of width 2ℓ can be written (Lamb,[2] 1932) as

$$W_1(z) = \frac{m_1}{2\pi} \log_e\left[\sinh \frac{\pi (z-\xi)}{2\ell}\right] \tag{3.17}$$

where z=x+iy.

This gives the complex velocity,

$$\frac{dW_1}{dz} = \frac{m_1}{4\ell} \coth\left[\frac{\pi (z-\xi)}{2\ell}\right] \tag{3.18}$$

Now, for an uniform source distribution of strength m_2/L per unit length extending from ξ =0 to ξ =L, we can by superimposition write the complex velocity as

$$\frac{dW_2}{dz} = \frac{m_2}{L} \frac{1}{4\ell} \int_0^L \coth\left[\frac{\pi (z-\xi)}{2\ell}\right] d\xi$$

i.e.

$$\frac{dW_2}{dz} = \frac{m_2}{L} \frac{1}{2\pi} \log_e\left[\frac{\sinh \frac{\pi z}{2\ell}}{\sinh \frac{\pi (z-L)}{2\ell}}\right] \tag{3.19}$$

We can superpose the potentials due to a source of strength $4\ell U_o \alpha^{(o)}$ at $x=\xi$, uniform source distribution of total strength $4\ell U_o \beta^{(o)}$ and uniform flow of velocity $(1+\alpha^{(o)}+\beta^{(o)})U_o$ to get the complex velocity,

$$\frac{1}{U_0}\frac{dW}{dz} = \frac{U_1^{(0)}(x,y)}{U_0} - i\frac{V_1^{(0)}(x,y)}{U_0}$$

$$= \alpha^{(0)} \coth\frac{\pi(z-\xi)}{2\ell} + 2\frac{\beta^{(0)}}{\pi}\left(\frac{\ell}{L}\right)\log_e\left\{\frac{\sinh\frac{\pi z}{2\ell}}{\sinh\frac{\pi(z-L)}{2\ell}}\right\}$$

$$+ \left[1 + \alpha^{(0)} + \beta^{(0)}\right] \qquad (3.20)$$

In the above equation, uniform flow is added such that the approach velocity at the far upstram is U_0. From the analysis of 3.1, we take $\ell/L \approx w_1/U_0$, where L is the length of the flame region. We also choose the total source strength such that $U_1^{(0)}(L)$ is approximately equal to the value obtained from the previous section.

3.2.1 RESULTS AND DISCUSSION: In the results discussed below, to generate acceptable flame envelopes, the source strengths selected are

$$\alpha^{(0)} = 0, \qquad \beta^{(0)} = 1 \qquad \text{for } \lambda = 4.5$$

and

$$\alpha^{(0)} = 0, \qquad \beta^{(0)} = 0.44 \qquad \text{for } \lambda = 2.25$$

This implies that we model the steady state flow field upstream of the flame by an uniform source distribution at the channel axis, extending over the entire flame region.

Typical flame envelopes for $w_1/U_0 = 0.1$, 0.2 and 0.4 are shown in Fig. 3.4 for $\lambda = 4.5$. Flame shape and streamlines upstream of the flame for $\lambda = 4.5$ are shown in Fig. 3.5 for $w_1/U_0 = 0.2$ and in Fig. 3.6 for $w_1/U_0 = 0.4$. This flow field is compared with the results of Ball (1951)

and the agreement is very good. The above potential solution, of course, does not describe the flow field downstream of the flame.

Velocity profiles for three axial locations, namely x/ℓ =-0.032, 0.238 and 0.758, are shown in the Figs. 3.7-3.9 for the flame configuration of Fig. 3.6. We notice that, in the early stages of flame spreading, the axial velocity $u_1^{(o)}(x,y)$ is strongly non-uniform over the cross section. This can also be seen from the flow pattern of Fig. 3.6.

To complete the formulation in chapter 2, we intend to obtain an approximation for $u_1^{(o)}(x,\eta^{(o)})/\bar{u}_1^{(o)}(x)$, where $\bar{u}_1^{(o)}$ is the mean axial velocity. Distributions of $u_1^{(o)}(x,\eta^{(o)})/\bar{u}_1^{(o)}(x)$ and $v^{(o)}(x,\eta^{(o)})/\bar{u}^{(o)}(x)$ are shown in Fig. 3.10 for the above stabilized flame. In Figs. 3.11 and 3.12, the $u_1^{(o)}(x,\eta^{(o)})/\bar{u}_1^{(o)}(x)$ profiles for w_1/U_o =0.4 and 0.2 are approximated by,

$$\left[1-\frac{u_1^{(o)}(x,\eta^{(o)})}{\bar{u}_1^{(o)}(x)}\right]\left(1+\delta\frac{x}{\ell}\right)=1 \qquad (3.21)$$

where δ =1/0.014

The above approximation, together with the matching conditions (2.13-2.16) provide all the velocity components at the flame surface for the steady state flame development. A similar modelling for the non-steady calculation is shown in section 4.2.

3.3 NUMERICAL SOLUTION OF THE STEADY STATE INTEGRAL RELATIONS:

The integral relations (2.31-2.34) are analyzed by a perturbation technique. The perturbation scheme consists of the dominant order solution representing the steady state flame development, together with the time dependent perturbations caused by the imposed disturbances. Let $\eta^{(0)}(x)$ represent the steady state flame shape and $\bar{p}_1^{(0)}(x)$, $\bar{p}_2^{(0)}(x)$ and $\bar{u}_1^{(0)}(x)$, $\bar{u}_2^{(0)}(x)$ denote the average static pressures and velocities in the two regions. We assume the time dependent perturbation quantities to be small compared to the corresponding steady state variables. Formally, we express the dependent variables in the integral relations as

$$\eta(x,t) = \eta^{(0)}(x) + \eta^{(1)}(x,t)$$
$$\bar{p}_1(x,t) = \bar{p}_1^{(0)}(x) + \bar{p}_1^{(1)}(x,t) \qquad (3.22)$$

etc.

and

$$\left|\eta^{(1)}(x,t)\right| << \left|\eta^{(0)}(x)\right| \quad \text{etc.}$$

Substituting equations (3.22) into the integral relations (2.31-2.34), we get for the steady state flame development,

$$\frac{d}{dx}\left[(1-\eta^{(0)})\,\bar{u}_1^{(0)}\right] + w_1 \sec\vartheta^{(0)} = 0 \qquad (3.23)$$

$$\bar{u}_1^{(0)}\frac{d\bar{u}_1^{(0)}}{dx} + \frac{1}{\rho_1}\frac{d\bar{p}_1^{(0)}}{dx} + \frac{1}{(1-\eta^{(0)})}\left[u_1^{(0)}(x,\eta^{(0)}) - \bar{u}_1^{(0)}\right] w_1 \sec\vartheta^{(0)} = 0 \qquad (3.24)$$

$$\frac{d}{dx}\left(\eta^{(0)}\bar{u}_2^{(0)}\right) - w_2 \sec\vartheta^{(0)} = 0 \tag{3.25}$$

$$\bar{u}_2^{(0)}\frac{d\bar{u}_2^{(0)}}{dx} + \frac{1}{\rho_2}\frac{d\bar{p}_2^{(0)}}{dx} + \frac{1}{\eta^{(0)}}\left[\bar{u}_2 - u_2^{(0)}(x,\eta^{(0)})\right] w_2 \sec\vartheta^{(0)} = 0 \tag{3.26}$$

In equations (3.24) and (3.26), $u_1^{(0)}(x,\eta^{(0)})$ is obtained from the approximation (3.21) and from equation (2.38) we have,

$$u_2^{(0)}(x,\eta^{(0)}) = u_1^{(0)}(x,\eta^{(0)}) + w_1(\lambda-1)\sin\vartheta^{(0)}$$

Further, the pressure fields in the two regions are related through the normal momentum balance (2.13),

$$\bar{p}_1^{(0)}(x) - \bar{p}_2^{(0)}(x) = (\lambda-1)\rho_1 w_1^2 \tag{3.27}$$

We assume a small flame holder of half width η_0 located at x=0 and also consider as in section 3.1, $\bar{u}_1^{(0)}(0) = \bar{u}_2^{(0)}(0)$ at $x=0$. This gives the initial conditions for the steady problem as

at x=0,

$$\eta^{(0)}(0) = \eta_0$$

$$\bar{u}_1^{(0)}(0) = \bar{u}_2^{(0)}(0) = \frac{U_0 \ell}{\ell - \eta_0 + \eta_0/\lambda}$$

and

$$\bar{p}_1^{(o)}(o) = p_o + \frac{1}{2}\rho_1\left[U_o^2 - \left(\bar{u}_1^{(o)}(o)\right)^2\right]$$

The above system of ordinary first order non-linear differential equations are integrated numerically to obtain $\eta^{(o)}(x)$, $\bar{u}_1^{(o)}(x)$, $\bar{u}_2^{(o)}(x)$ and $\bar{p}_1^{(o)}(x)$.

3.3.1 RESULTS AND DISCUSSION: Steady flame envelopes for three flame speeds, w_1/U_o =0.1, 0.2 and 0.4 and for an approach Mach number, $M_o = U_o/c_1$ =0.2 are shown in Fig. 3.13 for λ =4.5 and in Fig. 3.14 for λ =2.25. The flame shapes are not very sensitive to changes in the approach Mach number for low Mach numbers. These flame envelopes may be compared with Fig. 3.4 obtained from the source flow calculations. The agreement is very good. The flame shape and velocities in the two regions are compared in the figures 3.15 and 3.16 with the approximate analysis of section 3.1 for a flame speed w_1/U_o of 0.1 and show excellent agreement.

3.4 REFERENCES:

[1] Ball, G.A., "Combustion Aerodynamics. A Study of a Two-Dimensional Flame",Department of Engineering Science and Applied Physics, Harvard University, July, 1951.

[2] Lamb, H., "HYDRODYNAMICS", Sixth Edition, Dover Publications, p. 71, 1932.

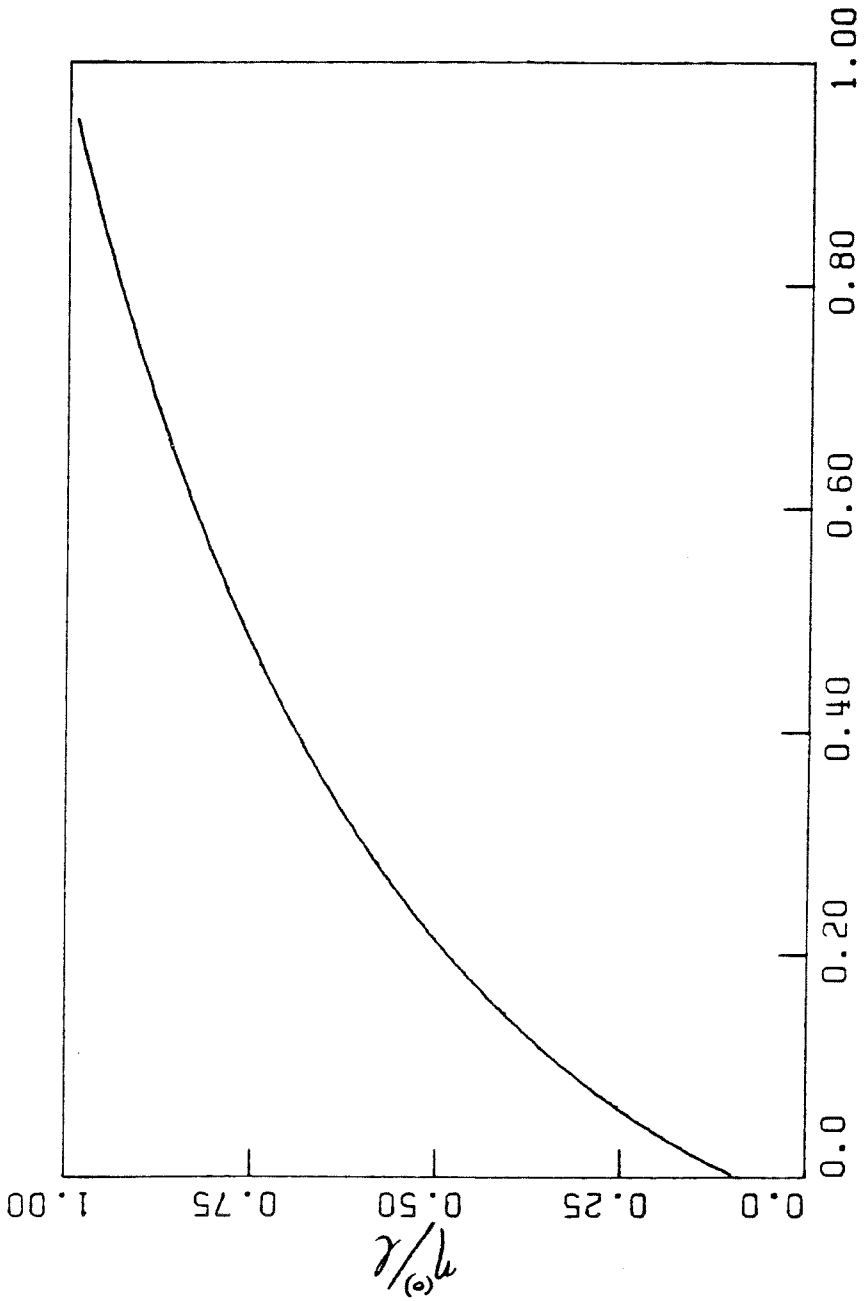

FIGURE 3.1 STEADY FLAME SHAPE, =4.5

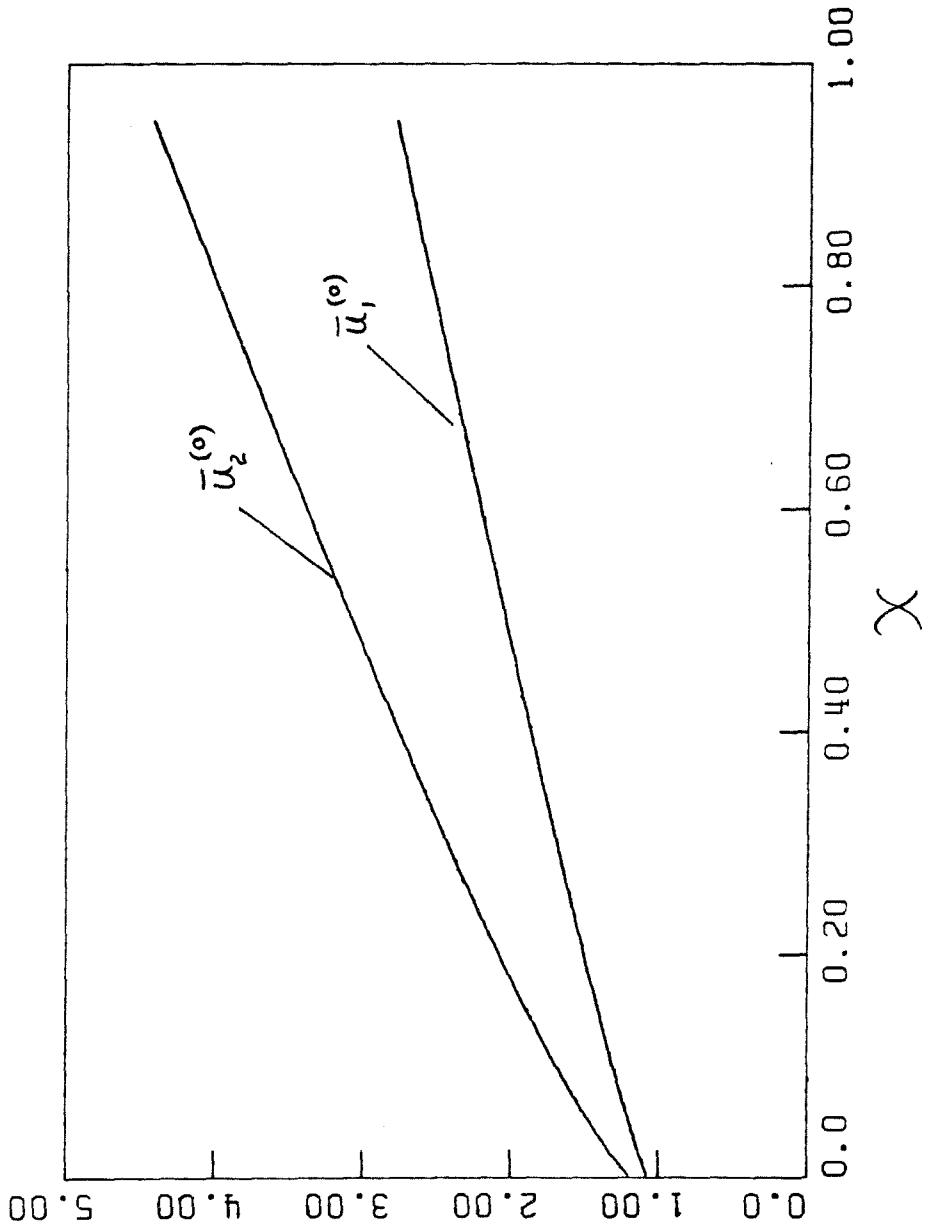

FIGURE 3.2 DISTRIBUTION OF AVERAGE AXIAL VELOCITIES, λ =4.5

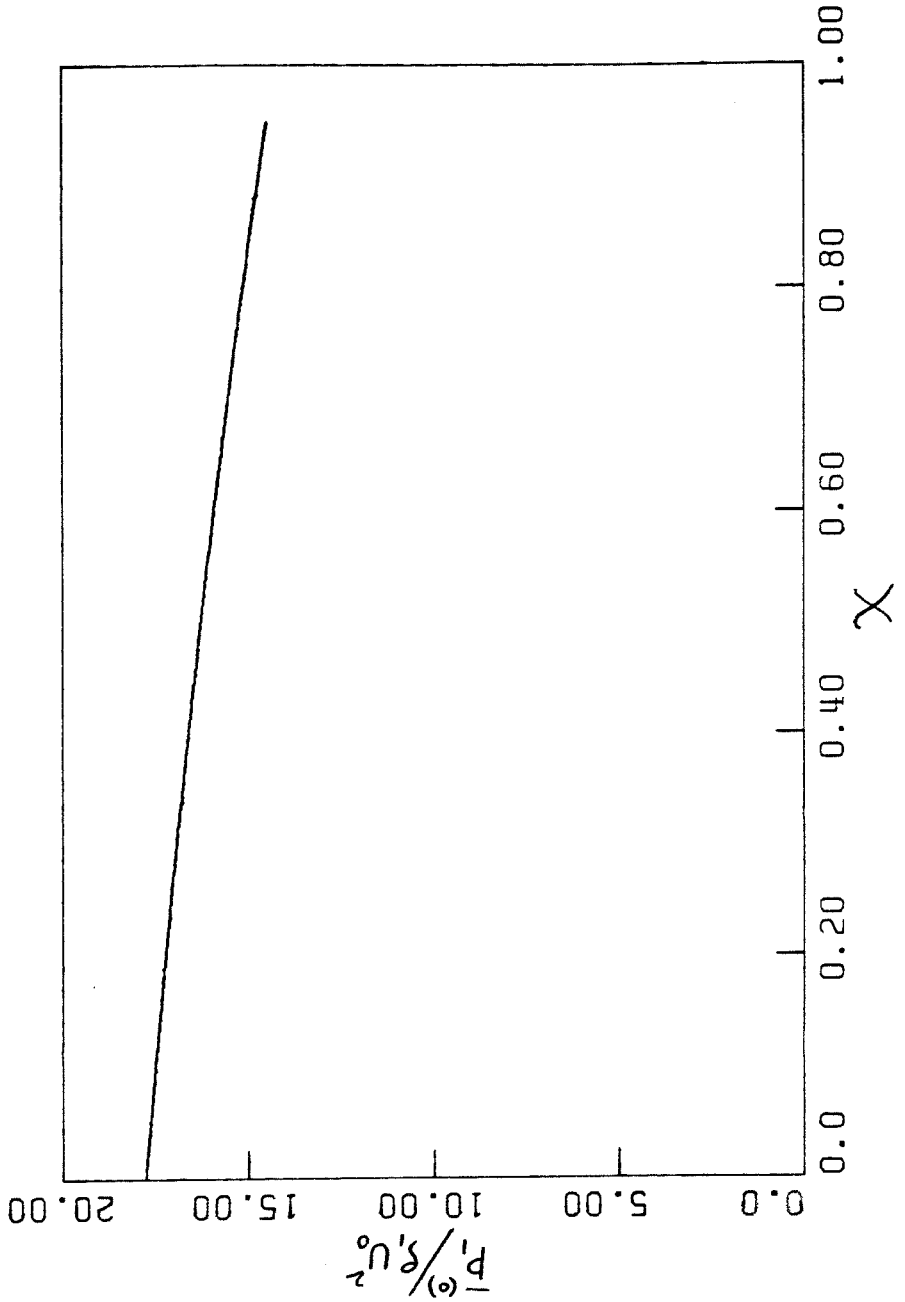

FIGURE 3.3 DISTRIBUTION OF AVERAGE STATIC PRESSURE, λ =4.5

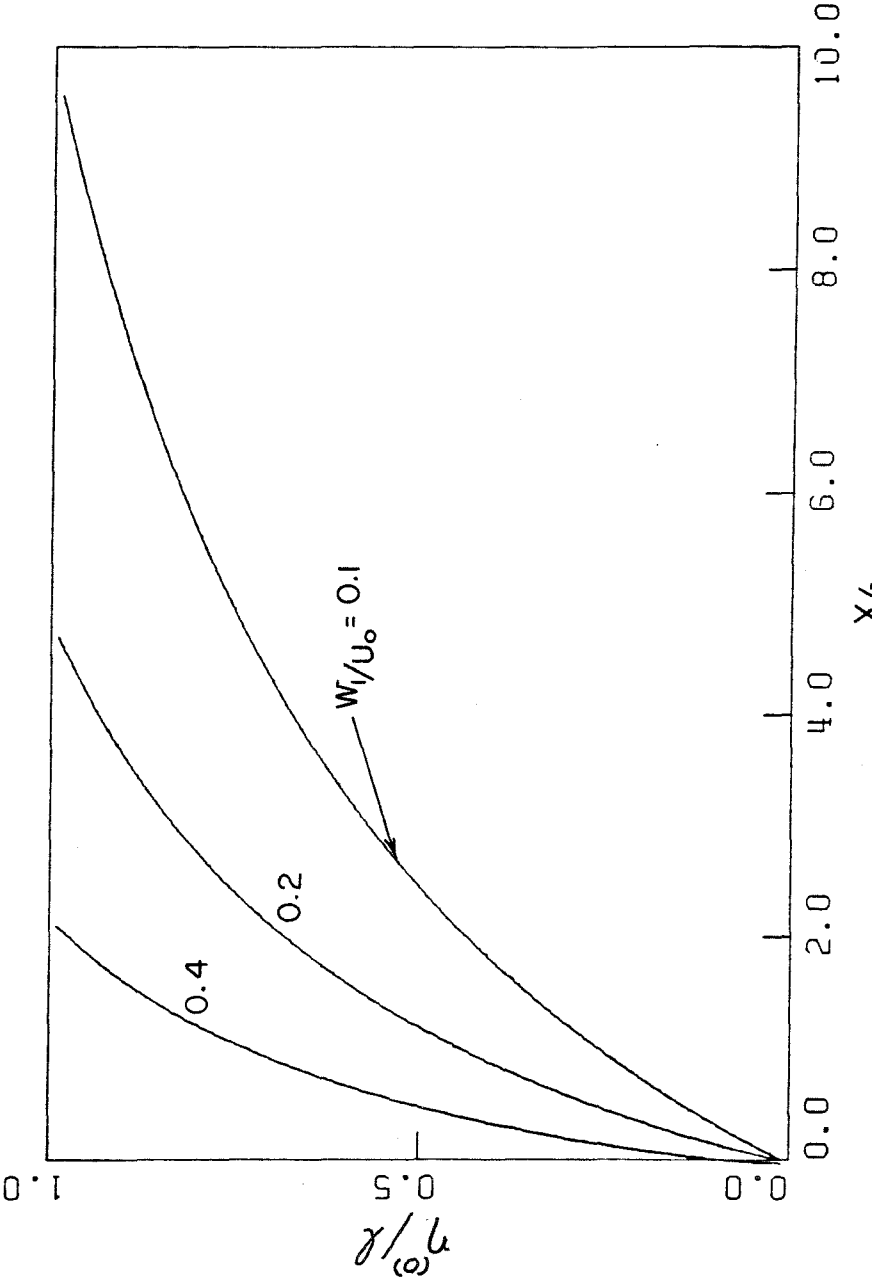

FIGURE 3.4 STEADY FLAME ENVELOPES, $\lambda = 4.5$, $\alpha^{(\infty)} = 0$, $\beta^{(\infty)} = 1.0$

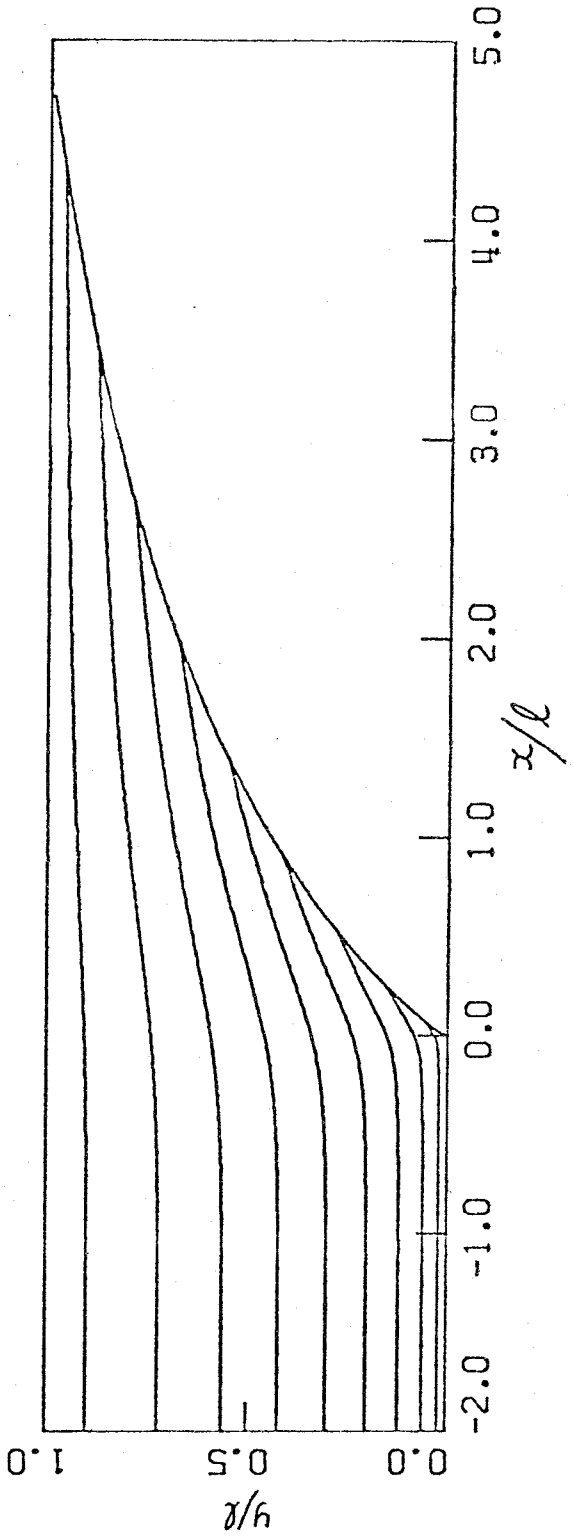

FIGURE 3.5 STREAMLINES UPSTREAM OF THE FLAME, $w_1/U_o = 0.1$

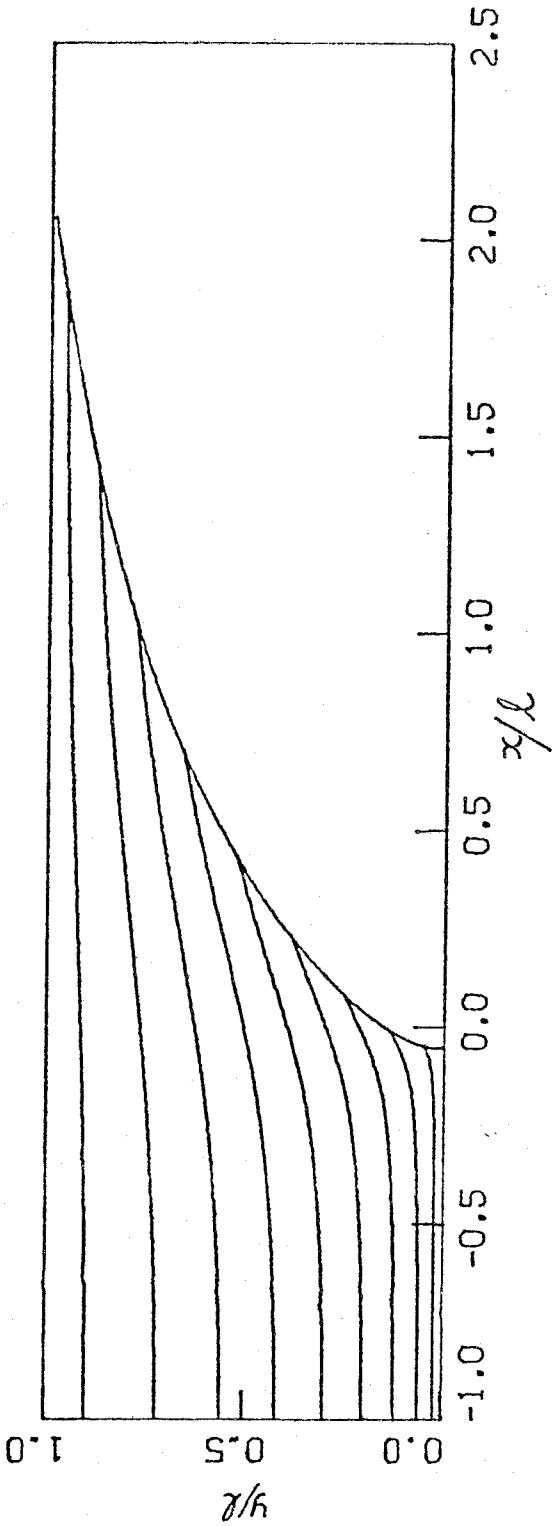

FIGURE 3.6 STREAMLINES UPSTREAM OF THE FLAME, $w_i/U_o = 0.4$

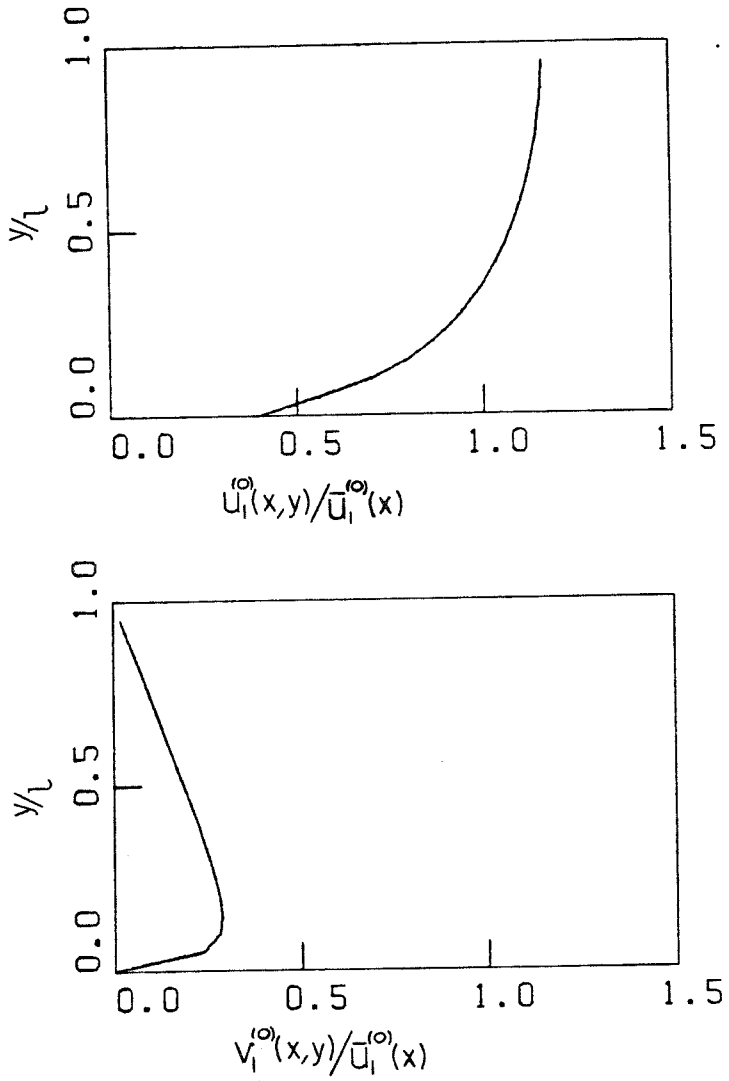

FIGURE 3.7 VELOCITY PROFILES UPSTREAM OF THE FLAME, X/l=-0.032

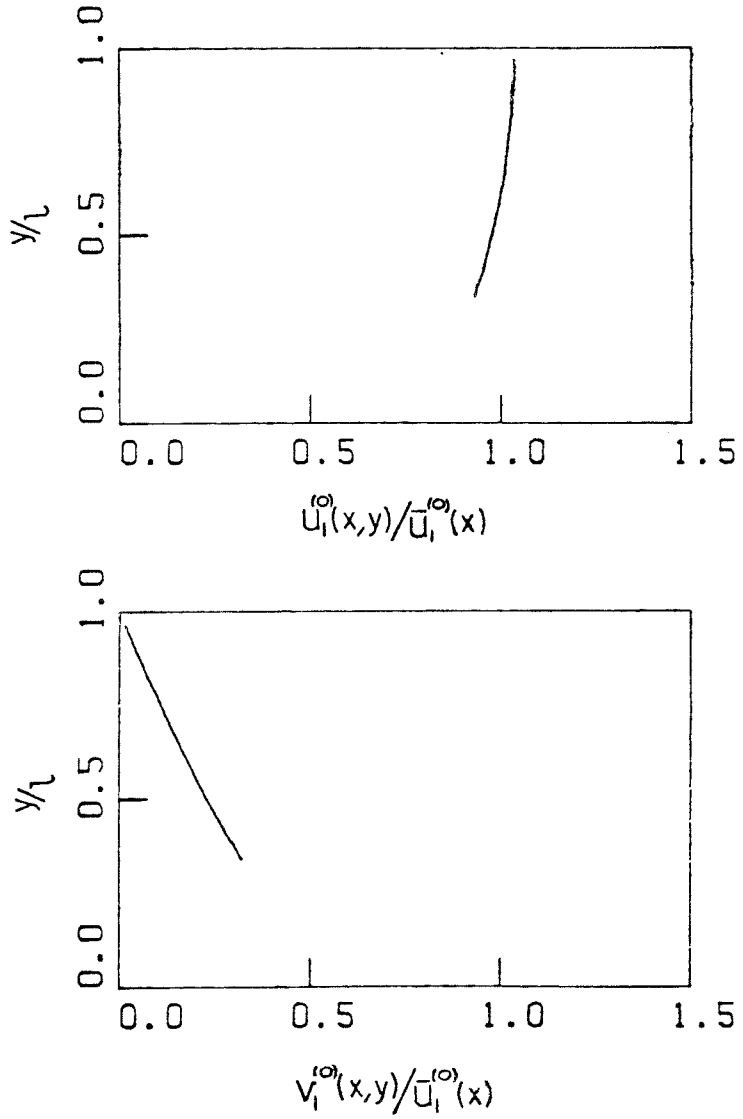

FIGURE 3.8 VELOCITY PROFILES UPSTREAM OF THE FLAME, X/l=0.238

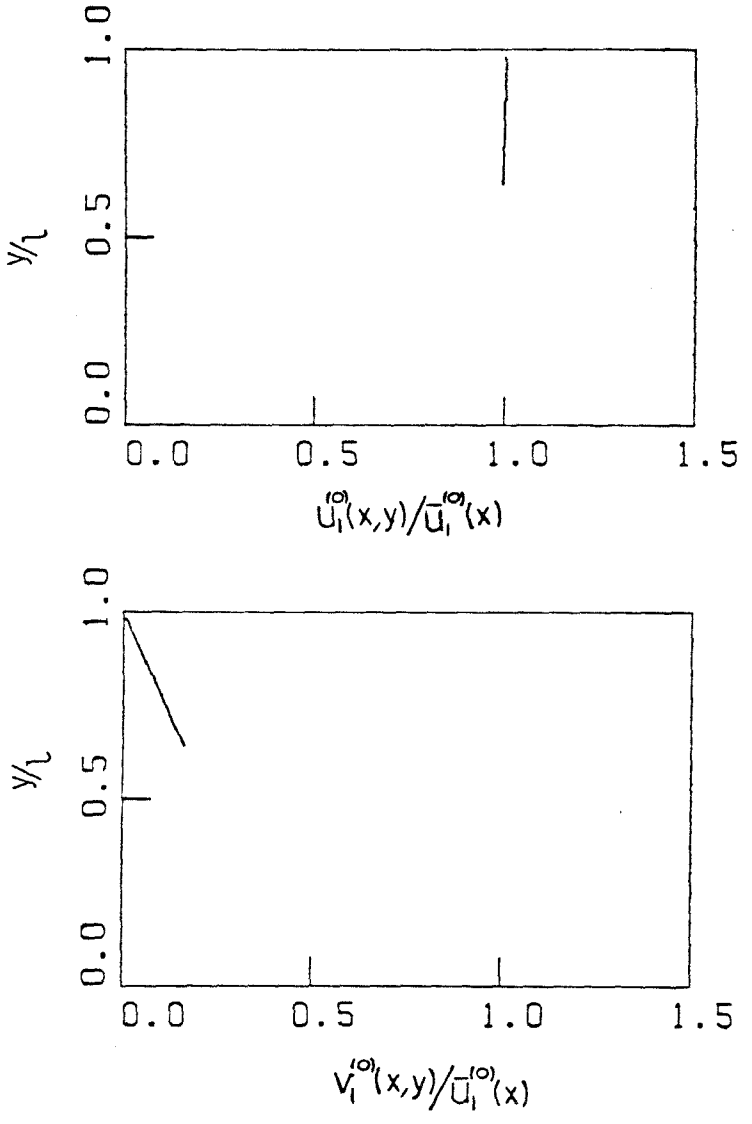

FIGURE 3.9 VELOCITY PROFILES UPSTREAM OF THE FLAME, X/l=0.758

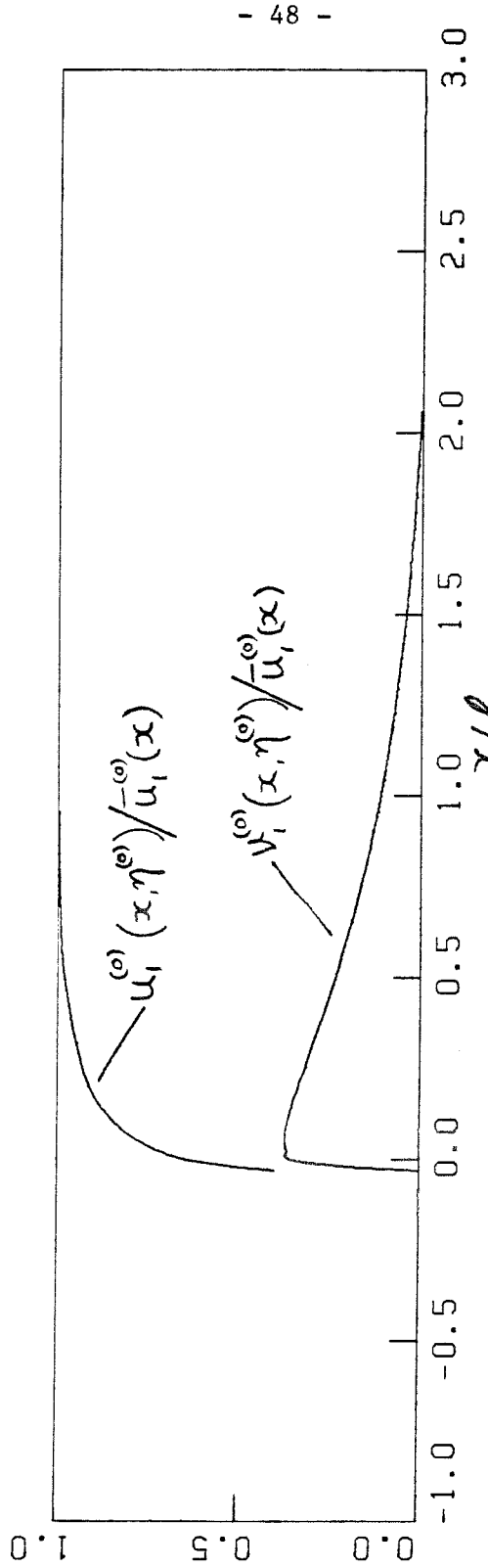

FIGURE 3.10 DISTRIBUTION OF UPSTREAM VELOCITIES AT THE FLAME EDGE, $w_1/u_o = 0.4$

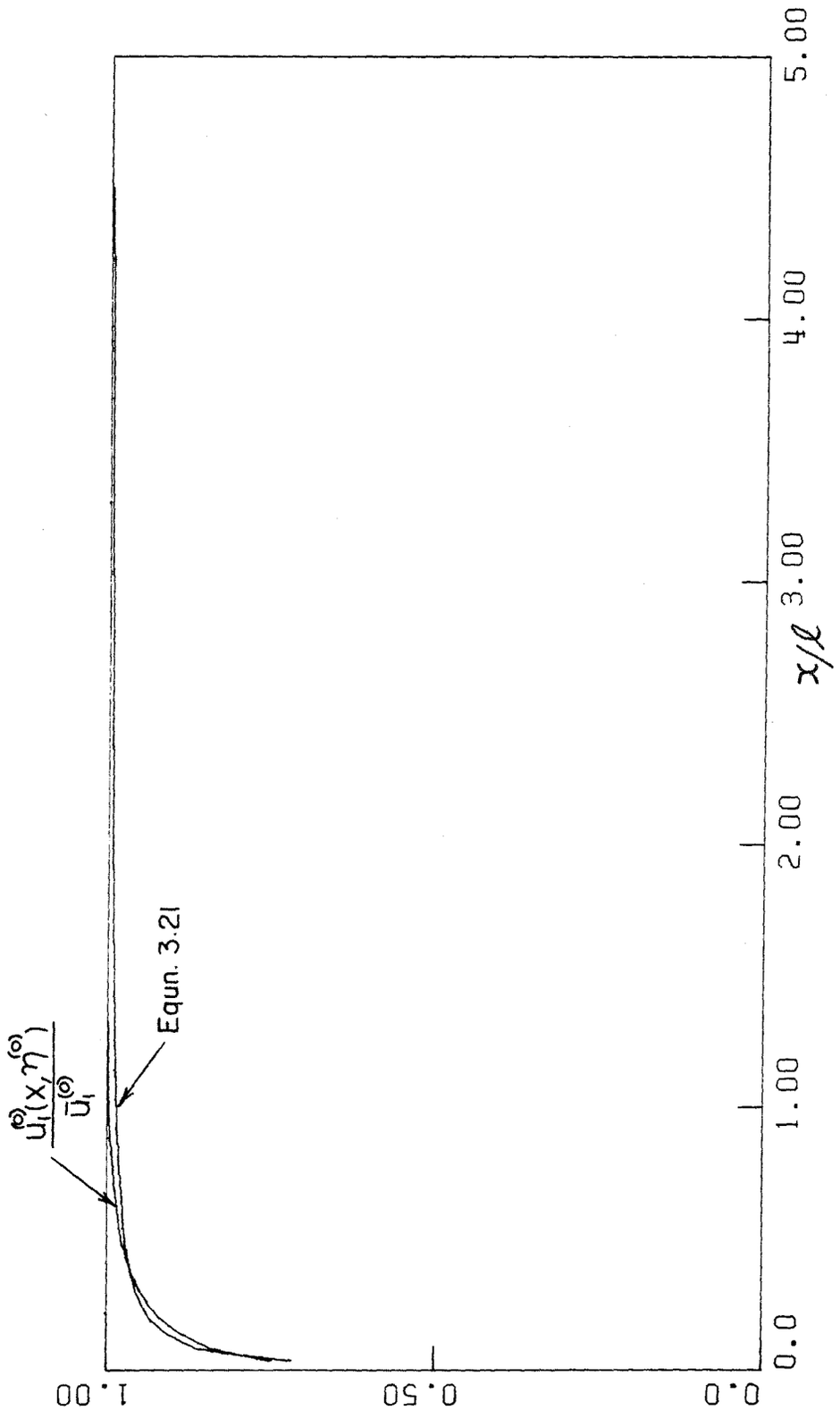

FIGURE 3.11 APPROXIMATION FOR THE UPSTREAM AXIAL VELOCITY AT THE FLAME SURFACE, $W_1/U_o=0.2$

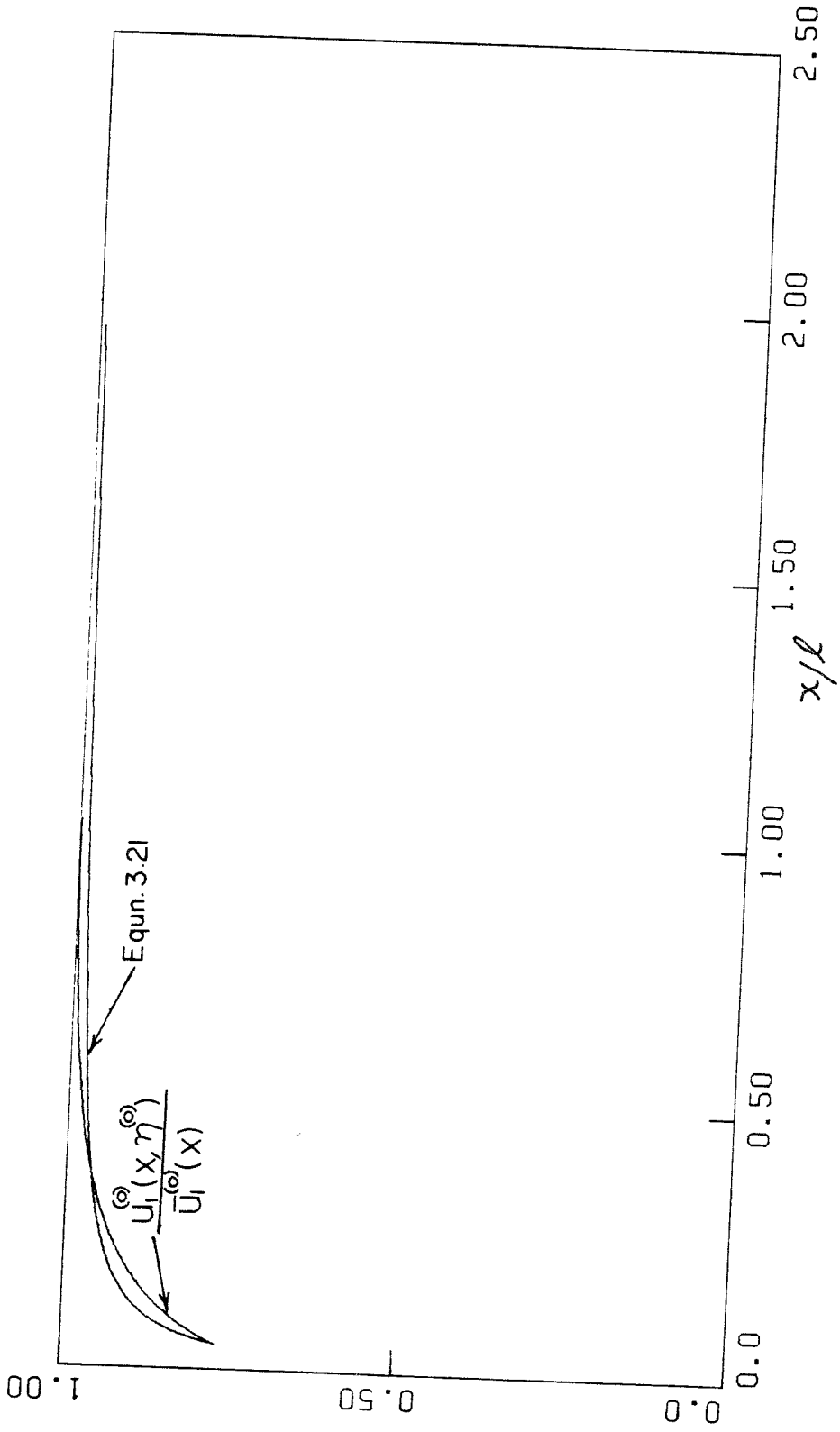

FIGURE 3.12 APPROXIMATION FOR THE UPSTREAM AXIAL VELOCITY AT THE FLAME SURFACE, $W/U_o=0.4$

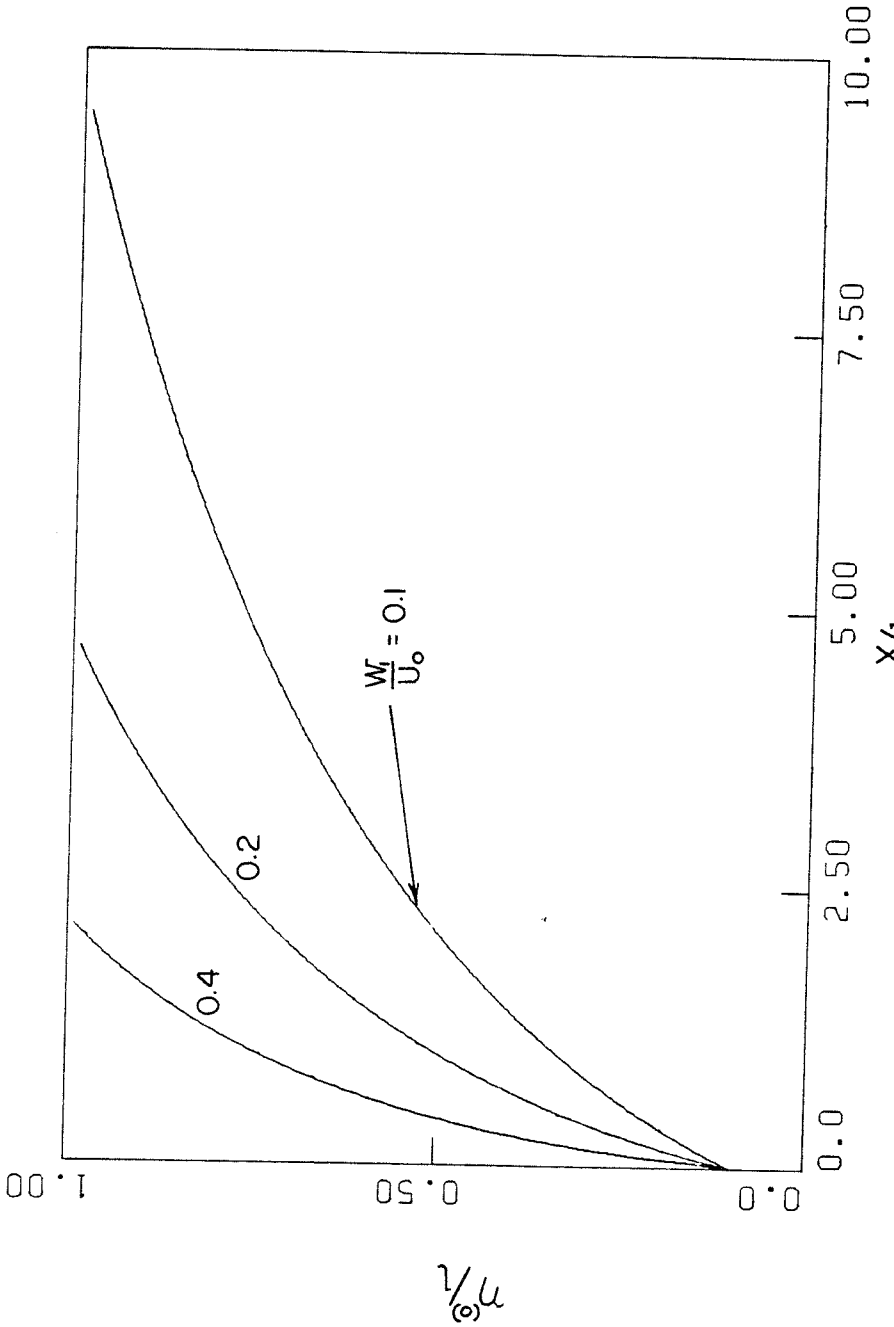

FIGURE 3.13 STEADY FLAME ENVELOPES, λ=4.5

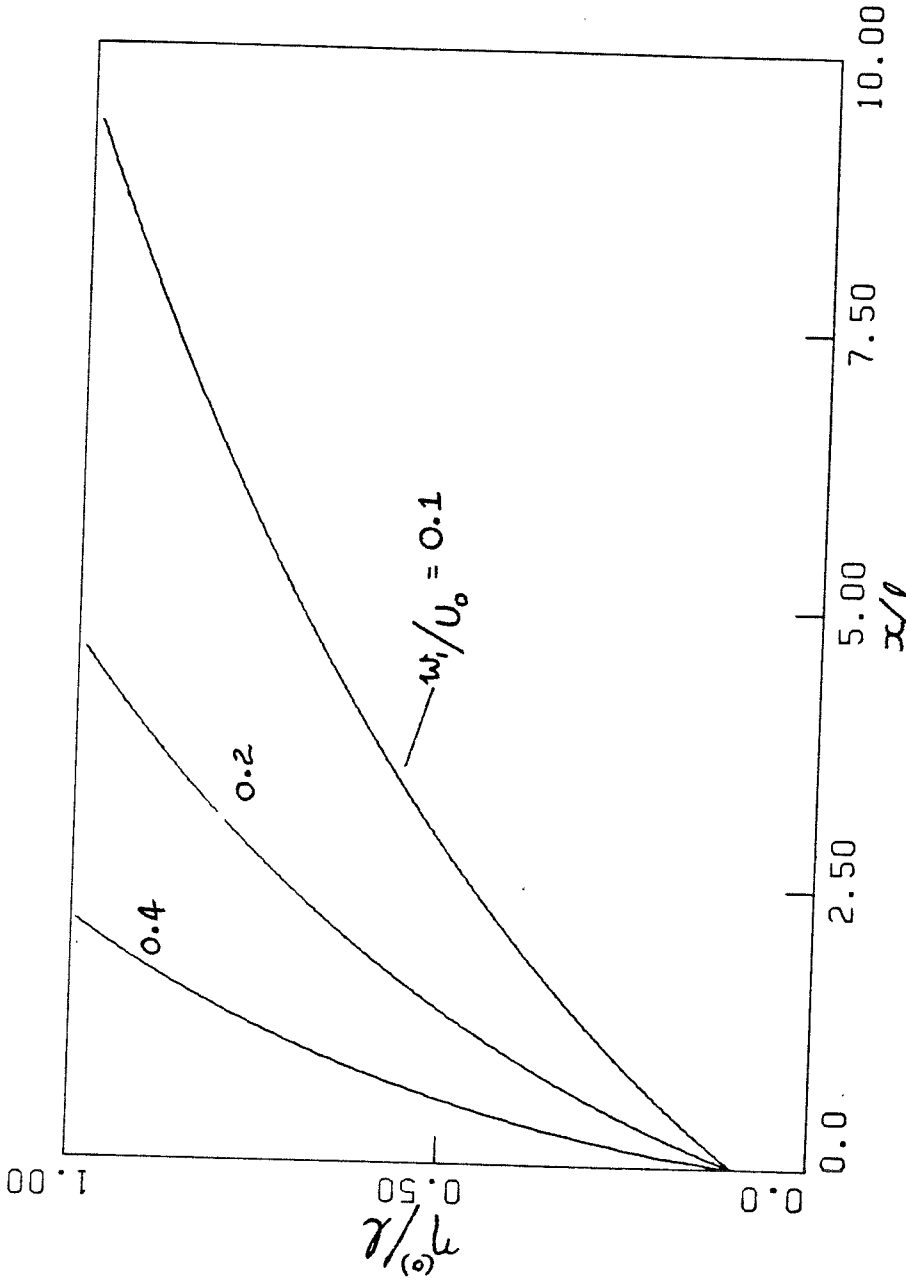

FIGURE 3.14 STEADY FLAME ENVELOPES, λ =2.25

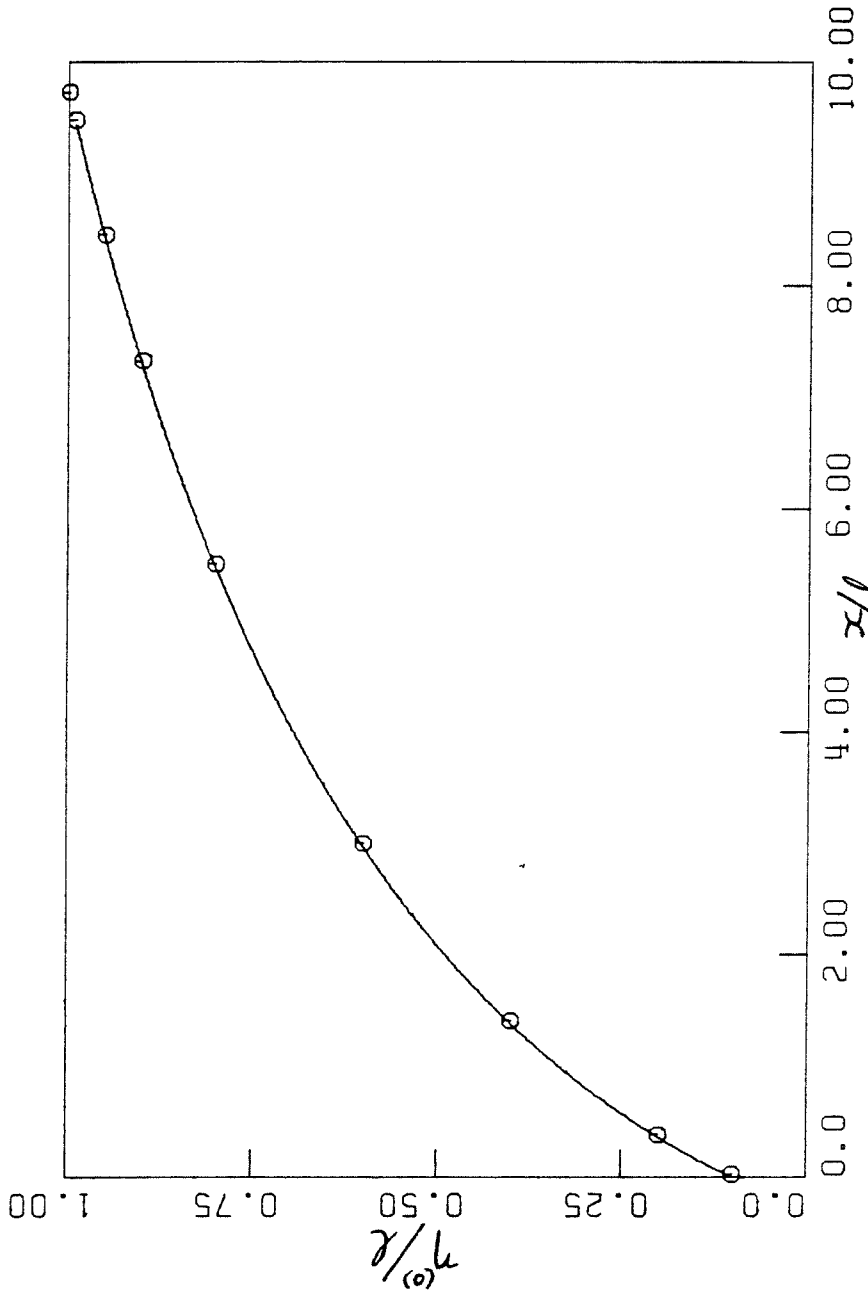

FIGURE 3.15 STEADY FLAME SHAPE, λ =4.5, ω_f/U_o=0.1
——From The Integral Relations of section 3.3
⊙ From The Approximate Analysis of section 3.1

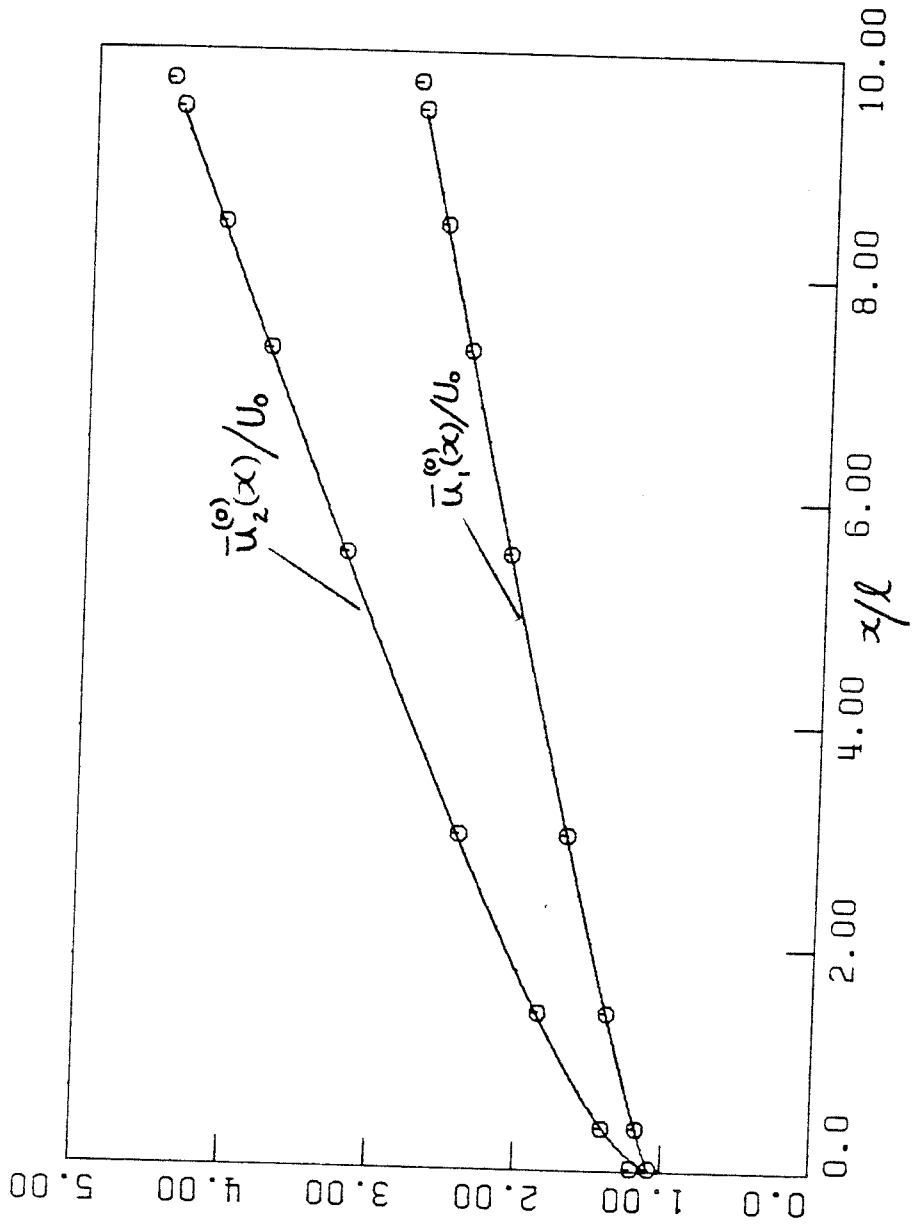

FIGURE 3.16 DISTRIBUTION OF AVERAGE AXIAL VELOCITIES, $\lambda = 4.5$, $\omega_1/U_o = 0.1$

——— From The Integral Relations of section 3.3

⊙ From The Approximate Analysis of section 3.1

4. TIME DEPENDENT FLAME CALCULATIONS

Non-steady behaviour of the flame stabilized in a two-dimensional duct is analyzed in the present chapter. Integral relations for the non-steady flow variables are studied in the first section. In the second section, the time dependent flame configuration is modelled by an unsteady source flow. By considering the flame as an unstable shear layer, a possible mechanism for the amplification of the disturbance in the flame region is discussed in the third section. The final section deals with the calculations of the transmission and reflection characteristics of the flame zone.

4.1 NON-STEADY PERTURBATION CALCULATIONS OF THE INTEGRAL RELATIONS:

The time-dependent counterpart to the steady analysis (section 3.3) of the integral relations is studied in this section. With the assumed decomposition (equations 3.22) of the dependent variables in the integral relations (2.31-2.34), we obtain the following governing equations for the non-steady variables. Only the terms linear in the perturbation quantities are retained. The axial velocity at the flame surface, $u_1(x,\eta,t)$ can be written as

$$u_1(x,\eta,t) = u_1^{(0)}(x,\eta^{(0)}) + \frac{\partial u_1^{(0)}}{\partial y}(x,\eta^{(0)})\,\eta^{(1)}(x,t) + u_1^{(1)}(x,\eta^{(0)},t) \qquad (4.1)$$

and $u_2(x,\eta,t)$ is obtained using equation 2.38 as

$$u_2(x,\eta,t) = u_1^{(0)}(x,\eta^{(0)}) + w_1(\lambda-1)\sin\vartheta^{(0)} + \frac{\partial u_1^{(0)}}{\partial y}(x,\eta^{(0)})\eta^{(1)} + u_1^{(1)}(x,\eta^{(0)},t) + w_1(\lambda-1)\cos^3\vartheta^{(0)}\frac{\partial\eta}{\partial x}^{(1)} \qquad (4.2)$$

In region 1,

Continuity equation

$$\frac{\partial\eta}{\partial t}^{(1)} + \left(\bar{u}_1^{(0)} - w_1\sin\vartheta^{(0)}\right)\frac{\partial\eta}{\partial x}^{(1)} + \frac{d\bar{u}_1^{(0)}}{dx}\eta^{(1)} + \frac{d\eta}{dx}^{(0)}\bar{u}_1^{(1)} - (1-\eta^{(0)})\frac{\partial\bar{u}_1^{(1)}}{\partial x} = 0 \qquad (4.3)$$

X-momentum equation

$$\frac{\partial\bar{u}_1^{(1)}}{\partial t} + \bar{u}_1^{(0)}\frac{\partial\bar{u}_1^{(1)}}{\partial x} + \frac{d\bar{u}_1^{(0)}}{dx}\bar{u}_1^{(1)} + \frac{1}{\rho_1}\frac{\partial\bar{p}_1^{(1)}}{\partial x} + \frac{w_1\sec\vartheta^{(0)}}{(1-\eta^{(0)})}\left[u_1^{(1)}(x,\eta^{(0)},t) + \frac{\partial u_1^{(0)}}{\partial y}(x,\eta^{(0)})\eta^{(1)} - \bar{u}_1^{(1)}\right] + \frac{w_1}{(1-\eta^{(0)})}\left[u_1^{(0)}(x,\eta^{(0)}) - \bar{u}_1^{(0)}\right] \times \left[\sin\vartheta^{(0)}\frac{\partial\eta}{\partial x}^{(1)} + \frac{1}{(1-\eta^{(0)})}\sec\vartheta^{(0)}\eta^{(1)}\right] = 0 \qquad (4.4)$$

In region 2,

Continuity equation

$$\frac{\partial \eta^{(1)}}{\partial t} + \left(\bar{u}_2^{(0)} - w_2 \sin\vartheta^{(0)}\right)\frac{\partial \eta^{(1)}}{\partial x} + \frac{d\bar{u}_2^{(0)}}{dx}\eta^{(1)} + \frac{d\eta^{(0)}}{dx}\bar{u}_2^{(1)} + \eta^{(0)}\frac{\partial \bar{u}_2^{(1)}}{\partial x} = 0 \qquad (4.5)$$

X-momentum equation

$$\frac{\partial \bar{u}_2^{(1)}}{\partial t} + \bar{u}_2^{(0)}\frac{\partial \bar{u}_2^{(1)}}{\partial x} + \frac{d\bar{u}_2^{(0)}}{dx}\bar{u}_2^{(1)} + \frac{1}{\rho_2}\frac{\partial \bar{p}_2^{(1)}}{\partial x}$$

$$+ \frac{w_2 \sec\vartheta^{(0)}}{\eta^{(0)}}\left[\bar{u}_2^{(1)} - u_1^{(1)}(x,\eta^{(0)},t) - \frac{\partial u_1^{(0)}}{\partial y}(x,\eta^{(0)})\eta^{(1)} - w_1(\lambda-1)\cos^3\vartheta^{(0)}\frac{\partial \eta^{(1)}}{\partial x}\right]$$

$$+ \frac{w_2}{\eta^{(0)}}\left[\bar{u}_2^{(0)} - u_1^{(0)}(x,\eta^{(0)}) - w_1(\lambda-1)\sin\vartheta^{(0)}\right] \times$$

$$\left[\sin\vartheta^{(0)}\frac{\partial \eta^{(1)}}{\partial x} - \frac{1}{\eta^{(0)}}\sec\vartheta^{(0)}\eta^{(1)}\right] = 0 \qquad (4.6)$$

The zeroth order solution, which describes the steady flame development, is discussed in section 3.3. It provides the steady state variables in the above system of differential equations for the perturbation quantities.

The normal momentum balance across the flame (equation 2.13) states that the pressure perturbation is continuous across the flame.

i.e. $$\bar{p}_1^{(1)}(x,t) = \bar{p}_2^{(1)}(x,t)$$

The steady axial velocity at the upstream flame edge, $u_1^{(0)}(x,\eta^{(0)})$, is approximated by equation 3.21.

In equations 4.4 and 4.6, $\frac{\partial u_1^{(0)}}{\partial x}(x,\eta^{(0)})$ is calculated as follows. For the steady irrotational, incompressible flow upstream of the flame, we have the governing equations

continuity

$$\frac{\partial u_1^{(0)}}{\partial x} + \frac{\partial v_1^{(0)}}{\partial y} = 0 \tag{4.7}$$

vorticity

$$\frac{\partial v_1^{(0)}}{\partial x} - \frac{\partial u_1^{(0)}}{\partial y} = 0 \tag{4.8}$$

kinematic condition (2.36)

$$u_1^{(0)}(x,\eta^{(0)})\frac{d\eta^{(0)}}{dx} = v_1(x,\eta^{(0)}) + w_1 \sec\vartheta^{(0)} \tag{4.9}$$

We differentiate 4.9 along the flame surface and utilize the equations 4.7 and 4.8 to obtain

$$\frac{\partial u_1^{(o)}}{\partial y}\left[1-\left(\frac{d\eta^{(o)}}{dx}\right)^2\right] = \left(u_1^{(o)} - w_1 \sin\vartheta^{(o)}\right)\frac{d^2\eta^{(o)}}{dx^2} + 2\frac{\partial u_1^{(o)}}{\partial x}\frac{d\eta^{(o)}}{dx} \tag{4.10}$$

$\frac{\partial u_1^{(o)}}{\partial y}(x,\eta^{(o)})$, in turn, is obtained from the equation 3.21.

In addition, we assume

$$u_1^{(1)}(x,\eta^{(o)},t) = \bar{u}_1^{(1)}(x,t) \tag{4.11}$$

Validity of the above approximation is verified in the next section, by generating the non-steady flame envelopes with a time-dependent source flow.

We consider the flame region to be excited by an harmonic pressure wave with wave number $\bar{K}_2$ from the downstream direction. This generates a transmitted wave of wave number $\bar{K}_1$ upstream of the flame and a reflected wave of wave number K_2^+ downstream of the flame. Let the transmitted wave upstream of the flame be represented by

$$\frac{\bar{p}_1'}{\gamma p_o} = \bar{P}_1 \exp\left[-i(\omega t + \bar{K}_1 x)\right]$$

Since there is no acoustic wave incident on the flame zone from the upstream direction, we can write the associated velocity perturbation upstream of the flame region as

$$\frac{\bar{u}_1'}{c_1} = -\bar{P}_1 \exp\left[-i(\omega t + \bar{K}_1 x)\right]$$

This gives the boundary conditions at x=0 for the pressure and velocity perturbations as

$$\frac{\bar{p}_1'}{\gamma p_0}(x=0,t) = \bar{P}_1^- e^{-i\omega t} \tag{4.12}$$

$$\frac{\bar{u}_1'}{c_1}(x=0,t) = -\bar{P}_1^- e^{-i\omega t} \tag{4.13}$$

With the assumed harmonic excitation, we consider

$$\frac{\eta^{(1)}(x,t)}{\ell} = \tilde{\eta}(x/\ell)\, e^{-i\omega t}$$

$$\frac{\bar{u}_1^{(1)}(x,t)}{U_0} = \tilde{u}_1(x/\ell)\, e^{-i\omega t}$$

$$\frac{\bar{u}_2^{(1)}}{U_0} = \tilde{u}_2(x/\ell)\, e^{-i\omega t}$$

and

$$\bar{p}^{(1)}/\rho_1 U_0^2 = \tilde{p}(x/\ell)\, e^{-i\omega t}$$

Substitution of the above equations into the governing equations (4.3-4.6) results in a system of four first order ordinary differential equations for the dependent variables $\tilde{\eta}$, $\tilde{u}_1$, $\tilde{u}_2$ and $\tilde{p}$. These are integrated numerically with the following boundary conditions at x=0.

The flame is attached to the flame holder at x=0,

$$\eta^{(1)}(x,t) = 0 \tag{4.14}$$

Velocity perturbation downstream of the flame holder is zero,

$$\bar{u}_2^{(1)}(0,t) = 0 \tag{4.15}$$

It should, however, be noted that in the present integral formulation, the flame development adjacent to the flame holder is not represented accurately. Detailed calculations near the flame holder should take into account the viscous and heat conduction effects. Present calculations indicated that the flame response is rather insensitive to the choice of $\bar{u}_2^{(1)}(0,t)$, suggesting that the behaviour of the non-steady wake downstream of the flame holder may not be of dominant influence on the non-steady flame development.

4.1.1 RESULTS AND DISCUSSION: As can be seen from section 3.1, the principal parameters that affect the steady flame development are the upstream translational speed U_0, duct width 2ℓ, flame speed w_1/U_0 and the density ratio across the flame, $\lambda = \rho_1/\rho_2 = T_2/T_1$. For the non-steady response of the flame region, in addition, the radian frequency ω of the disturbance is an important parameter. We utilize the reduced frequency $\Omega = \omega\ell/U_0$ to evaluate the burner response.

In equations 4.12 and 4.13, let $\bar{P}_1 = M_0^2$, where $M_0 = U_0/C_1$ is the approach Mach number. This gives at x=0,

$$\tilde{p}(0) = 1 \tag{4.16}$$

and

$$\tilde{u}_1(0) = -M_0 \tag{4.17}$$

A flame speed of $w_1/U_o = 0.1$, density ratio $\lambda = 4.5$, approach Mach number $M_o = 0.2$ and reduced frequency $\omega\ell/U_o = 4.85$ are chosen to describe the burner operation for the results presented here.

Figure 4.1 shows the non-steady flame envelope for the above operating conditions of the burner. The flame envelopes are shown for three different time intervals given by $\omega t = 0$, $\pi/4$ and $\pi/2$. The velocity perturbations, $\tilde{u}_1(x/\ell)$ and $\tilde{u}_2(x/\ell)$, are shown in figures 4.2 and 4.3. The flame perturbation exhibits a travelling wave pattern with considerable amplification in the downstream direction. This has to be differentiated from the classical Landau instability of plane flames, wherein the flame perturbation is stationary, with no associated phase speed.

For the present case of the confined stabilized flame, there is vorticity production by the steady flame due to the curvature of the flame. A possible mechanism to explain the calculated growth of the disturbance in the flame region is the amplification of the shed vorticity, behaving as an unstable shear layer. This aspect is explored in some detail in section 4.3. In the case of plane flames, there is no vorticity production by the steady flame.

The development of the pressure perturbation $\tilde{p}(x/\ell)$ is shown in figure 4.4. The velocity and pressure perturbations enable us to obtain the acoustic transmission and reflection properties of the compact flame region, as will be shown in section 4.4.

4.2 SOURCE FLOW MODELLING FOR THE NON-STEADY FLAME:

We generate a non-steady flame shape similar to the one calculated in the previous section, by a suitable time dependent source distribution on the duct axis. The primary need for such a modelling is to verify the approximation (4.11) on the axial velocity perturbation at the flame edge. The method of simulation of the non-steady flame envelopes is similar to the exact representation of the steady flow upstream of the flame, discussed in section 3.2.

We have the kinematic condition (2.36) for the compatible deformation of the upstream flow and the flame surface,

$$\frac{\partial \eta}{\partial t} + u_1(x,\eta,t)\,\frac{\partial \eta}{\partial x} = v_1(x,\eta,t) + w_1\left[1+\left(\frac{\partial \eta}{\partial x}\right)^2\right]^{1/2} \qquad (4.18)$$

The dependent variables are decomposed as in equations (3.22),

$$u_1(x,y,t) = u_1^{(0)}(x,y) + u_1^{(1)}(x,y,t) \qquad (4.19)$$

etc.

where

$$\left|\frac{u_1^{(1)}}{u_1^{(0)}}\right| << 1$$

Substituting equations (4.19) into (4.18) and retaining only the first order terms in the perturbation quantities, we obtain the following differential equation for the non-steady flame shape.

$$\frac{\partial \eta^{(1)}}{\partial t} + u_1^{(o)}(x,\eta^{(o)})\frac{\partial \eta^{(1)}}{\partial x} + \frac{\partial u_1^{(o)}}{\partial y}(x,\eta^{(o)})\frac{d\eta^{(o)}}{dx}\eta^{(1)}$$
$$+ u_1^{(1)}(x,\eta^{(o)},t)\frac{d\eta^{(o)}}{dx} = V_1^{(1)}(x,\eta^{(o)},t) + \frac{\partial V_1^{(o)}}{\partial y}(x,\eta^{(o)})\eta^{(1)}$$
$$+ w_1 \sin\vartheta^{(o)}\frac{\partial \eta^{(1)}}{\partial x} \qquad (4.20)$$

The steady field is represented by an uniform source distribution on the duct axis, extending over the flame region (section 3.2). To generate the non-steady flame envelopes, we utilize a source distribution on the duct axis with the perturbation velocities upstream of the flame in the form,

$$\frac{u_1^{(1)}}{U_o}(x,y,t) = \int_o^{L/\ell} \alpha'_{\xi/L} \exp\left(-i\omega\left[t - \frac{\xi}{U_o(A_1 + A_2\,\xi/L)}\right]\right) \times$$
$$\left\{R\left(\coth\left[\frac{\pi(z-\xi)}{2\ell}\right]\right)+1\right\} d(\xi/\ell)$$
$$+ (\beta' + i\beta')e^{-i\omega t}\left\{\frac{2}{\pi}\frac{\ell}{L}R\left(\mathrm{Log_e}\left[\frac{\sinh \pi z/2\ell}{\sinh \frac{\pi(z-L)}{2\ell}}\right]\right)+1\right\}$$
$$- M_o e^{-i\omega t} \qquad (4.21)$$

$$-\frac{V_1^{(1)}}{U_o}(x,y,t) = \int_0^{L/\ell} \alpha'\,\xi/L \exp\left(-i\omega\left[t - \frac{\xi}{U_o(A_1 + A_2\,\xi/L)}\right]\right) \times$$

$$\mathcal{I}_m\left(\coth\left[\frac{\pi(z-\xi)}{2\ell}\right]\right) d(\xi/\ell)$$

$$+ (\beta' + i\beta')\, e^{-i\omega t}\, \frac{2}{\pi}\, \frac{\ell}{L}\, \mathcal{I}_m\left(\mathrm{Log}_e\left[\frac{\sinh \pi z/2\ell}{\sinh \frac{\pi(z-L)}{2\ell}}\right]\right) \qquad (4.22)$$

In the above perturbation velocities, the first term is due to a distribution of fluctuating sources with the source strength and phase varying with the distance from the flame holder. The second term is due to an uniform distribution of sources fluctuating in phase. In equation (4.21), an axial velocity $-M_o e^{-i\omega t}$ is also added to have the same velocity perturbation at the flame holder as in the numerical calculations discussed earlier.

The steady flow variables, $\eta^{(o)}(x)$, $u_1^{(o)}(x,y)$ and $u_2^{(o)}(x,y)$ are given by the results of section 3.2. As in the previous section, let

$$\frac{\eta^{(1)}(x,t)}{\ell} = \tilde{\eta}(x)\, e^{-i\omega t} \qquad (4.23)$$

$$\frac{u_1^{(1)}}{U_o}(x,y,t) = \tilde{U}_1(x,y)\, e^{-i\omega t} \qquad (4.24)$$

$$\frac{V_1^{(1)}}{U_o}(x,y,t) = \tilde{V}_1(x,y)\, e^{-i\omega t} \tag{4.25}$$

4.2.1 RESULTS AND DISCUSSION: Equation 4.20 is integrated numerically with the initial condition $\eta^{(1)}(x,t) = 0$ at $x = x_o$ to obtain the non-steady flame envelope. Calculations for the burner operating conditions as given in the previous section are presented here. The reduced frequency of the disturbance is again chosen as $\omega l/U_o = 4.85$. $\alpha' = 0.5$, $\beta' = 0.2$, $A_1 = 1.0$ and $A_2 = 1.0$ in the expressions for the source distributions (equations 4.21 and 4.22) yield the non-steady flame envelope (Fig. 4.5). The associated velocity perturbations at the flame edge, $\tilde{U}_1(x,\eta^{(o)})$ and $\tilde{V}_1(x,\eta^{(o)})$ are shown in figures 4.6 and 4.7.

Using the above flow field upstream of the flame, we calculate the avearage axial velocity,

$$\frac{\bar{U}_1}{U_o}(x,t) = \frac{\bar{U}_1^{(o)}}{U_o}(x) + \tilde{u}_1(x)\, e^{-i\omega t}$$

$$= \frac{1}{[l-\eta(x,t)]} \int_{\eta(x,t)}^{l} \frac{u_1(x,y,t)}{U_o}\, dy \tag{4.26}$$

Figures 4.8 and 4.9 compare $\tilde{u}_1(x)$ with the axial velocity perturbation at the steady flame surface, $\tilde{U}_1(x,\eta^{(o)})$. The comparison suggests that equation 4.11 is a valid approximation.

4.3 MODELLING OF THE NON-STEADY FLAME AS AN UNSTABLE SHEAR LAYER:

In this section, we explore a possible mechanism to explain the non-steady behaviour of the stabilized flame, by studying the stability of a fluid interface. The technique is classical and is similar to that of Blackshear[1] (1956), but explicitly considers the spatial development of the disturbance in the flame region. In the steady state, the interface coincides with the x-axis, separating region 1 with density ρ_1 and uniform velocity U_1 and region 2 with density ρ_2 and a linear velocity profile, as shown in figure 4.10. Let ℓ_1 and ℓ_2 be the distances of the interface from the top wall and centerline of the channel respectively. The steady velocity profile in region 2 is written as

$$U_2(y) = a - \frac{(b-a)}{\ell_2}\, y \qquad (4.27)$$

where a and b are constants to be chosen.

This gives the average velocity in region 2, $\bar{U}_2 = (a+b)/2$. Let $\eta^{(1)}(x,t)$ be the perturbed interface with the associated velocity perturbations as $U_1^{(1)}(x,y,t)$ and $V_1^{(1)}(x,y,t)$ in region 1 and $U_2^{(1)}(x,y,t)$ and $V_2^{(1)}(x,y,t)$ in region 2.

For an inviscid, incompressible flow with conservative body forces, Helmholtz equation takes the form

$$\frac{\partial \underset{\sim}{\Sigma}}{\partial t} + (\underset{\sim}{u}\cdot\nabla)\underset{\sim}{\Sigma} = (\underset{\sim}{\Sigma}\cdot\nabla)\underset{\sim}{u} \qquad (4.28)$$

where $\underset{\sim}{\Sigma} = \nabla \wedge \underset{\sim}{u}$ is the vorticity.

For plane flows, $(\underset{\sim}{\zeta}.\nabla)\underset{\sim}{u} = 0$

Region 1 is irrotational and in region 2, $\underset{\sim}{\zeta} = \zeta_2 \underset{\sim}{e}_z$, where

$$\zeta_2 = \zeta_2^{(0)} + \zeta_2^{(1)}$$

$$= \left(\frac{b-a}{l_2}\right) + \left(\frac{\partial v_2^{(1)}}{\partial x} - \frac{\partial u_2^{(1)}}{\partial y}\right) \qquad (4.29)$$

Since the steady vorticity $\zeta_2^{(0)}$ is constant, we get from equation 4.28,

$$\frac{\partial \zeta_2^{(1)}}{\partial t} + (\underset{\sim}{u}\cdot\nabla)\,\zeta_2^{(1)} = 0 \qquad (4.30)$$

The above equation guarantees that there is no transfer of vorticity from the mean flow to the disturbance flow field. Hence, we can represent the perturbation field in region 2 by a scalar potential $\varphi_2(x,y,t)$. Let $\varphi_1(x,y,t)$ be the velocity potential in region 1. Then, the formulation to study the stability of the interface can be written as follows.

Region 1,

$$\underset{\sim}{u}_1(x,y,t) = U_1 \underset{\sim}{e}_x + \nabla \varphi_1 \qquad (4.31)$$

$$\nabla^2 \varphi_1 = 0 \qquad (4.32)$$

Normal velocity is zero at the solid wall, $y = \ell_1$,

$$\frac{\partial \varphi_1}{\partial y}(x, \ell_1, t) = 0 \tag{4.33}$$

Kinematic condition at the interface, valid at $y = \eta(x,t)$, can be written as

$$\frac{\partial \eta^{(1)}}{\partial t} + \left(U_1 + \frac{\partial \varphi_1}{\partial x}\right)\frac{\partial \eta^{(1)}}{\partial x} = \frac{\partial \varphi_1}{\partial y} \tag{4.34}$$

which on linearization becomes (on $y = 0$)

$$\frac{\partial \eta^{(1)}}{\partial t} + U_1 \frac{\partial \eta^{(1)}}{\partial x} = \frac{\partial \varphi_1}{\partial y} \tag{4.35}$$

Similarly in region 2,

$$u_2(x,y,t) = a - \zeta_2^{(0)} y + \frac{\partial \varphi_2}{\partial x} \tag{4.36}$$

$$v_2(x,y,t) = \frac{\partial \varphi_2}{\partial y} \tag{4.37}$$

$$\nabla^2 \varphi_2 = 0 \tag{4.38}$$

$$\frac{\partial \varphi_2}{\partial y}(x, -\ell_2, t) = 0 \tag{4.39}$$

Linearized kinematic condition at y=0

$$\frac{\partial \eta^{(1)}}{\partial t} + a \frac{\partial \eta^{(1)}}{\partial x} = \frac{\partial \varphi_2}{\partial y} \tag{4.40}$$

Next we match the pressure gradient along the interface,

$$\left.\frac{\partial p}{\partial x}\right)_{y=\eta} + \left.\frac{\partial p}{\partial y}\right)_{y=\eta} \times \frac{\partial \eta^{(1)}}{\partial x}$$

on either side of the interface. With the present linearization, this becomes (on y=0)

$$\frac{\partial p_1}{\partial x} = \frac{\partial p_2}{\partial x} \tag{4.41}$$

From the axial momentum equations,

$$-\frac{\partial p_i}{\partial x} = \rho_i \left(\frac{\partial u_i}{\partial t} + u_i \frac{\partial u_i}{\partial x} + v_i \frac{\partial u_i}{\partial y} \right) \tag{4.42}$$

$$i = 1,2$$

Using the above representation for the flow field in regions 1 and 2, we can write equation 4.41 as

$$\rho_1 \left(\frac{\partial^2 \varphi_1}{\partial t \partial x} + U_1 \frac{\partial^2 \varphi_1}{\partial x^2} \right)$$

$$= \rho_2 \left(\frac{\partial^2 \varphi_2}{\partial t \partial x} + a \frac{\partial^2 \varphi_2}{\partial x^2} - \zeta_2^{(0)} \frac{\partial \varphi_2}{\partial y} \right) \tag{4.43}$$

In the above equation, only the first order terms in the perturbation quantities are retained.

4.3.1 RESULTS AND DISCUSSION: We assume the perturbation of the interface to be in the form,

$$\eta^{(1)}(x,t) = \mathcal{D} \exp\left[i\,(\omega t - Kx)\right] \tag{4.44}$$

where ω is the radian frequency and K is the wave number. We consider ω as real and K is, in general, complex quantity. We consider solutions for $\varphi_1(x,y,t)$ and $\varphi_2(x,y,t)$ in the form,

$$\varphi_1(x,y,t) = A_1 \exp\left[i\,(\omega t - Kx)\right] \frac{\cosh K(y-\ell_1)}{\sinh K\ell_1} \tag{4.45}$$

$$\varphi_2(x,y,t) = A_2 \exp\left[i\,(\omega t - Kx)\right] \frac{\cosh K(y+\ell_2)}{\sinh K\ell_2} \tag{4.46}$$

Clearly, φ_1 and φ_2 as given above, satisfy the Laplace equation and the boundary conditions 4.33 and 4.39. Substituting the above equations for $\eta^{(1)}$, φ_1 and φ_2 into the remaining boundary conditions, we obtain

from equation 4.35

$$i\mathcal{D}\,(\omega - U_1 K) = -A_1 K \tag{4.47}$$

from equation 4.40

$$i\mathcal{D}\,(\omega - aK) = A_2 K \tag{4.48}$$

equation 4.43 gives

$$\begin{aligned}\rho_1 A_1 \coth(Kl_1)\left(\omega K - U_1 K^2\right) \\ = \rho_2 A_2 \coth(Kl_2)\left(\omega K - aK^2\right) \\ - A_2 \rho_2 \zeta_2^{(0)} K\end{aligned} \tag{4.49}$$

For the non-trivial solution of the above system of linear, homogeneous, simultaneous equations, the determinant of the coefficient matrix has to identically vanish. This gives

$$\begin{vmatrix} 1 & 0 & (\omega - U_1 K) \\ 0 & -1 & (\omega - aK) \\ \rho_1(\omega - U_1 K)\coth(Kl_1) & -\rho_2(\omega - aK)\coth(Kl_2) + \rho_2 \zeta_2^{(0)} & 0 \end{vmatrix} = 0 \tag{4.50}$$

If we assume compactness of regions 1 and 2 with respect to the wave length of the disturbance, and thus approximate equation 4.50, for $|Kl_1| \ll 1$ and $|Kl_2| \ll 1$, we obtain

$$\rho_1 (\omega - U_1 K)^2 \ell_2 + \rho_2 (\omega - aK)^2 \ell_2$$

$$- \rho_2 (b-a)(\omega - aK) \ell_1 K = 0 \qquad (4.51)$$

The solution of the above equation is used as an initial guess to solve equation 4.50 by successive approximation and obtain

$$K = \frac{\omega}{\sigma} + i \Delta \qquad (4.52)$$

where σ is the phase speed and Δ is the growth rate of the disturbance.

At this stage, we postulate that the above analysis provides a local representation of the non-steady flame development. We consider two separate cases for comparing the above results with those of section 4.1. In the first case, the vorticity in region 2 is considered as localized near the flame, and accordingly we take $U_1 = \bar{u}_1^{(o)}$ and $a = b = \bar{u}_2^{(o)}$. The steady flow variables, $\bar{u}_1^{(o)}$, $\bar{u}_2^{(o)}$, $\ell_2 = \eta^{(o)}$ and $\ell_1 = (\ell - \eta^{(o)})$ are obtained from the results of section 3.3 for a flame speed, $w_1/U_o = 0.1$. Figure 4.11 compares the local phase speed obtained from equation 4.50 with that calculated from the integral relations. The agreement is very good away from the flame holder.

Analysis of section 4.1 for $w_1/U_o = 0.1$, $\lambda = 4.5$, $M_o = 0.2$ and $\omega \ell / U_o = 4.85$ gives the amplitude of the non-steady flame envelope as shown in figure 4.12. This has to be compared with figure 4.13, calculated from the growth rate Δ obtained from equation 4.50.

In the second case, we consider the case of constant vorticity at any cross section in region 2. From equation 2.38, for the steady flow

$$u_2^{(o)}(x,\eta^{(o)}) = u_1^{(o)}(x,\eta^{(o)}) + w_1(\lambda-1)\sin\vartheta^{(o)} \tag{4.53}$$

Accordingly we consider, $a = u_2^{(o)}(x,\eta^{(o)})$ and $b = 2\bar{u}_2^{(o)} - a$. This flow configuration yields a neutrally stable interface and does not explain the growth rates calculated in section 4.1. This case can be interpreted as the case of symmetric disturbance in the analysis of Blackshear.

4.3.2 VORTICITY PRODUCTION BY THE FLAME: To further examine the assumption of concentrated vorticity near the flame surface, we calculate the vorticity produced by the flame using the exact solution of section 3.2 for the upstream flow.

For the steady flame development, we can write the matching conditions at the flame surface, $y = \eta^{(o)}(x)$, as

$$u_1^{(o)}(x,\eta^{(o)})\frac{d\eta}{dx}^{(o)} = v_1^{(o)}(x,\eta^{(o)}) + w_1 \sec\vartheta^{(o)} \tag{4.54}$$

$$u_2^{(o)}(x,\eta^{(o)})\frac{d\eta}{dx}^{(o)} = v_2^{(o)}(x,\eta^{(o)}) + w_2 \sec\vartheta^{(o)} \tag{4.55}$$

$$P_1^{(o)}(x) - P_2^{(o)}(x) = \rho_1(\lambda-1)\, w_1^2 \tag{4.56}$$

and

$$u_1^{(o)}(x,\eta^{(o)}) + v_1^{(o)}(x,\eta^{(o)})\frac{d\eta}{dx}^{(o)} = u_2^{(o)}(x,\eta^{(o)}) + v_2^{(o)}(x,\eta^{(o)})\frac{d\eta}{dx}^{(o)} \tag{4.57}$$

Differentiating equation 4.56 along the flame surface, we get

$$\frac{\partial p_1}{\partial x} + \frac{\partial p_1}{\partial y}\frac{d\eta}{dx}^{(o)} = \frac{\partial p_2}{\partial x} + \frac{\partial p_2}{\partial y}\frac{d\eta}{dx}^{(o)} \qquad y = \eta^{(o)}(x) \tag{4.58}$$

From the momentum equations in region 2, we can write defining

$$\frac{d^*}{dx} \equiv \left(\frac{\partial}{\partial x} + \frac{d\eta}{dx}^{(o)}\frac{\partial}{\partial y}\right)_{y=\eta^{(o)}(x)},$$

$$\frac{d^* p_2}{dx} = -\rho_2\zeta_2^{(o)}\left(u_2^{(o)}\frac{d\eta}{dx}^{(o)} - v_2^{(o)}\right) - \rho_2\frac{d^*}{dx}\left[\frac{(u_2^{(o)})^2 + (v_2^{(o)})^2}{2}\right] \tag{4.59}$$

where

$$\zeta_2^{(o)}(x,\eta^{(o)}(x)) = \left(\frac{\partial v_2}{\partial x}^{(o)} - \frac{\partial u_2}{\partial y}^{(o)}\right)_{y=\eta^{(o)}(x)}$$

is the vorticity produced by the steady flame.

Similarly, utilizing the momentum equations in region 1 and noting that the flow field upstream of the flame is irrotational, we obtain from equation 4.58

$$-\rho_1 \frac{d^*}{dx}\left[\frac{(u_1^{(o)})^2+(v_1^{(o)})^2}{2}\right] = -\rho_2 \zeta_2^{(o)}\left(u_2^{(o)}\frac{d\eta^{(o)}}{dx} - v_2^{(o)}\right) - \rho_2 \frac{d^*}{dx}\left[\frac{(u_2^{(o)})^2+(v_2^{(o)})^2}{2}\right] \tag{4.60}$$

From equations 4.54, 4.55 and 4.57, we get

$$u_2^{(o)}(x,\eta^{(o)}) = u_1^{(o)}(x,\eta^{(o)}) + w_1(\lambda-1)\sin\vartheta^{(o)} \tag{4.61}$$

$$v_2^{(o)}(x,\eta^{(o)}) = u_1^{(o)}\frac{d\eta^{(o)}}{dx} - w_1 \sin\vartheta^{(o)}\frac{d\eta^{(o)}}{dx} - w_2 \cos\vartheta^{(o)} \tag{4.62}$$

Substituting these values into equation 4.60, we can express the vorticity produced by the flame, $\zeta_2^{(o)}(x,\eta^{(o)})$ as

$$\zeta_2^{(o)}(x,\eta^{(o)}) = \frac{-1}{2w_2 \sec\vartheta^{(o)}}\frac{d^*}{dx}\left[\left(u_1^{(o)} + v_1^{(o)}\frac{d\eta^{(o)}}{dx}\right)^2 \cos^2\vartheta^{(o)} - \lambda\left[(u_1^{(o)})^2 + (v_1^{(o)})^2\right]\right] \tag{4.63}$$

The above equation relates the vorticity generated by the flame with the flow field upstream of the flame alone. The upstream flow field is known exactly from the representation of section 3.2. For plane flames, $\frac{d\eta^{(o)}}{dx}$ = constant, $v_1^{(o)}=0$ and $u_1^{(o)} = w_1 \operatorname{Cosec}\vartheta^{(o)}$, and from equation 4.63 we notice that there is no voriticity produced by the steady plane

flame.

Figure 4.14 shows the distribution of the vorticity produced by the stabilized flame, $\zeta_2^{(o)}(x, \eta^{(o)})$ for a flame speed of $w_1/U_o = 0.1$ and density ratio of 4.5. The total voritcity, ζ_T in region 2 is obtained as

$$\zeta_T = \int_0^L \int_0^{\eta^{(o)}(x)} \zeta_2^{(o)} \, dy \, dx \tag{4.64}$$

and gives a value of 12.8 $U_o \ell$ for the 0.1 flame speed and 2.9 $U_o \ell$ for the 0.4 flame speed. We compare these values with the circulations

$$\Gamma_T = \int_0^L \left[\bar{u}_2^{(o)}(x) - \bar{u}_1^{(o)}(x) \right] dx \tag{4.65}$$

(9.2 $U_o \ell$ for $w_1/U_o = 0.1$ and 2.3 $U_o \ell$ for $w_1/U_o = 0.4$) around the flame surface, with the velocities $\bar{u}_1^{(o)}(x)$ and $\bar{u}_2^{(o)}(x)$ on either side. This implies that the bulk of the vorticity produced by the flame is concentrated near the flame surface in region 2.

4.4 TRANSMISSION AND REFLECTION CHARACTERISTICS OF THE STABILIZED FLAME

The velocity and pressure perturbations in the flame region, as calculated in section 4.1, enable us to determine the acoustic transmission and reflection coefficients of the burner. These, in a practical combustion system like the aircraft afterburner or the utility boiler, couple the non-steady flame response with the acoustics of the combustion chamber. A typical application to an afterburner is discussed in the next chapter.

We consider two different cases for the calculation of the reflection and transmission coefficients of the flame region. In the first case, an acoustic input

$$\bar{P}_2 \exp\left[-i\left(\omega t + \bar{k}_2(x-L)\right)\right]$$

is incident on the flame region from downstream, giving rise to a reflected wave

$$P_2^+ \exp\left[-i\left(\omega t - k_2^+(x-L)\right)\right]$$

downstream of the flame and a transmitted wave

$$\bar{P}_1 \exp\left[-i\left(\omega t + \bar{k}_1 x\right)\right]$$

upstream of the flame region. k_1^-, k_1^+ and k_2^-, k_2^+ are the wave numbers upstream and downstream of the flame zone respectively. Thus, with acoustic input from downstream, we have at the downstream edge of the flame (i.e. x=L),

$$\frac{\bar{P}_2^{(1)}}{\gamma P_0} = \left(P_2^+ + \bar{P}_2\right) e^{-i\omega t} \qquad (4.66)$$

$$\frac{\bar{u}_2^{(1)}}{c_2} = \left(P_2^+ - P_2^-\right) e^{-i\omega t} \tag{4.67}$$

Equations 4.66 and 4.67 give

$$P_2^+ e^{-i\omega t} = \frac{1}{2}\left[\frac{\bar{P}_2^{(1)}}{\gamma P_0} + \frac{\bar{u}_2^{(1)}}{c_2}\right]_{x=L} \tag{4.68}$$

$$P_2^- e^{-i\omega t} = \frac{1}{2}\left[\frac{\bar{P}_2^{(1)}}{\gamma P_0} - \frac{\bar{u}_2^{(1)}}{c_2}\right]_{x=L} \tag{4.69}$$

Similarly at the upstream edge of the flame,

$$\left.\frac{\bar{P}_1^{(1)}}{\gamma P_0}\right|_{x=0} = -\left.\frac{\bar{u}_1^{(1)}}{c_1}\right|_{x=0} = P_1^- e^{-i\omega t} \tag{4.70}$$

The transmission and reflection coefficients, R_1 and T_1 can then be written as $T_1 = \bar{P}_1^- / P_2^-$ and $R_1 = P_2^+ / P_2^-$. The method of calculation is to prescribe P_1^- and integrate the perturbation equations with the prescribed conditions at x=0, as shown in section 4.1.

For the second case, let the flame region be excited by

$$P_1^+ \exp\left[-i\left(\omega t - k_1^+ x\right)\right]$$

from upstream. This gives rise to a reflected wave

$$\bar{P}_1^- \exp\left[-i\left(\omega t + k_1^- x\right)\right]$$

upstream and a transmitted wave downstream of the flame region. Similar to case 1 above, we can write

$$P_1^+ e^{-i\omega t} = \frac{1}{2}\left[\frac{\bar{P}_1^{(1)}}{\gamma P_0} + \frac{\bar{u}_1^{(1)}}{c_1}\right]_{x=0} \tag{4.71}$$

$$P_1^- e^{-i\omega t} = \frac{1}{2}\left[\frac{\bar{P}_1^{(1)}}{\gamma P_0} - \frac{\bar{u}_1^{(1)}}{c_1}\right]_{x=0} \tag{4.72}$$

and

$$P_2^+ e^{-i\omega t} = \left.\frac{\bar{u}_2^{(1)}}{c_2}\right|_{x=L} \tag{4.73}$$

The transmission and reflection coefficients are $T_2 = P_2^+ / P_1^+$ and $R_2 = P_1^- / P_1^+$. But, in this case the pressure and velocity perturbations cannot be specified a priori at x=0. Instead, we calculate a special case wherein, $P_1^+ = 1$ and $P_1^- = 0$ and obtain

$$P_{2*}^+ e^{-i\omega t} = \frac{1}{2}\left[\frac{\bar{P}_2^{(1)}}{\gamma P_0} + \frac{\bar{u}_2^{(1)}}{c_2}\right]_{x=L} \tag{4.74}$$

$$P_{2*}^- e^{-i\omega t} = \frac{1}{2}\left[\frac{\bar{P}_2^{(1)}}{\gamma P_0} - \frac{\bar{u}_2^{(1)}}{c_2}\right]_{x=L} \tag{4.75}$$

This solution is combined with the results of case 1 to obtain the transmission and reflection coefficients for case 2 as

$$T_2 = P_{2*}^{+} - R_1 P_{2*}^{-} \tag{4.76}$$

and

$$R_2 = -T_1 P_{2*}^{-} \tag{4.77}$$

where R_1 and T_1 are the reflection and transmission coefficients as obtained in the first case.

4.4.1 RESULTS AND DISCUSSION: Calculations for a flame speed ω_1/U_o=0.1, density ratio λ=4.5 and approach Mach number M_o=0.2 are presented here. Figure 4.15 shows the magnitude $|T_1|$ and phase Φ_1 of the transmision coefficient of the flame region, when excited by an acoustic input from downstream. Considerable amplification in the transmitted wave is observed at certain discrete frequencies. The corresponding reflection coefficient, $R_1 = |R_1| e^{i\Psi_1}$ is shown in figure 4.16. It should be noted that considerable acoustic energy can be added to the system by the active flame and the transmission and reflection of the flame region should not be interpreted in the conventional way. Since in the present case, there is no wave incident on the flame region from upstream, the transmission coefficient is a measure of the upstream velocity fluctuation at x=0, and suggests that the non-steady response of the flame region peaks with the fluid injection by the flame region. The transmission and reflection coefficients, T_2 and R_2, when the flame region is excited by acoustic disturbance from upstream (case 2) are shown in figures 4.17 and 4.18.

The calculations are done for a range of flame speeds and density ratios. The amplification by the flame region decreases with the reduction in the density ratio, λ. Calculations for lower flame speeds give rise to peaks at correspondingly reduced frequencies, with no appreciable change in the amplification. From the analysis of section 3.1, we recognize that the steady flame shapes exhibit a similarity representation with the independent variable $\chi = (x/l)(w_1/U_0)$. It is then appropriate to consider a reduced frequency based on the flame length. Let $\bar{\sigma}$ be the average phase speed of the flame perturbation in the flame region, as can be calculated from the previous section. The frequencies at which the flame response exhibits local maxima are found to be approximately at $\frac{\omega L}{\bar{\sigma}} = 3\pi/2$, $7\pi/2$, $11\pi/2$ etc.

4.5 REFERENCE:

[1] Blackshear Jr., P.L., "Growth of Disturbances in a Flame Generated Shear Region", NACA 3830, 1956.

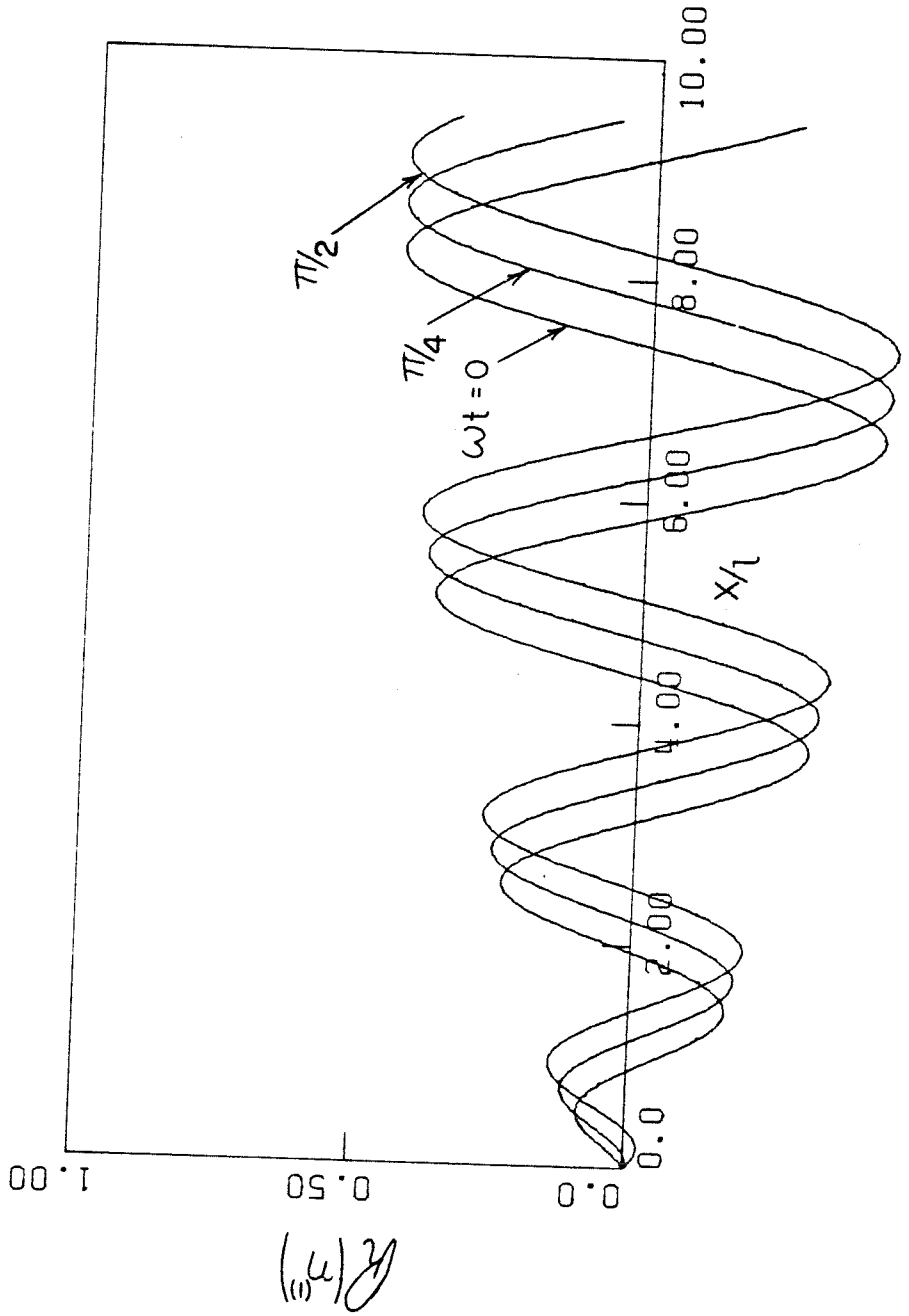

FIGURE 4.1 NON-STEADY FLAME ENVELOPES, $W_1/U_o=0.1$, $\lambda=4.5$, $M_o=0.2$ and $\omega l/U_o=4.85$

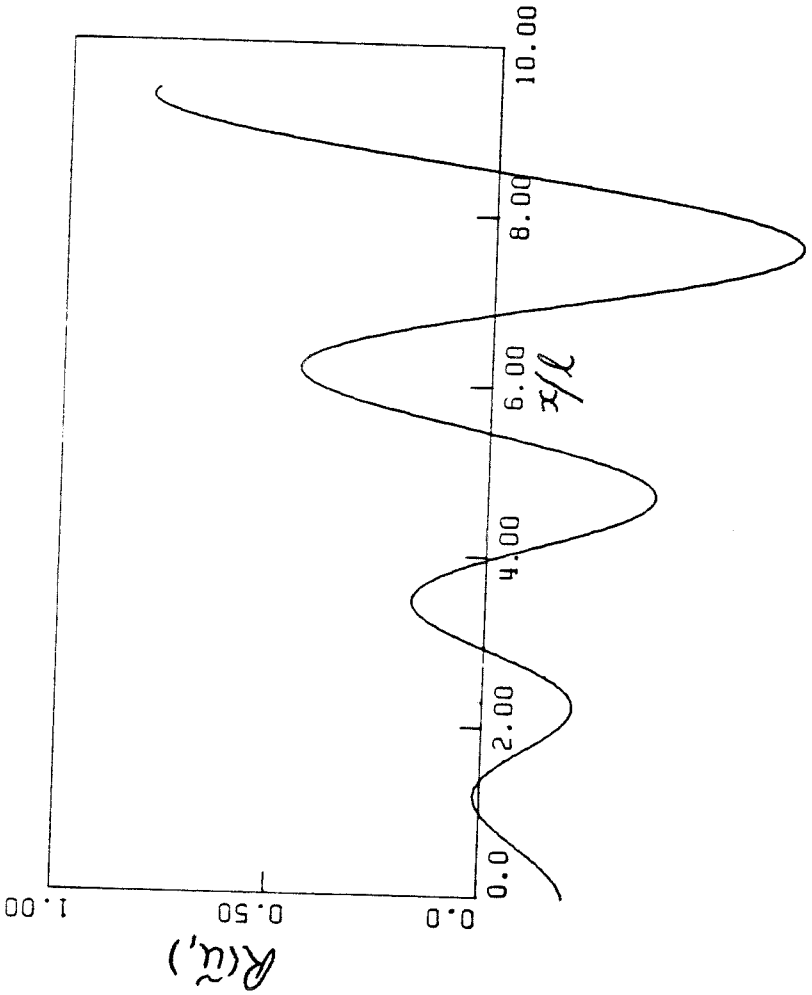

FIGURE 4.2 AVERAGE AXIAL VELOCITY PERTURBATION UPSTREAM OF THE FLAME

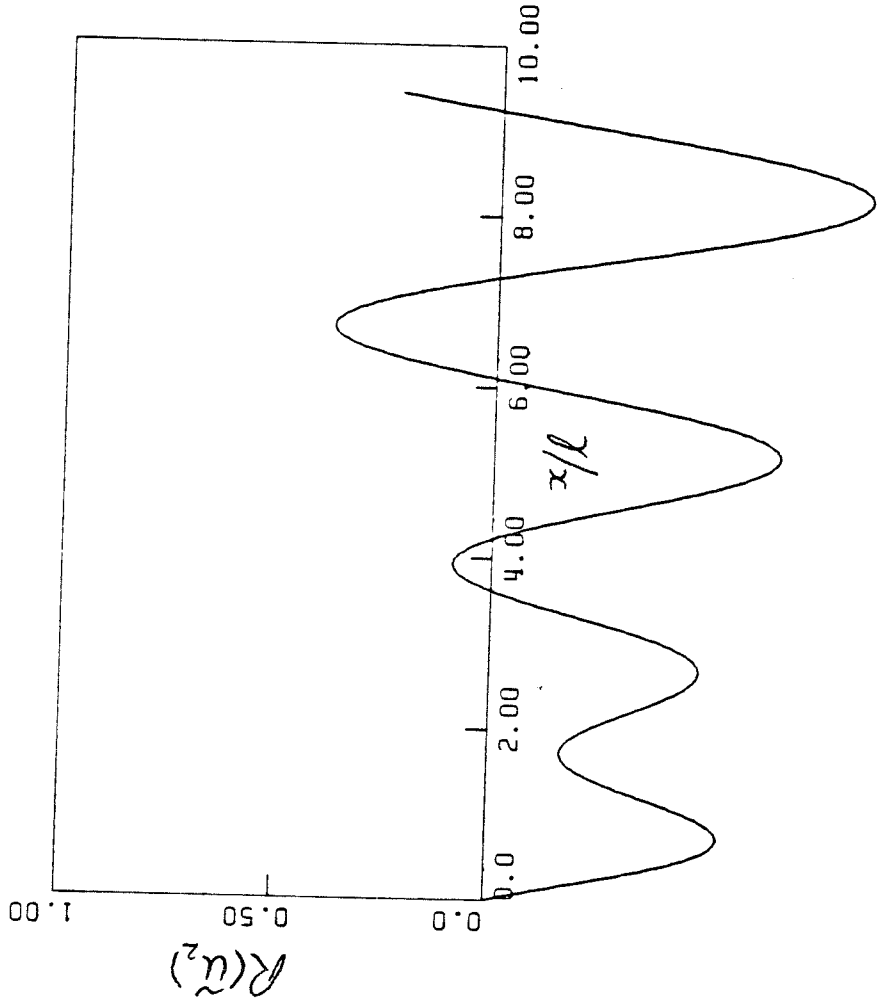

FIGURE 4.3 AVERAGE AXIAL VELOCITY PERTURBATION DOWNSTREAM OF THE FLAME

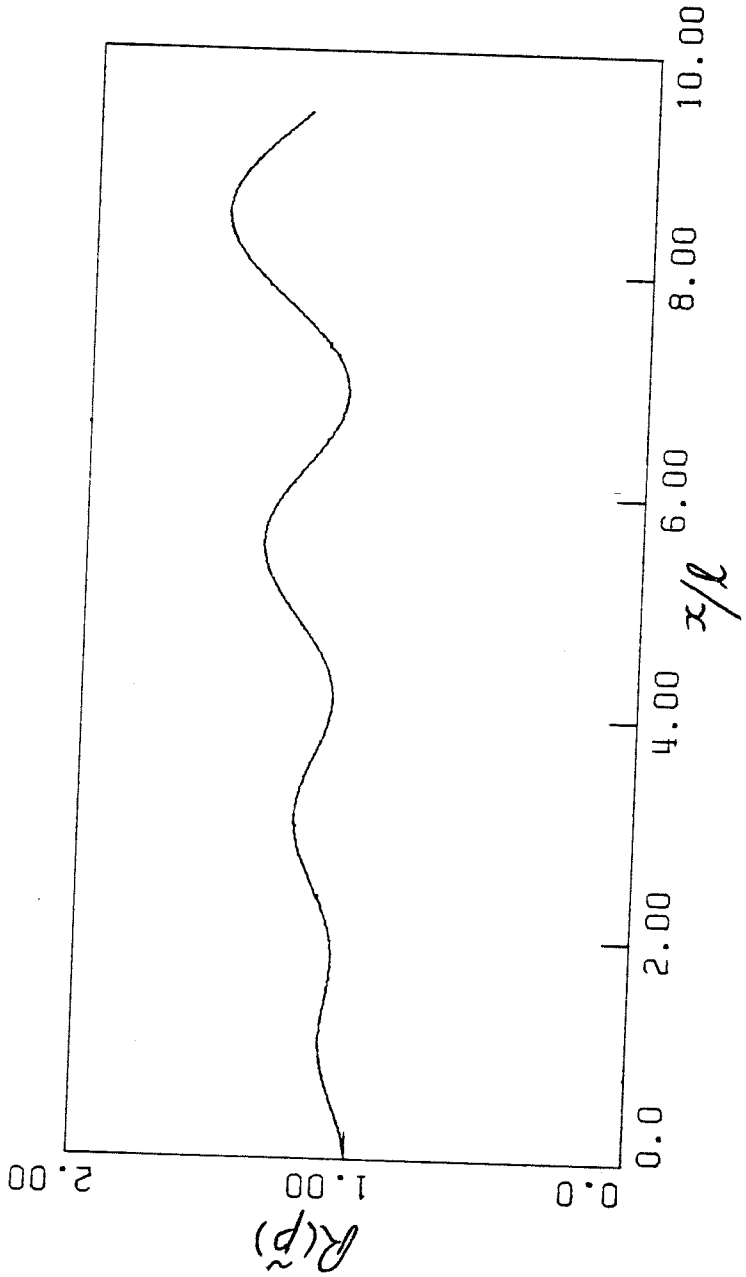

FIGURE 4.4 PRESSURE PERTURBATION IN THE FLAME REGION

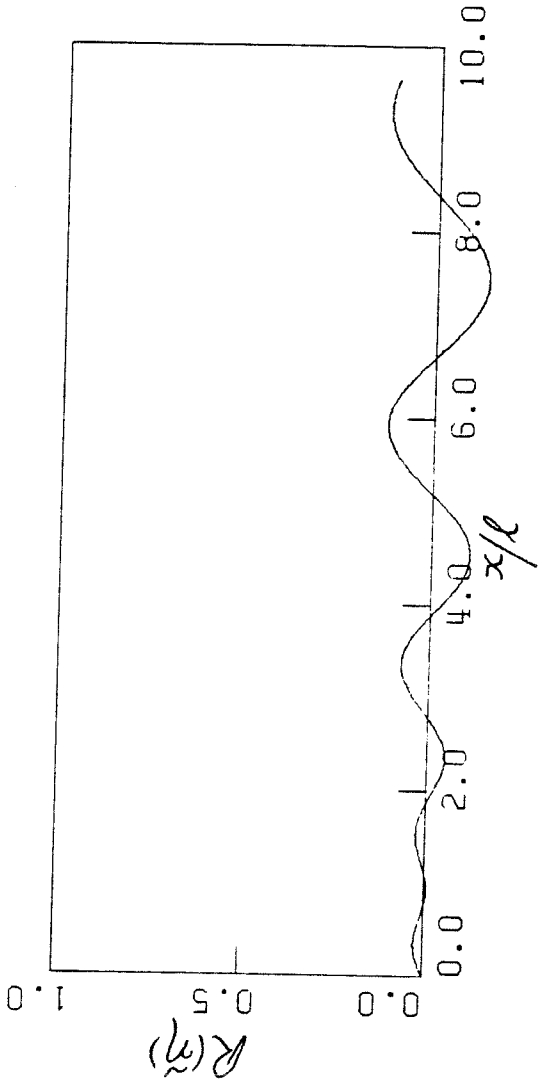

FIGURE 4.5 NON-STEADY FLAME ENVELOPE GENERATED BY SOURCE FLOW, $\omega\ell/U_o = 4.85$

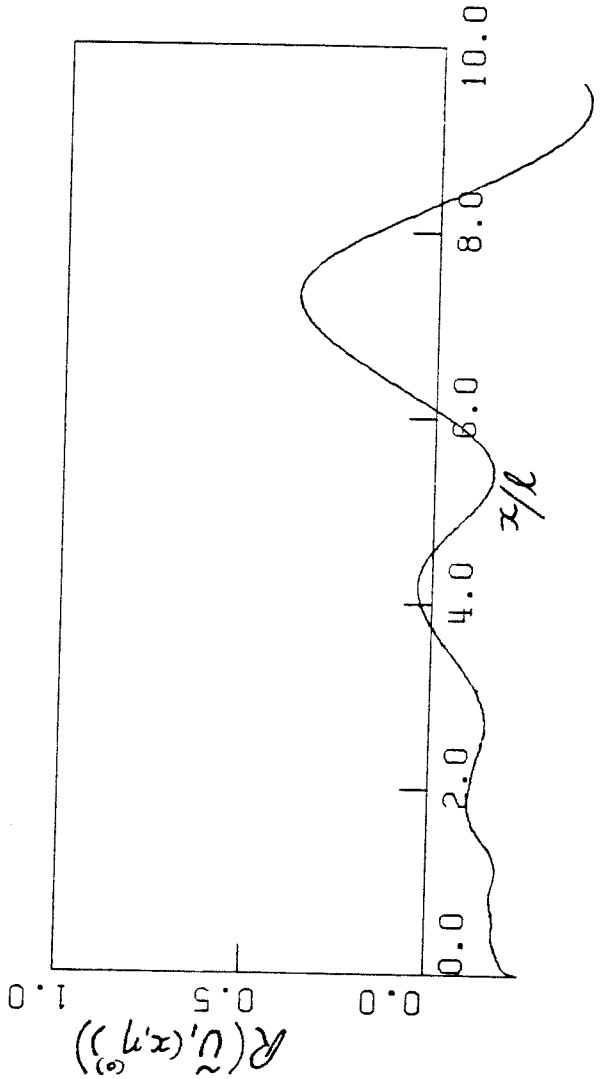

FIGURE 4.6 AXIAL VELOCITY PERTURBATION AT THE UPSTREAM FLAME SURFACE

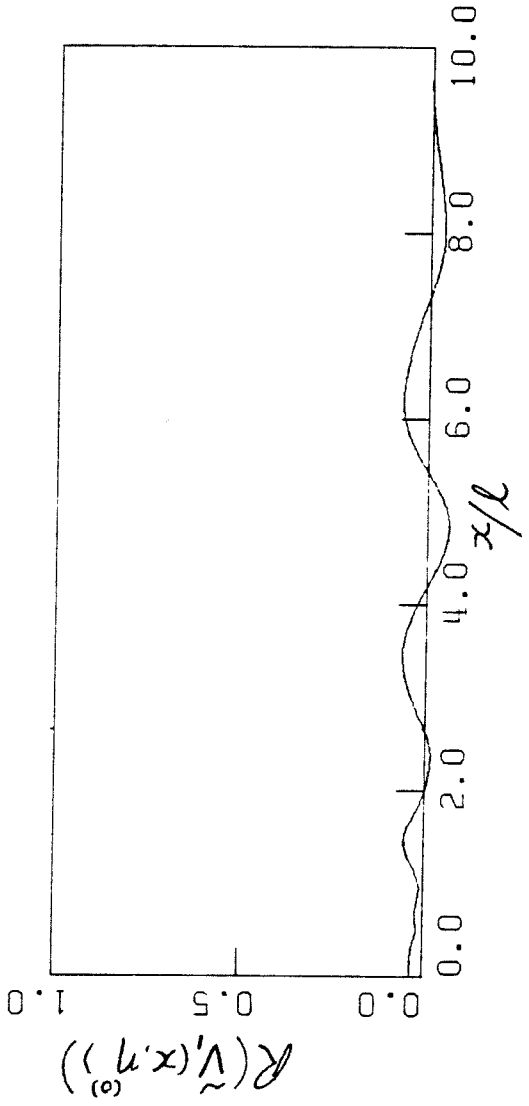

FIGURE 4.7 NORMAL VELOCITY PERTURBATION AT THE UPSTREAM FLAME SURFACE

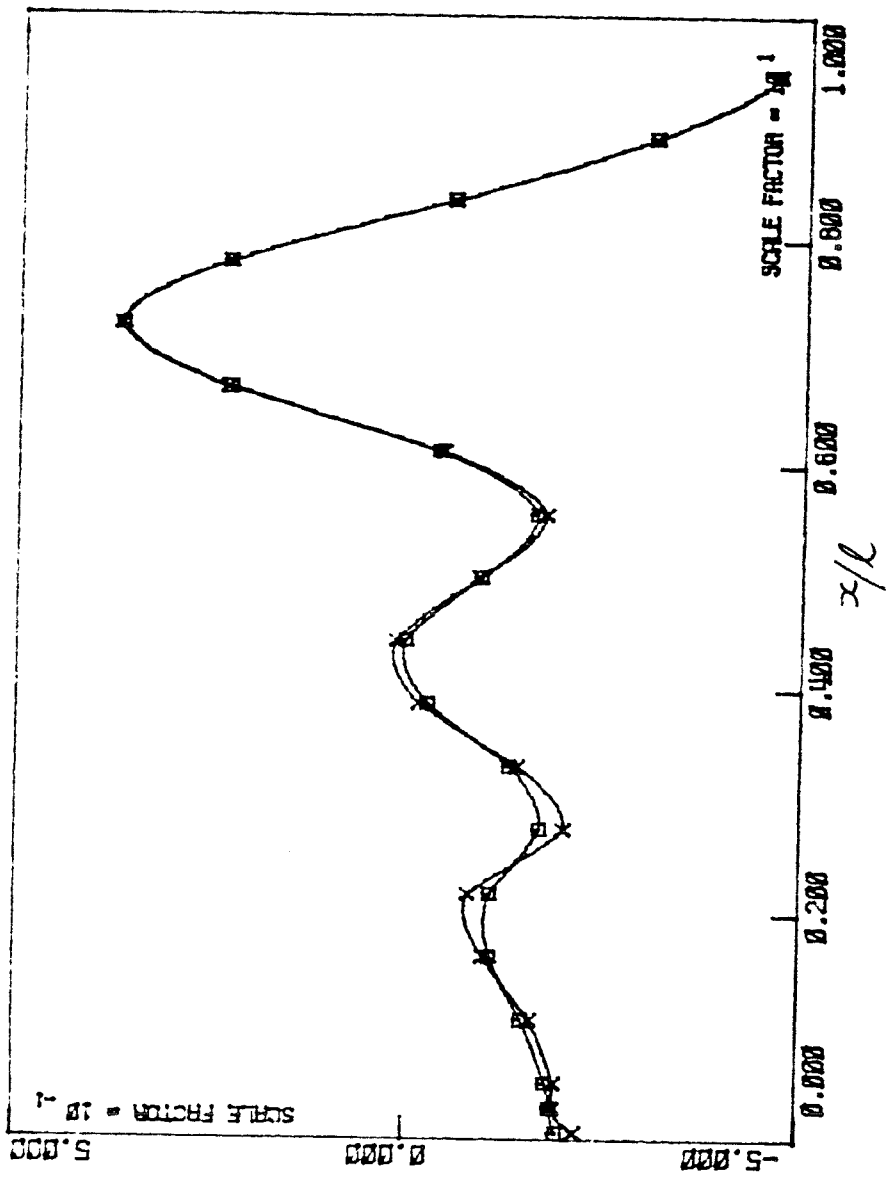

FIGURE 4.8 AXIAL VELOCITY PERTURBATION (Real Part)

□ $R(\tilde{u}_1(x))$; × $R(\tilde{U}_1(x,\eta^{(o)}))$

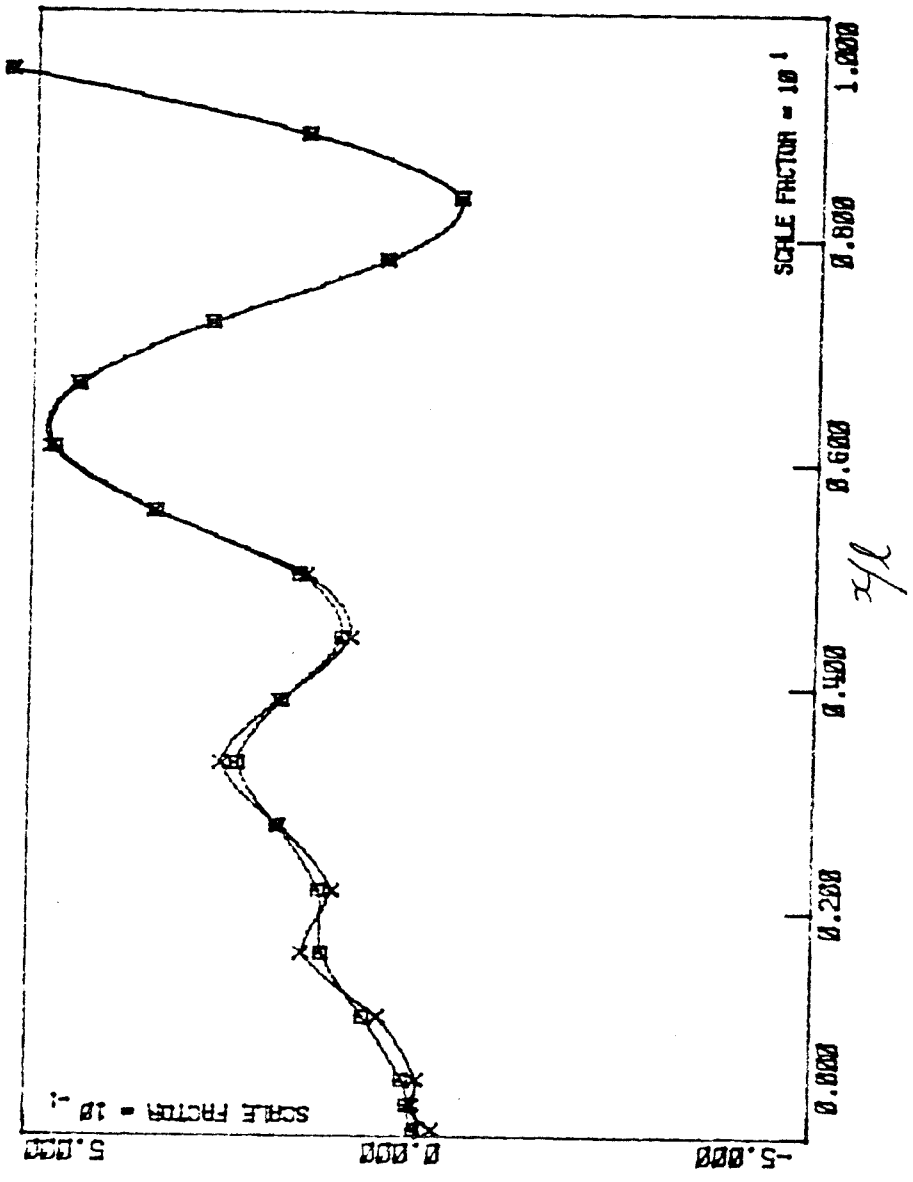

FIGURE 4.9 AXIAL VELOCITY PERTURBATION (Imaginary Part)
□ $\mathcal{I}_m(\tilde{u}, (x)) \; ; \; \times \; \mathcal{I}_m(\tilde{U}_1(x, \eta^{(o)}))$

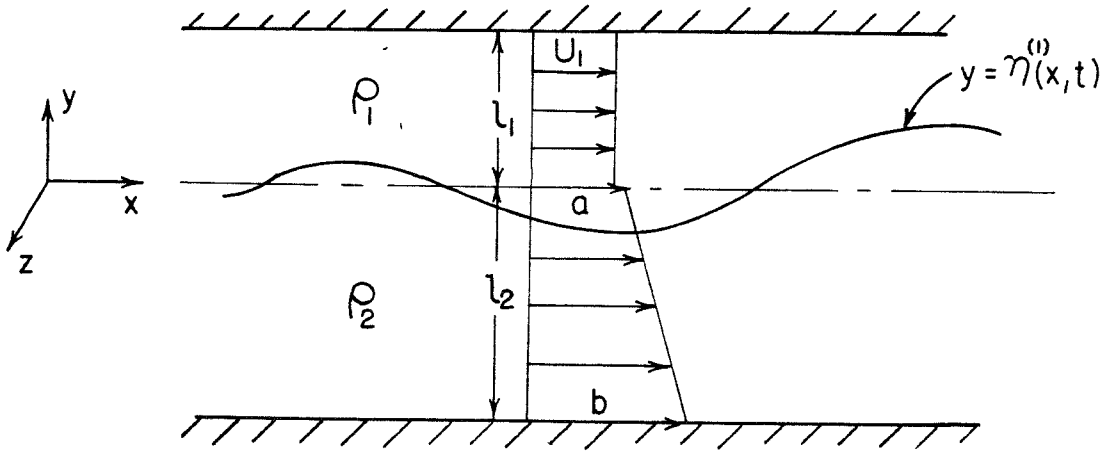

FIGURE 4.10 NOTATION FOR THE STABILITY OF THE INTERFACE

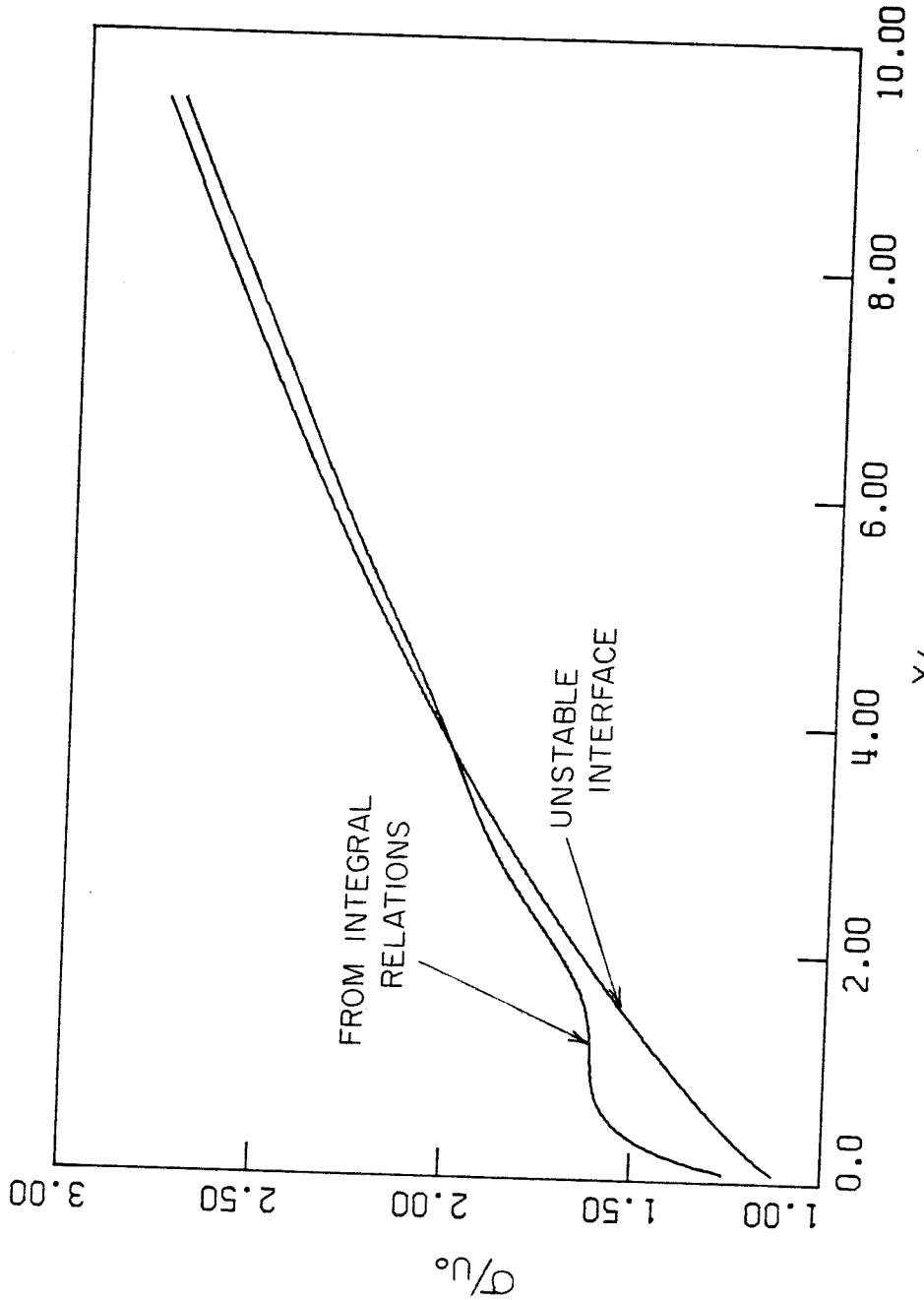

FIGURE 4.11 LOCAL PHASE SPEED OF THE FLAME PERTURBATION

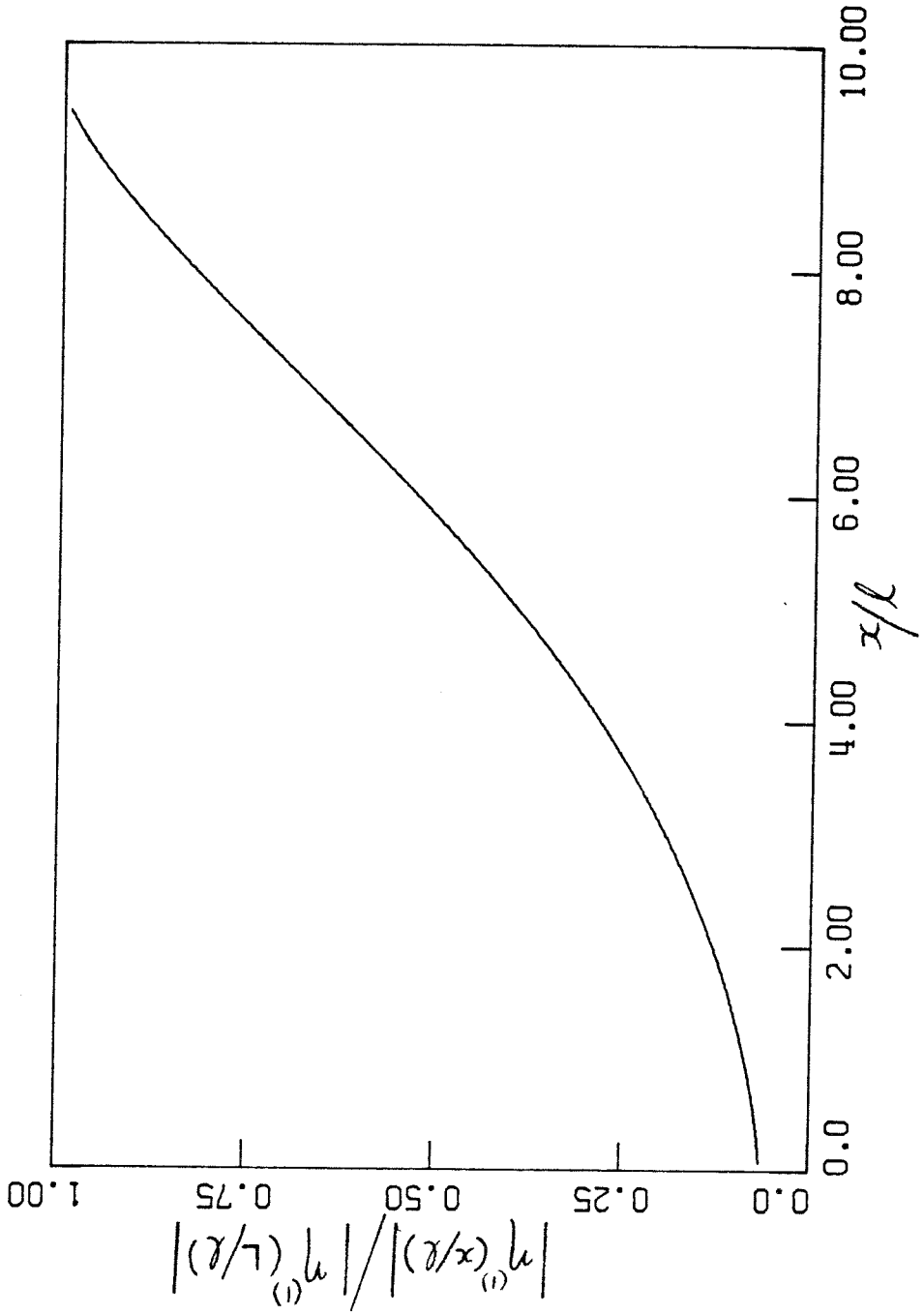

FIGURE 4.12 GROWTH OF THE DISTURBANCE TO THE INTERFACE

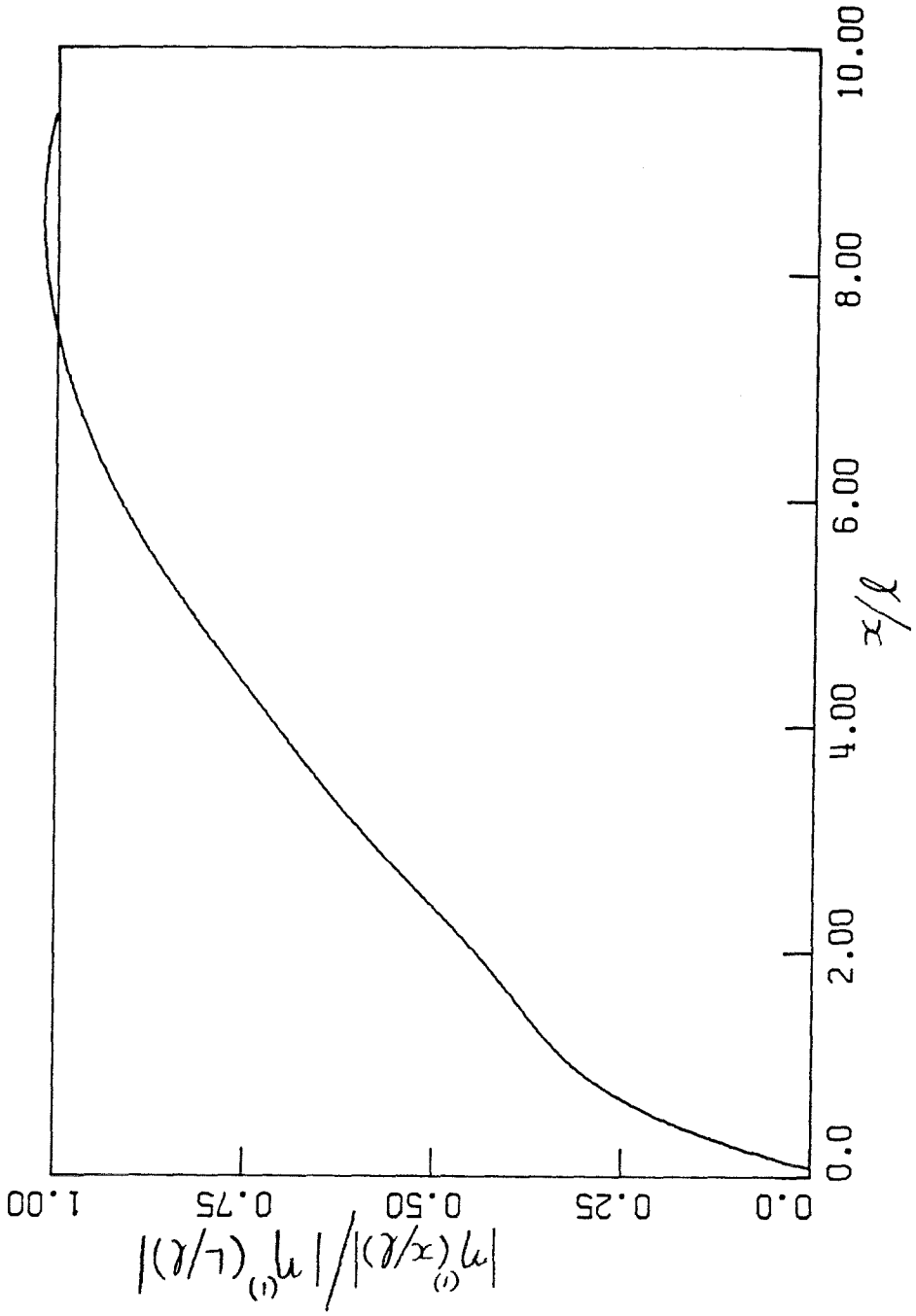

FIGURE 4.13 GROWTH OF THE FLAME PERTURBATION, From Section 4.1

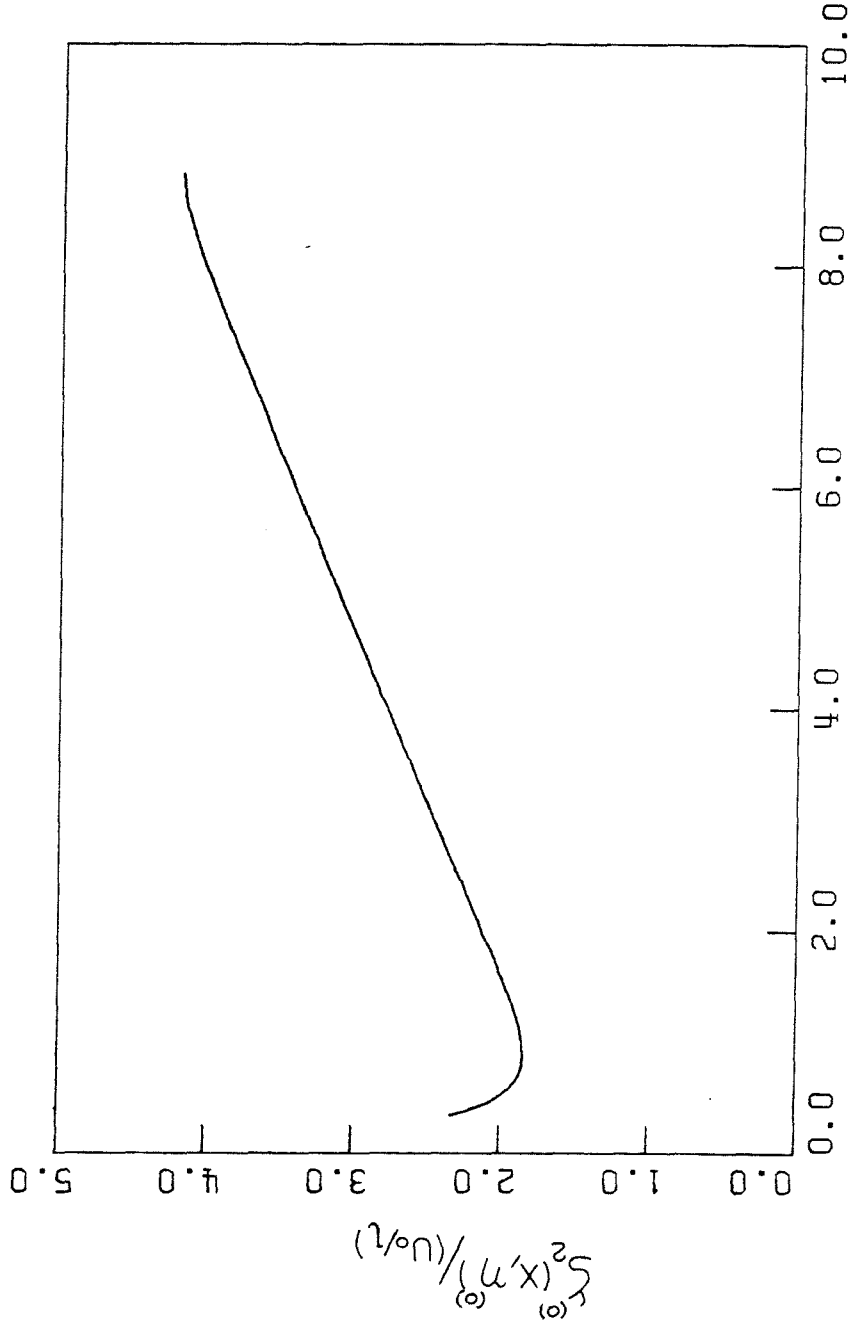

FIGURE 4.14 VORTICITY PRODUCED BY THE FLAME

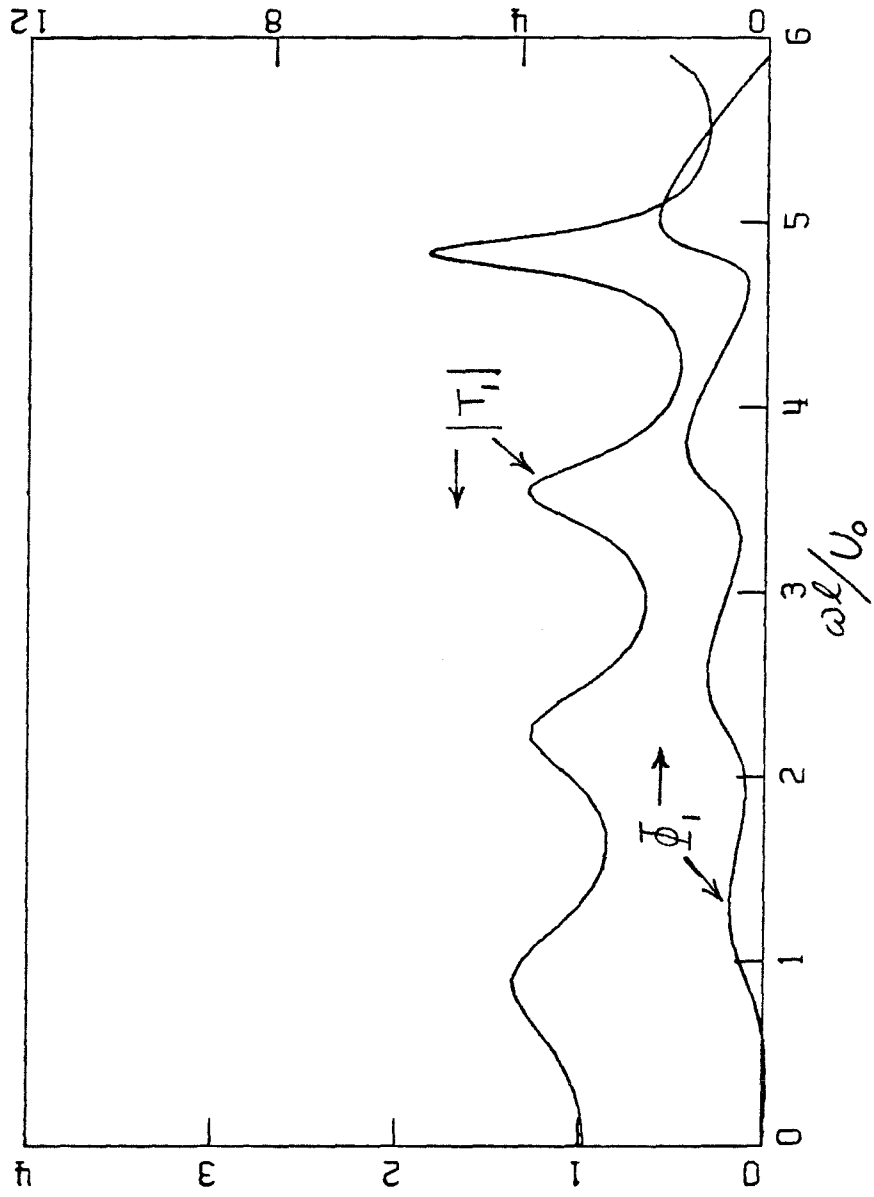

FIGURE 4.15 TRANSMISSION COEFFICIENT - WAVE FROM DOWNSTREAM

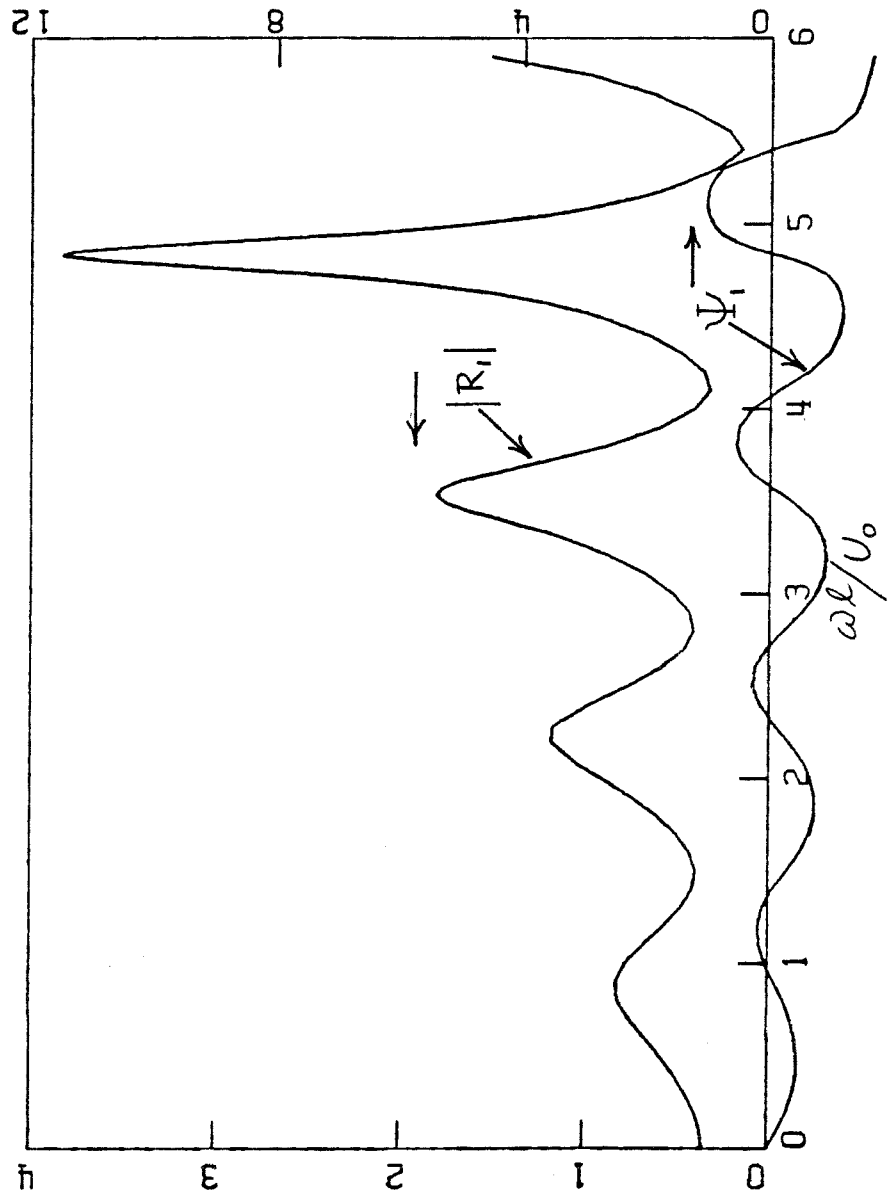

FIGURE 4.16 REFLECTION COEFFICIENT - WAVE FROM DOWNSTREAM

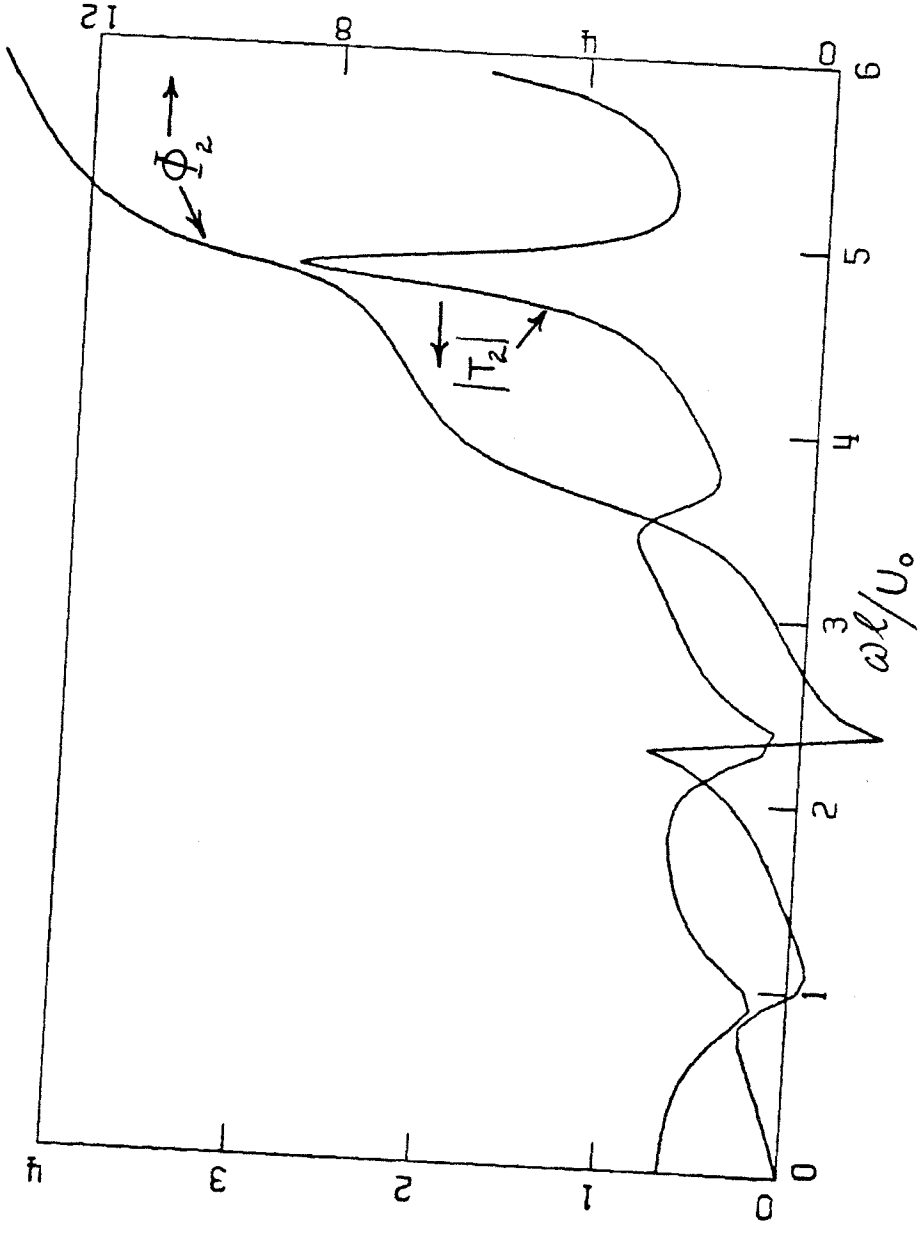

FIGURE 4.17 TRANSMISSION COEFFICIENT - WAVE FROM UPSTREAM

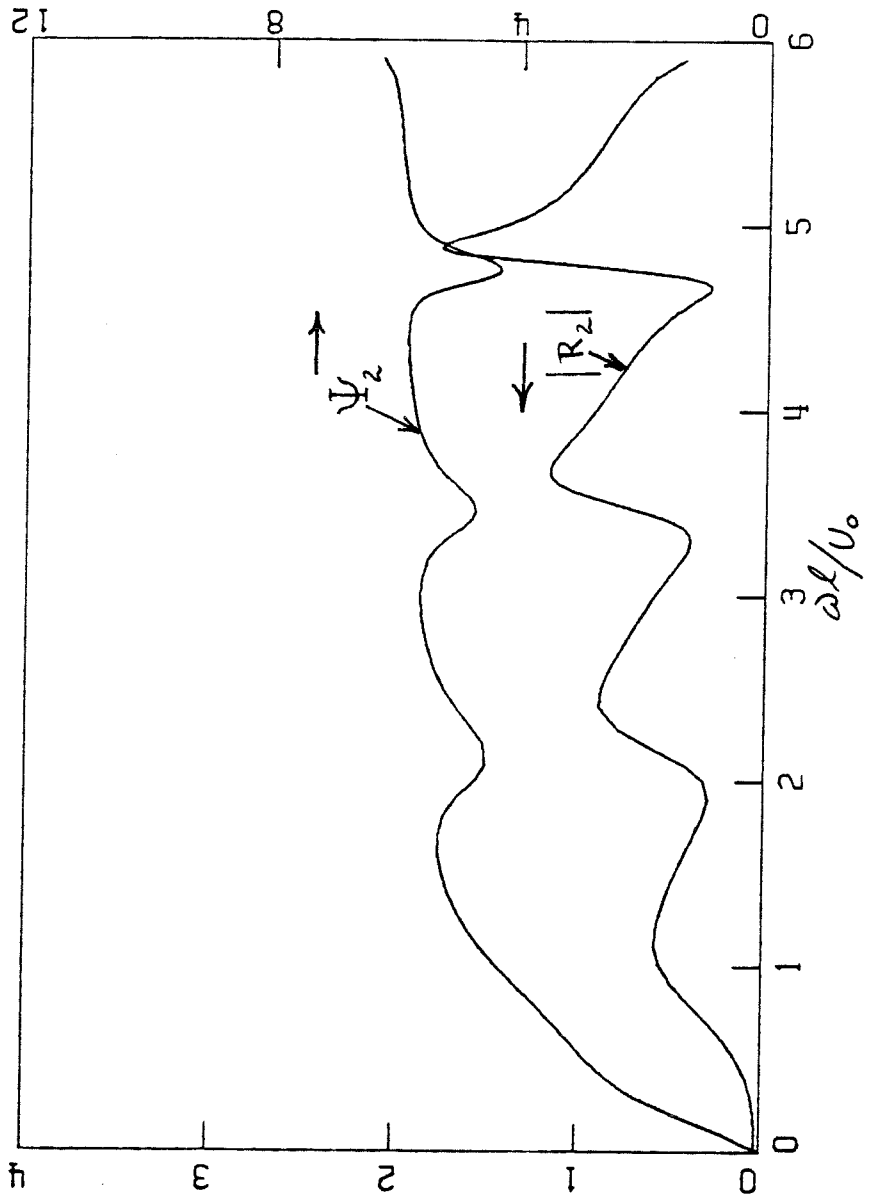

FIGURE 4.18 REFLECTION COEFFICIENT - WAVE FROM UPSTREAM

5. ANALYSIS OF LOW FREQUENCY DISTURBANCES IN AFTERBURNERS

Combustion oscillations in afterburners often arise due to the effects of local pressure and velocity fluctuations on the combustion processes and on the acoustic characteristics of the system[1,2,3]. The high frequency oscillations, known as screech, involve the chemical reaction times in an essential way[4,5]. The low frequency oscillations, on the other hand, primarily depend on the fluid mechanical adjustments in the flame region[6,7]. Chemical reaction times are not very important for the low frequency spectrum (less than, say, 100Hz). Non-steady response of stabilized flames exhibits certain well-defined energetic modes as calculated in the previous chapter. This active response to acoustic input, by the stabilized flame, can feed considerable acoustic energy into the system. When such a flame is situated in a practical combustion system like an aircraft afterburner or an utility boiler, it plays a major role in amplifying the low frequency disturbances to objectionable levels, even leading to instability in some instances. The transient response of an elementary afterburner configuration of an aircraft gas turbine is analyzed in the present chapter. The simple example considered here constitutes the first step towards a rational model for the study of low frequency disturbances in the afterburners.

Let us consider a rudimentary afterburner configuration of constant cross sectional area, as shown in figure 5.1. The flame holder, located at $x = 0$, has two rings, resulting in four flame holder points across the cross section. The half duct width (ℓ) in the flame calculations can then be approximated by $D/8$, where D is the diameter of the burner. Let L be the length of the flame zone. The turbine discharge

is located at $x = -L_1$ and the nozzle throat is located at $x = (L+L_2)$. Consistent with the non-steady flame calculations of chapter 4, we consider the flame region, the turbine and the nozzle to be compact to the acoustic disturbance. Consequently, the turbine and the nozzle can be characterized by appropriate admittance functions at $x = -L_1$ and $x = (L+L_2)$. Upstream of the flame holder, let U_o and C_o be the local fluid velocity and sound speed and P_1^+ and P_1^- be the complex amplitudes of the downstream and the upstream running waves. U_2, C_2, P_2^+ and P_2^- represent the corresponding quantities downstream of the flame zone.

Pressure and velocity fluctuations of a plane wave acoustic field may be written as

upstream of the flame holder,

$$\frac{\bar{P}_1^{(1)}}{\gamma P_o} = P_1^+ e^{-i\omega\left(t - \frac{x}{c_o+U_o}\right)} + P_1^- e^{-i\omega\left(t + \frac{x}{c_o-U_o}\right)} \quad (5.1)$$

$$\frac{\bar{U}_1^{(1)}}{C_o} = P_1^+ e^{-i\omega\left(t - \frac{x}{c_o+U_o}\right)} - P_1^- e^{-i\omega\left(t + \frac{x}{c_o-U_o}\right)} \quad (5.2)$$

downstream of the flame zone,

$$\frac{\bar{P}_2^{(1)}}{\gamma P_o} = P_2^+ e^{-i\omega\left(t - \frac{x}{c_2+U_2}\right)} + P_2^- e^{-i\omega\left(t + \frac{x}{c_2-U_2}\right)} \quad (5.3)$$

$$\frac{\bar{u}_2^{(1)}}{c_2} = P_2^+ e^{-i\omega\left(t - \frac{x}{c_2+U_2}\right)} - P_2^- e^{-i\omega\left(t + \frac{x}{c_2-U_2}\right)} \tag{5.4}$$

We define an acoustic admittance function,

$$\xi(x) = \frac{\bar{u}^{(1)}(x,t)}{\bar{p}^{(1)}(x,t)} \left(\frac{\gamma p_0}{c}\right) \tag{5.5}$$

Substituting from equations 5.1-5.4, we obtain

Upstream of the flame holder $(-L_1 < x < 0)$

$$\frac{P_1^+}{P_1^-} = \frac{1+\xi(x)}{1-\xi(x)} e^{-i\left(\frac{2\omega x}{c_0}\right)\left(\frac{1}{1-M_0^2}\right)} \tag{5.6}$$

and downstream of the flame region $[L < x < (L+L_2)]$

$$\frac{P_2^-}{P_2^+} = \frac{1-\xi(x)}{1+\xi(x)} e^{i\left(\frac{2\omega x}{c_2}\right)\left(\frac{1}{1-M_2^2}\right)} \tag{5.7}$$

Let α_T and α_N be the acoustic reflection coefficients of the turbine and the nozzle, defined as

$$\alpha_T = \left|\frac{P_1^+}{P_1^-}\right|_{x=-L_1} = \frac{1+\xi(-L_1)}{1-\xi(-L_1)} \tag{5.8}$$

and

$$\alpha_N = \left| \frac{P_2^-}{P_2^+} \right|_{x = L+L_2} = \frac{1-\xi(L+L_2)}{1+\xi(L+L_2)} \tag{5.9}$$

We then match the one-dimensional wave fields upstream of the flame holder with the turbine admittance at $x = -L_1$ and the flame reflection coefficient at $x = 0$. Similarly, the wave fields downstream of the flame region are matched at the end of the flame zone and with the nozzle admittance at $x = (L+L_2)$.

Let the transmission and reflection coefficients of the flame region be denoted by T_1 and R_1 for a wave incident from the downstream and by T_2 and R_2 for a wave incident from the upstream of the flame region. These coefficients are obtained from section 4.4 for a flame speed, $\omega_1/U_0 = 0.1$, $\lambda = \rho_1/\rho_2 = 4.5$ and $M_0 = U_0/C_0 = 0.2$. The matching conditions can then be written as follows.

At the turbine discharge $(x = -L_1)$,

$$P_1^+ e^{-i\omega\left(t + \frac{L_1}{C_0+U_0}\right)} = \alpha_T P_1^- e^{-i\omega\left(t - \frac{L_1}{C_0-U_0}\right)} \tag{5.10}$$

At the nozzle throat $(x = L+L_2)$,

$$P_2^- e^{-i\omega\left(t + \frac{L+L_2}{C_2-U_2}\right)} = \alpha_N P_2^+ e^{-i\omega\left(t - \frac{L+L_2}{C_2+U_2}\right)} \tag{5.11}$$

Across the flame region,

$$P_1^- e^{-i\omega t} = R_2 P_1^+ e^{-i\omega t} + T_1 P_2^- e^{-i\omega\left(t + \frac{L}{c_2 - U_2}\right)} \tag{5.12}$$

and

$$P_2^+ e^{-i\omega\left(t - \frac{L}{c_2 + U_2}\right)} = T_2 P_1^+ e^{-i\omega t} + R_1 P_2^- e^{-i\omega\left(t + \frac{L}{c_2 - U_2}\right)} + \frac{P_i(t)}{\gamma P_0} \tag{5.13}$$

where $P_i(t) = \tilde{P}_i e^{-i\omega t}$ is the input excitation of radian frequency ω at $x = 0$. In a practical device this can arise, for example, due to combustion roughness.

5.1 RESULTS AND DISCUSSION:

Equations 5.10-5.13 give a system of four inhomogeneous simultaneous equations for the unknowns P_1^+, P_1^-, P_2^- and P_2^+. Calculations were made for the operating conditions, $M_0 = 0.2$, $w_1/U_0 = 0.1$ and $\lambda = 4.5$. The reduced frequency, $\omega \ell / U_0$ is varied from 0 to 6. The pressure responses at four stations along the afterburner are shown in figures 5.2-5.5. These are made dimensionless by the imposed excitation, P_i. For the burner geometry, $L_1/\ell = 5.2$, $L_2/\ell = 26$ are selected. The flame length for a flame speed of $w_1/U_0 = 0.1$ is approximately given by $L/\ell = 10$ from the calculations of chapter 3. The values of the acoustic admittance at the turbine and the nozzle are chosen as $\xi(-L_1) = -0.25$ and $\xi(L + L_2) = 0.11$. Comparing with the responses of the flame zone (figures 4.15-4.18), we notice that the energetic

modes of the flame region are clearly noticed in the pressure responses at the turbine (figure 5.2), the flame holder (figure 5.3), end of the flame zone (figure 5.4) and the plane of the nozzle (figure 5.5). The dominant response of the system is at about a reduced frequency of $\omega\ell/U_o$ = 2.2, while the flame zone itself is most active at about $\omega\ell/U_o$ = 4.8. At $\omega\ell/U_o$ = 2.2, the normalized pressure response is about 15 at the end of the flame zone and at the nozzle.

The frequency spectrum of the pressure response is very sensitive to the afterburner geometry and to the acoustic admittance of the turbine and the nozzle. In the present illustrative example, we study only the effects of burner to turbine distance, L_1 and the admittance of the turbine discharge. Figures 5.6-5.9 show the pressure responses at the previous four stations for L_1/ℓ = 5.55. The response in this configuration is maximum at a higher frequency and approximately corresponds to the next higher burner mode. The maximum pressure response now occurs at $\omega\ell/U_o$ = 3.37 and has increased from 5 at the turbine when L_1/ℓ =5.2 to about 38 (figure 5.6) for $L_1/1$=5.55. The response is correspondingly higher at the other stations.

To systematically study this effect, the pressure reponse at the turbine for $\omega\ell/U_o$ = 3.37 is shown in figure 5.10 as a function of the turbine to the flame holder distance. It can be seen from the figure that the response at the turbine increases by a factor of 8 within a 10% change in the distance L_1/ℓ. This points out the importance of the flame holder location on the low frequency oscillations of the afterburner. Also, the figure 5.10 clearly demonstrates the need to consider the geometry of the system more accurately.

Next, we study the effect of the turbine acoustic admittance on the response of the afterburner. The flame holder to turbine distance is fixed at L_1/ℓ = 5.55 and corresponds to the geometry for the figures 5.6-5.9. The nozzle admittance is unaltered at $\xi(L+L_2) = 0.11$. Figures 5.11-5.14 show the pressure responses for a turbine admittance of $\xi(-L_1) = -0.43$. The maximum response (about 22 at the nozzle) occurs at about a frequency of $\omega\ell/U_0 = 2.2$. Change in the turbine admittance to $\xi(-L_1) = -0.27$ causes a significant change in the response spectrum. For this configuration, the afterburner becomes unstable (figures 5.15-5.18) at a frequency of 3.37. This is accompanied by a reduction in the response at the lower mode.

The sensitivity of the afterburner response to the turbine admittance is shown in figure 5.19. The pressure response at the turbine for the mode $\omega\ell/U_0 = 3.37$ is shown as a function of the turbine acoustic reflection coefficient, α_T. The flame holder is located at $L_1/\ell = 5.55$ and corresponds to the location for the maximum response (from figure 5.10) for a turbine reflection coefficient of 0.6. We notice that a slight reduction in the reflection coefficient causes a sharp increase in the pressure fluctuation at the turbine discharge. The burner becomes unstable at a reflection coefficient of 0.57. It is clear, from the figures 5.10 and 5.19, that one has to consider the details of the geometry and the flow conditions at the turbine and the nozzle more accurately.

To summarize, the above analysis proposes a possible mechanism of low-frequency instability and demonstrates the factors to which it should be sensitive. This gives a basis for scaling experiments on small burners

and making configurational changes that will suppress the instability. The non-steady flame model is an important tool to analyze this type of low-frequency instability. It is clear that the model can be easily adapted to configurations that are more complex than the example considered here.

5.2 REFERENCES:

[1] Crocco, L., "Aspects of Combustion Stability in Liquid Propellant Rocket Motors", J. Amer. Rocket Soc., volume 21, 1951, pp. 163-178; volume 22, 1952, pp. 7-16.

[2] Tsien, H.S., "Servo-Stabilization of Combustion in Rocket Motors", J. Amer. Rocket Soc., volume 22, 1952, pp. 256-262.

[3] Marble, F.E. and Cox Jr., D.W., "Servo-Stabilization of Low-Frequency Oscillations in a Liquid Bipropellant Rocket Motor", J. Amer. Rocket Soc., volume 23, 1953, pp. 63-81.

[4] Rogers, D.E. and Marble, F.E., "A Mechanism For High-Frequency Oscillations in Ramjet Combustors and Afterburners", Jet Propulsion, June 1966, pp. 456-462.

[5] Barker, C.L., "Experiments Concerning the Occurrence of High Frequency Combustion Instability", Ph.D. Thesis, California Institute of Technology, Pasadena, California, 1958.

[6] Marble, F.E. and Candel, S.M., "An Analytical Study of the Non-Steady Behaviour of Large Combustors", Seventeenth Symposium (International) on Combustion, August 1978, pp. 761-769 .

[7] Marble, F.E., Subbaiah, M.V. and Candel, S.M., "Analysis of Low-Frequency Disturbances in Afterburners", Proceedings, Specialists Meeting on Combustion Modelling, AGARD Propulsion and Energetics Panel, Cologne, 1979.

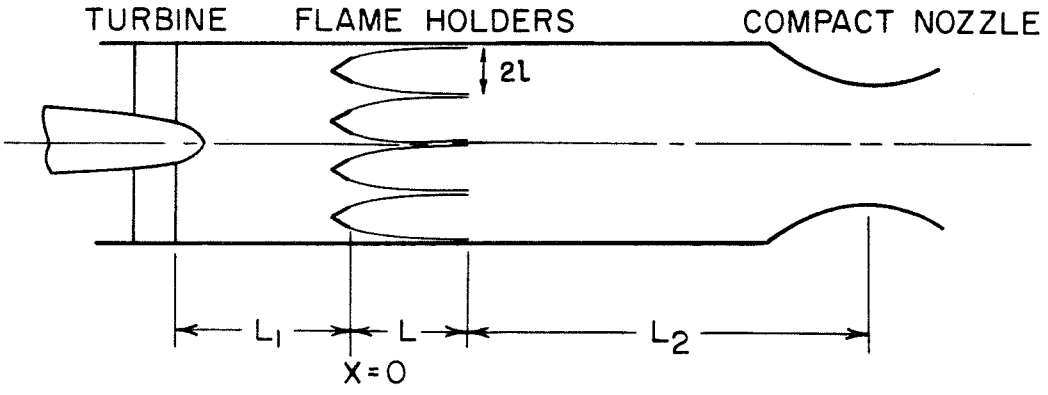

FIGURE 5.1 NOTATION FOR THE AFTERBURNER GEOMETRY

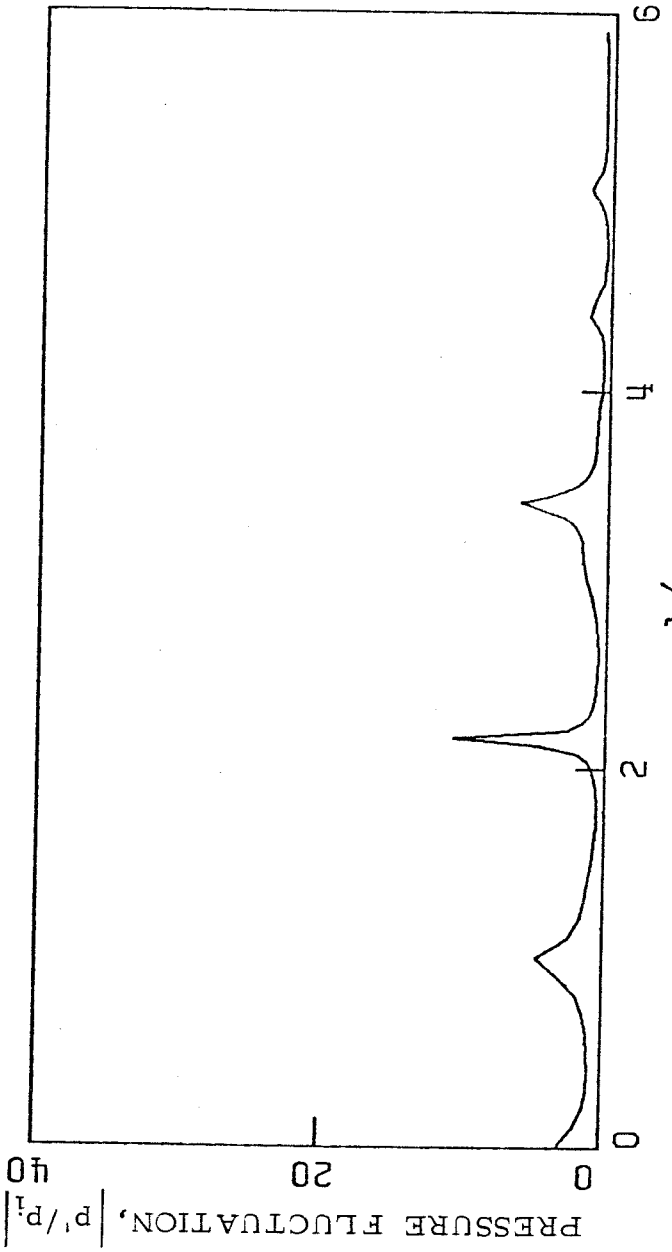

Figure 5.2 Pressure Fluctuation Spectrum, L_1/ℓ =5.2
Turbine Discharge

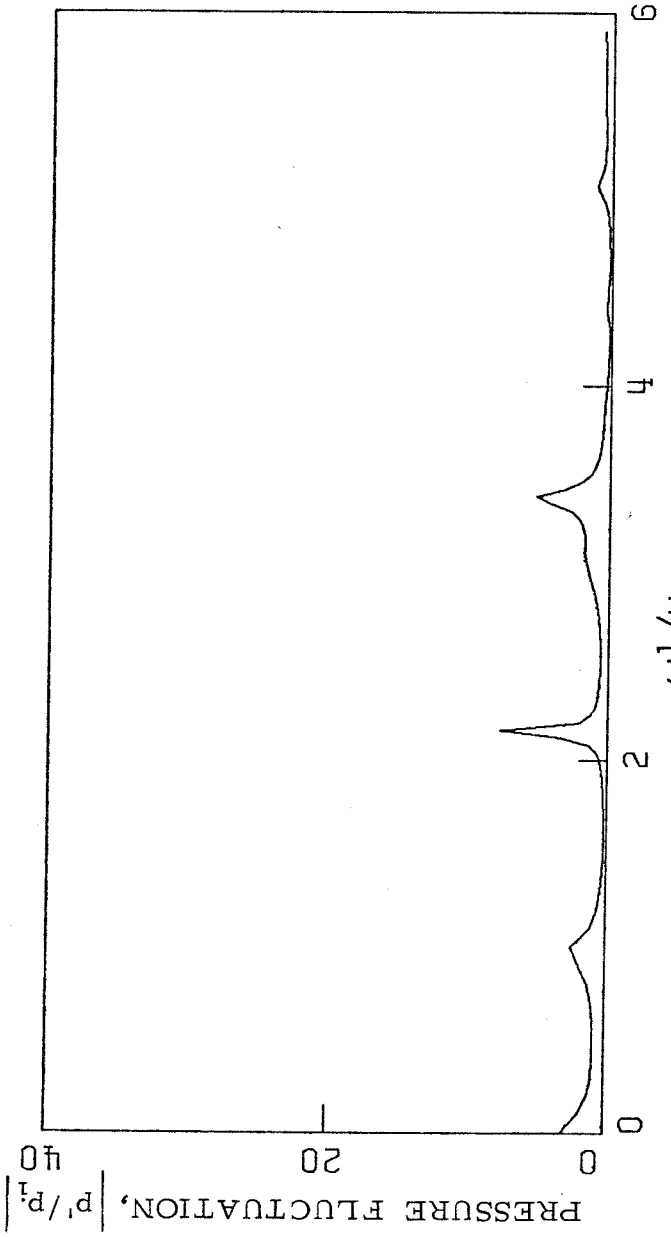

Figure 5.3 Pressure Fluctuation Spectrum, $L_1/\ell = 5.2$
Flame Holder

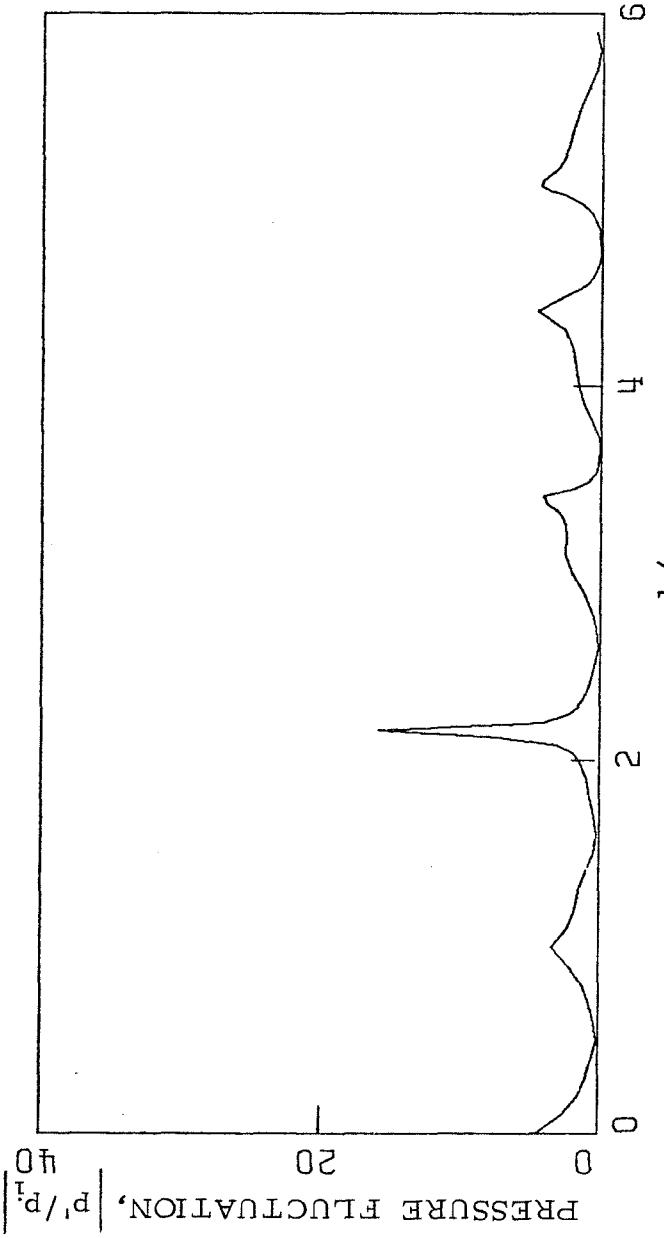

Figure 5.4 Pressure Fluctuation Spectrum, L_1/ℓ =5.2
End of Flame Zone

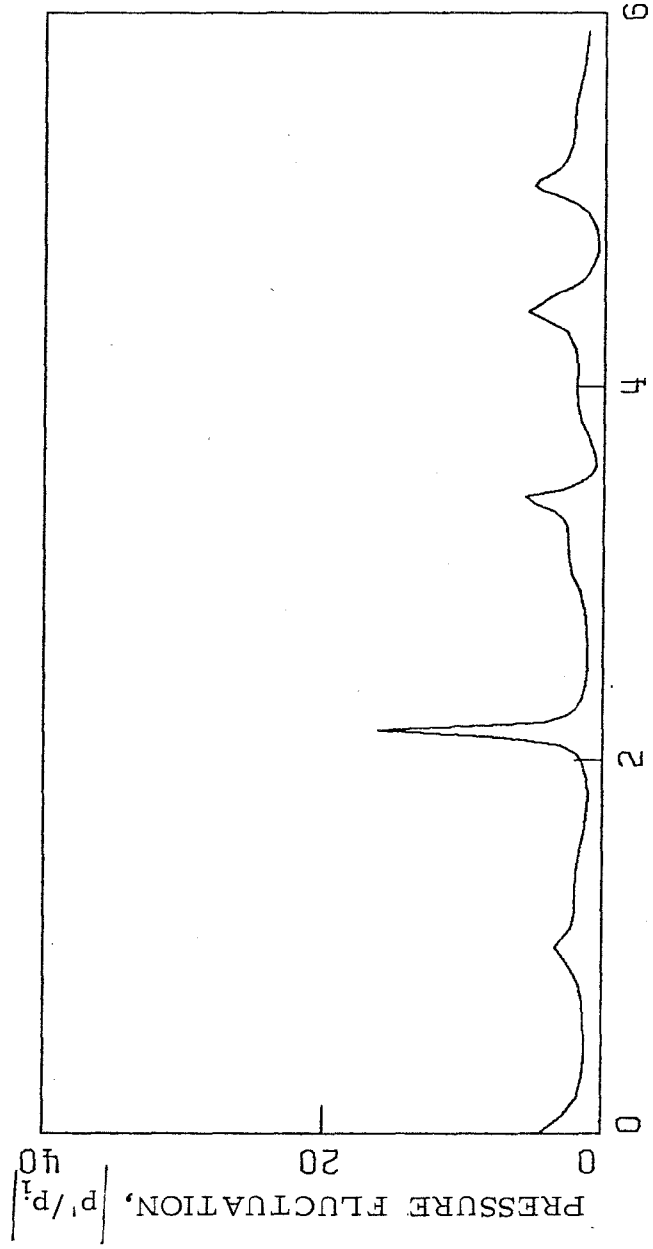

Figure 5.5 Pressure Fluctuation Spectrum, L_1/ℓ =5.2
Nozzle Inlet

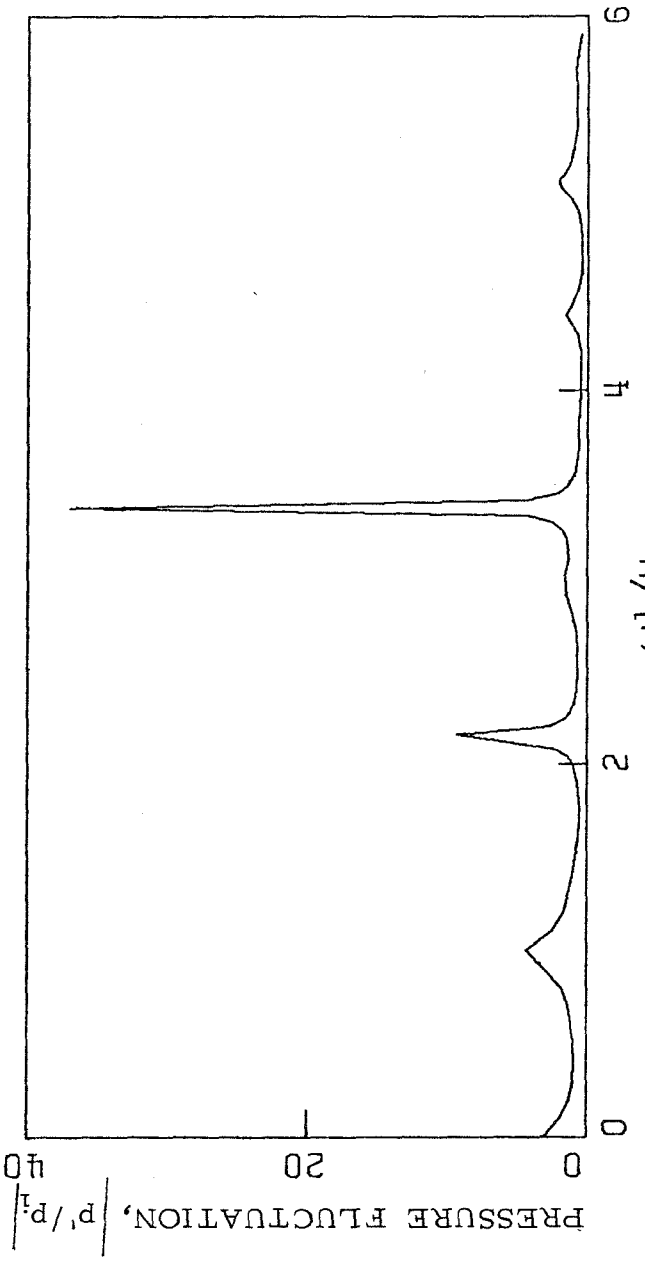

Figure 5.6 Pressure Fluctuation Spectrum, L_1/ℓ =5.55
Turbine Discharge

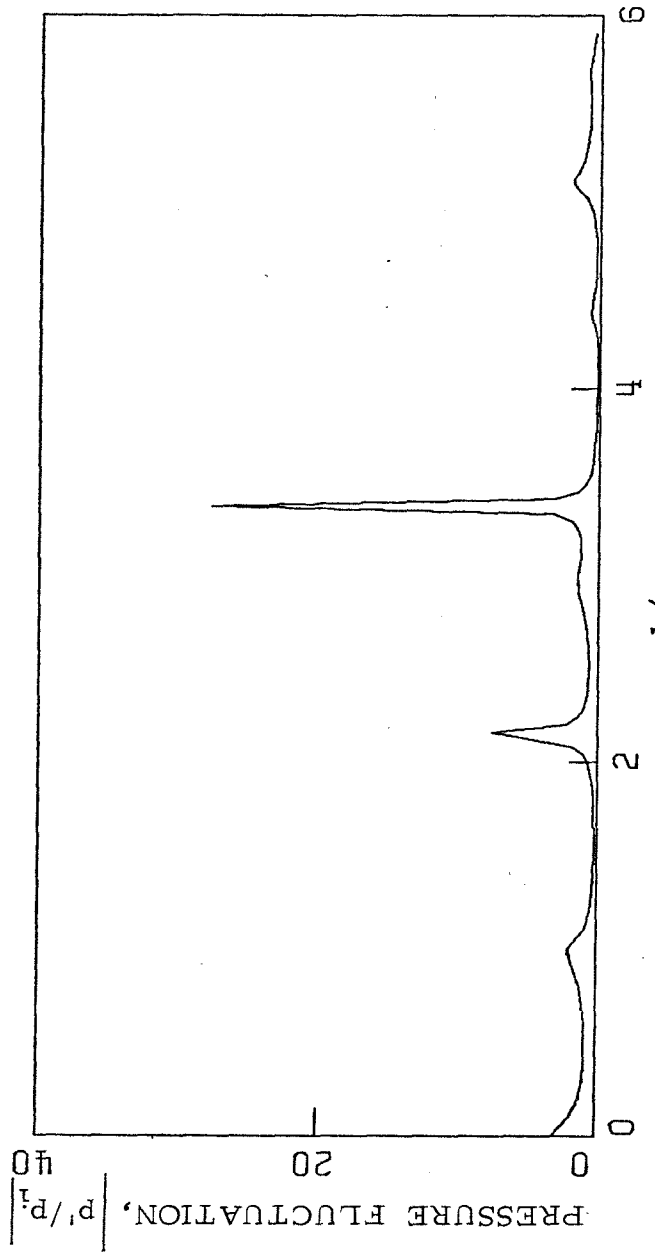

Figure 5.7 Pressure Fluctuation Spectrum, $L_1/\ell = 5.55$
Flame Holder

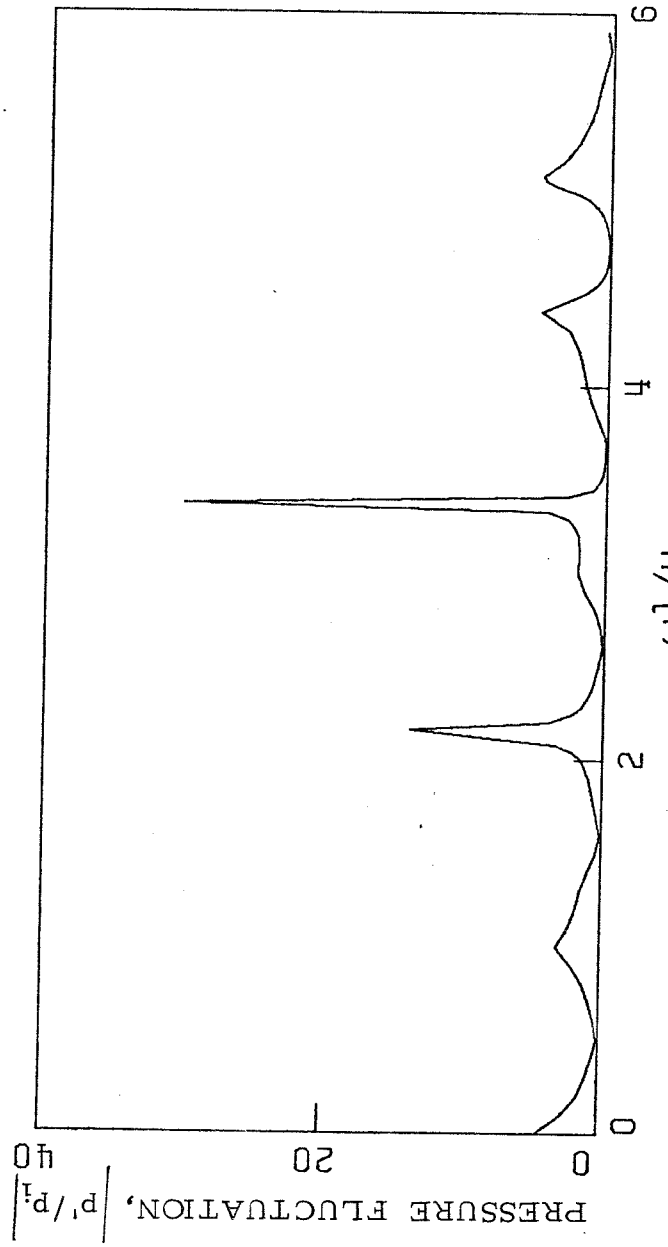

Figure 5.8 Pressure Fluctuation Spectrum, $L_1/\ell = 5.55$
End of Flame Zone

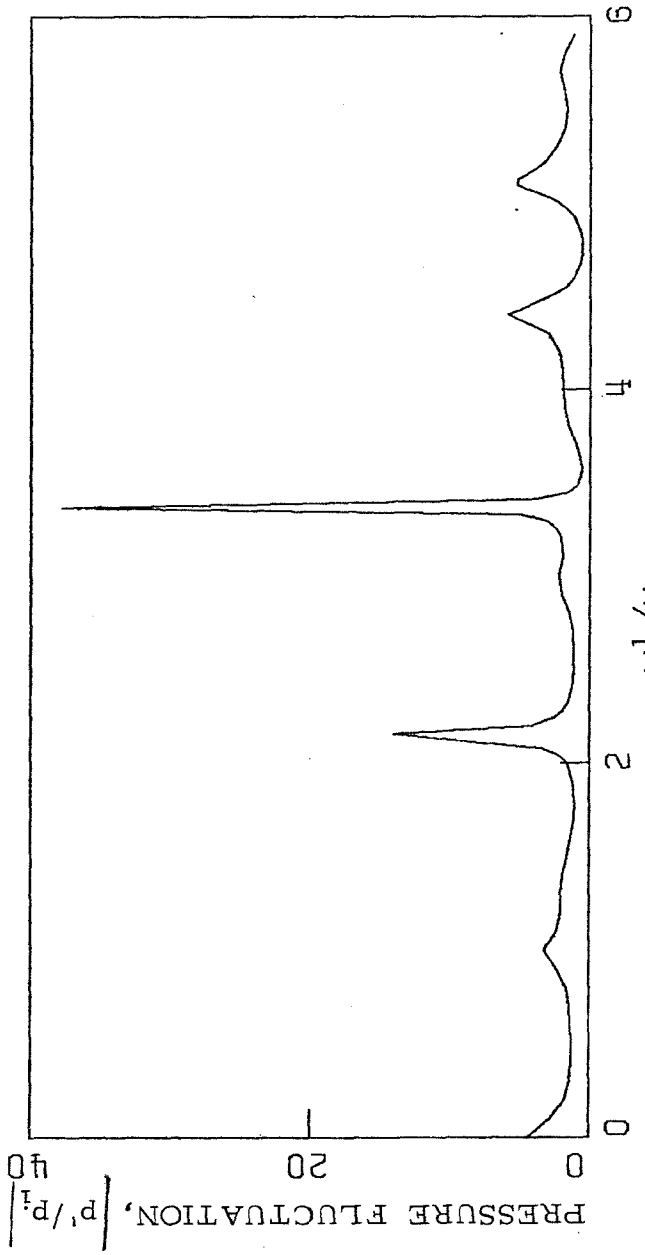

Figure 5.9 Pressure Fluctuation Spectrum, L_1/ℓ =5.55
Nozzle Inlet

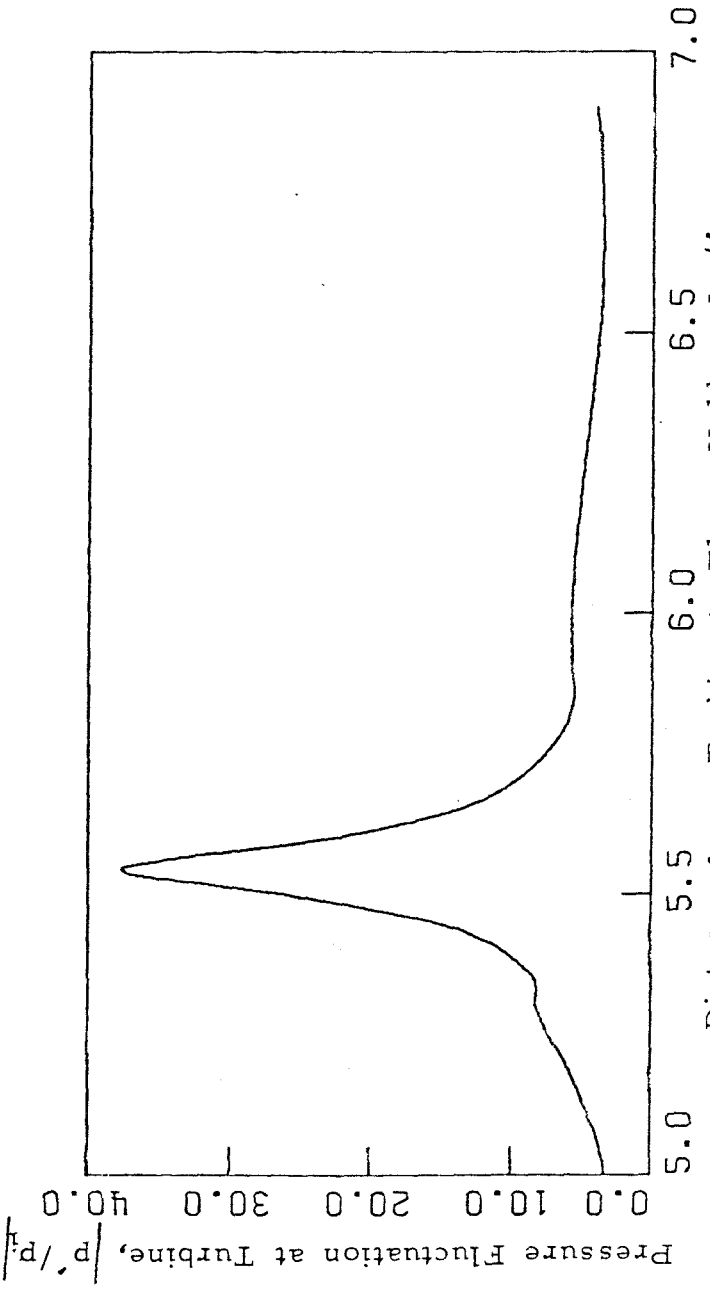

Figure 5.10 Pressure Fluctuation as a Function of Distance from Turbine to Flame Holder.

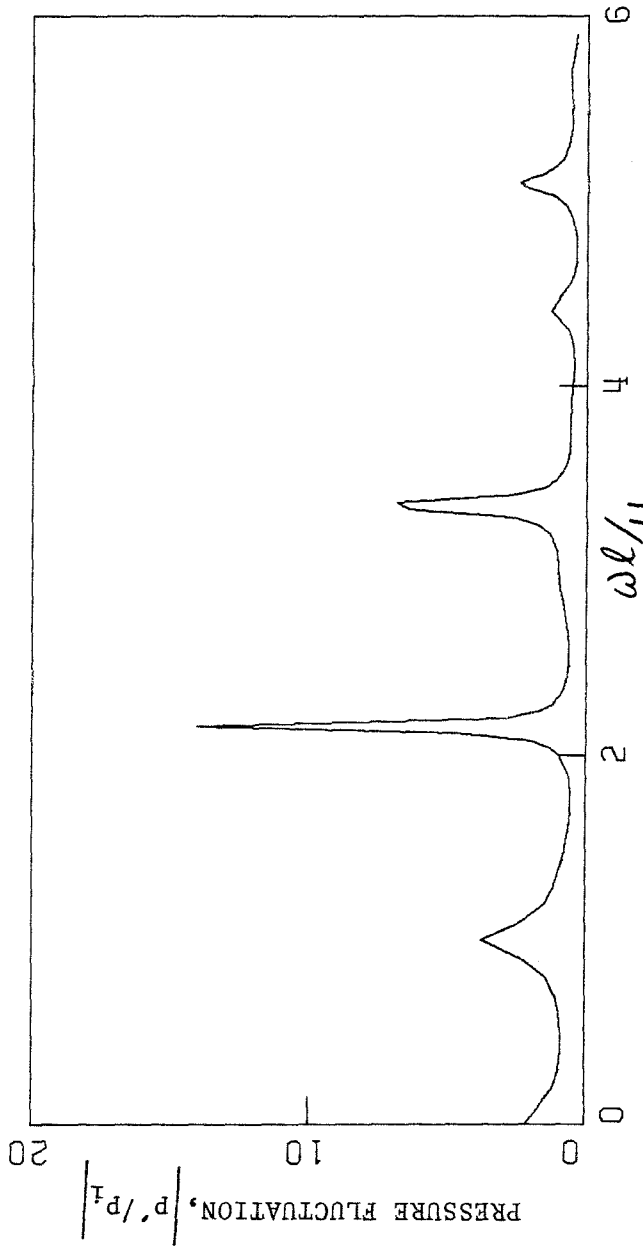

Figure 5.11 Pressure Fluctuation Spectrum, α_T =0.4
Turbine Discharge

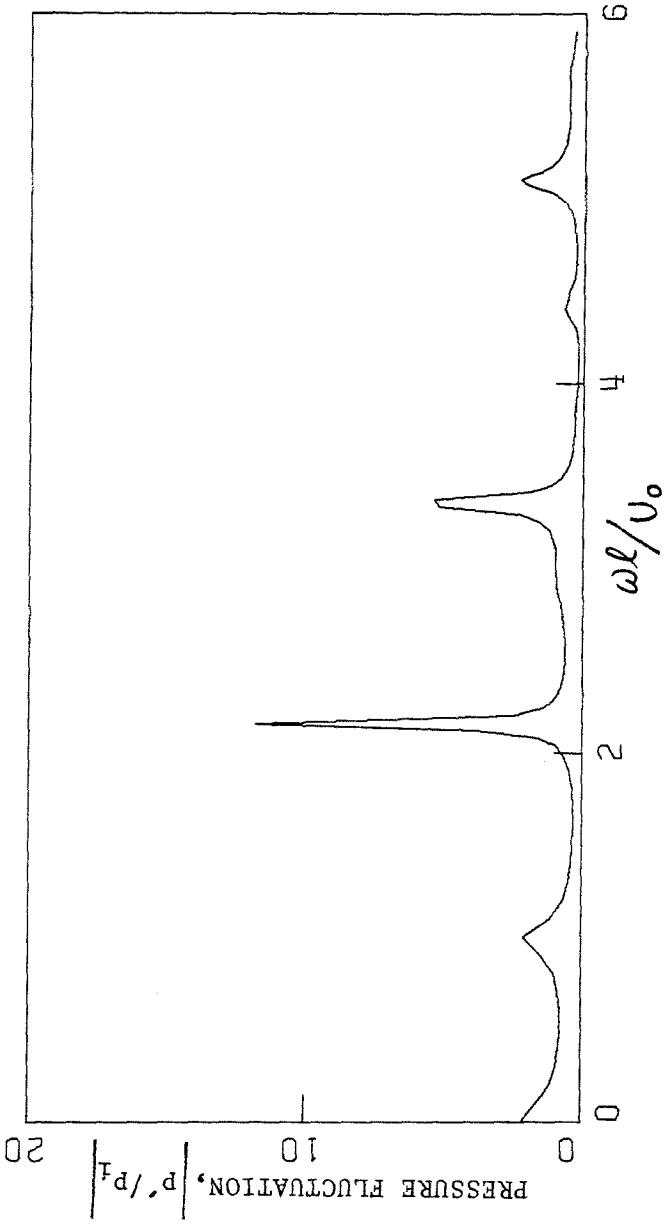

Figure 5.12 Pressure Fluctuation Spectrum, α_T =0.4
Flame Holder

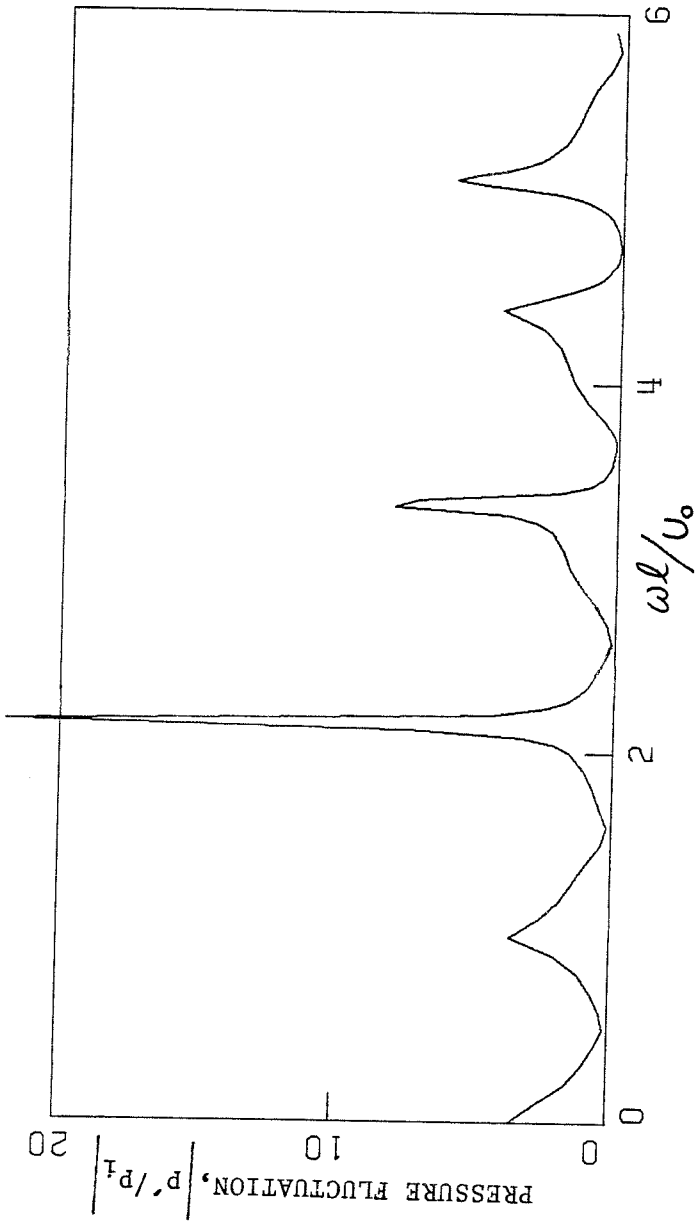

Figure 5.13 Pressure Fluctuation Spectrum, $\alpha_T = 0.4$
End of Flame Zone

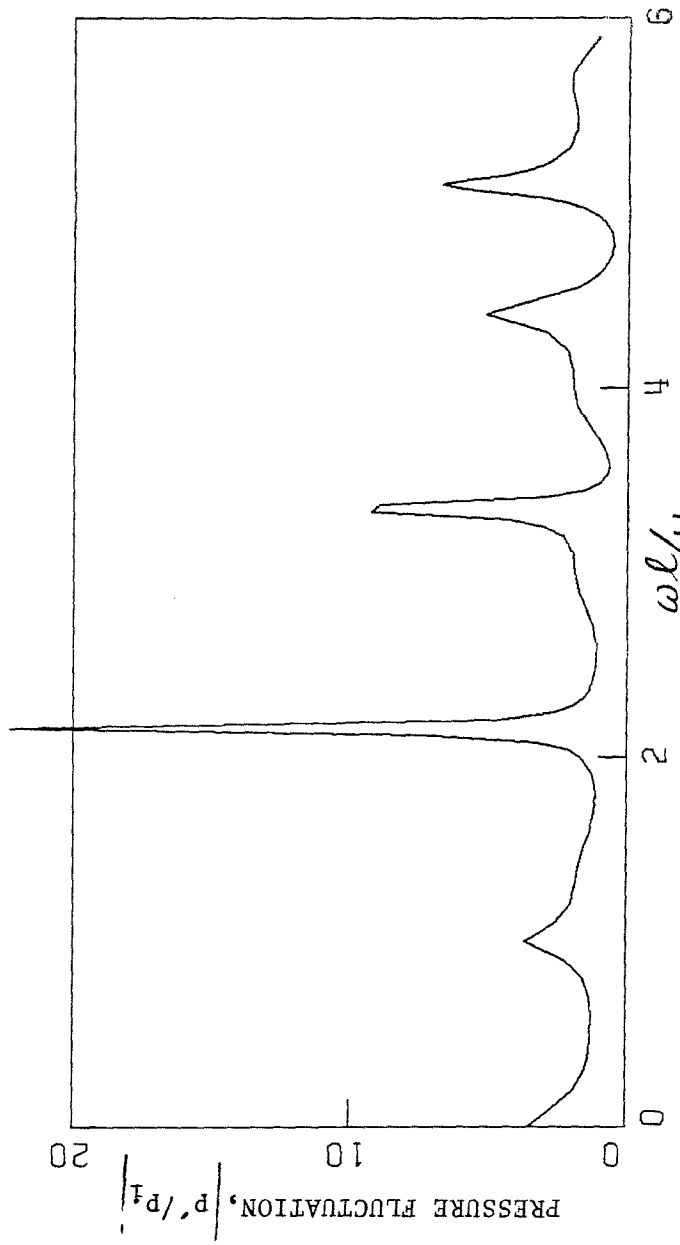

Figure 5.14 Pressure Fluctuation Spectrum, α_T =0.4
Nozzle Inlet

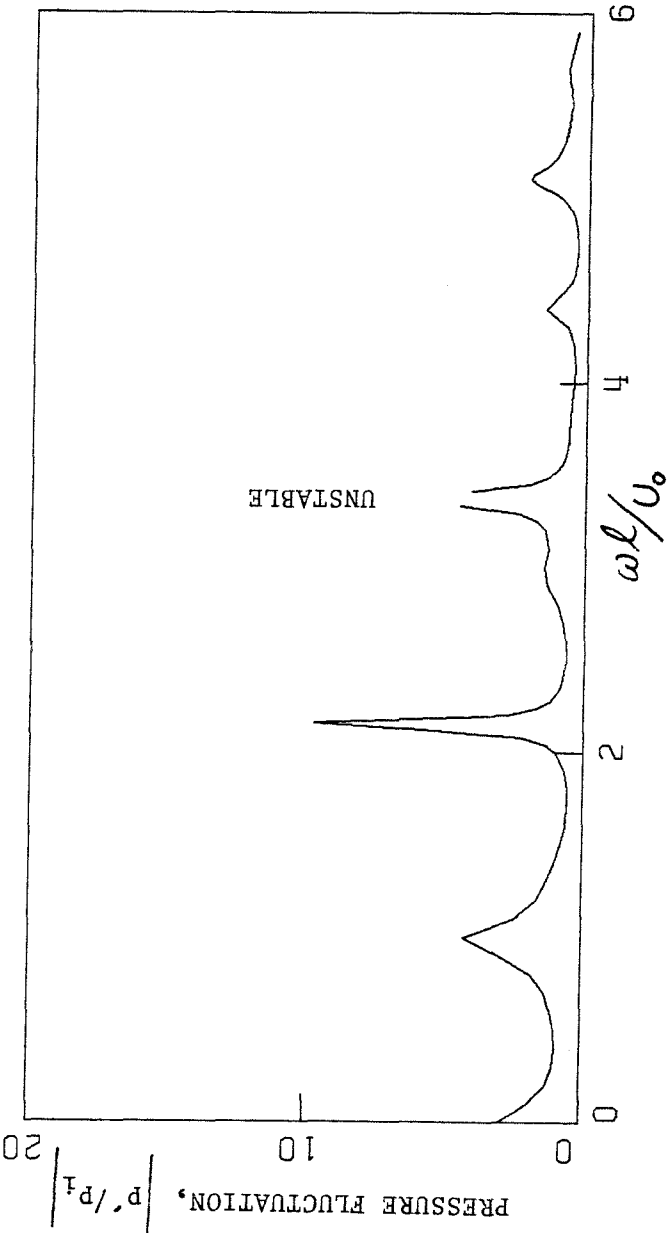

Figure 5.15 Pressure Fluctuation Spectrum, α_T =0.57
Turbine Discharge

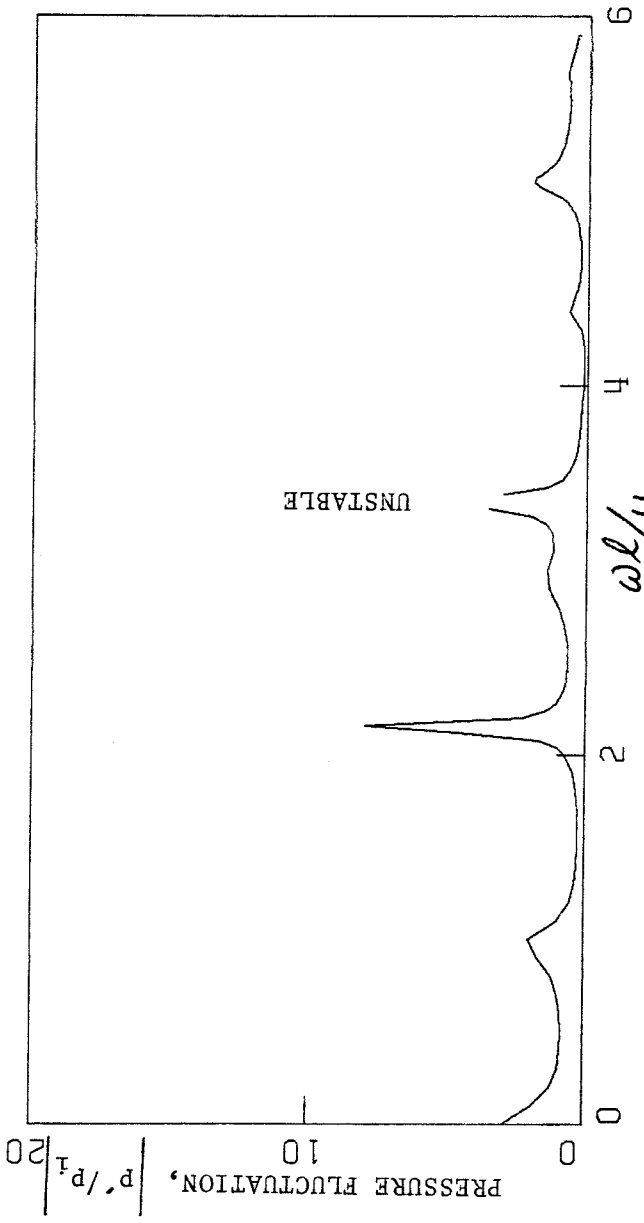

Figure 5.16 Pressure Fluctuation Spectrum, $\alpha_T = 0.57$
Flame Holder

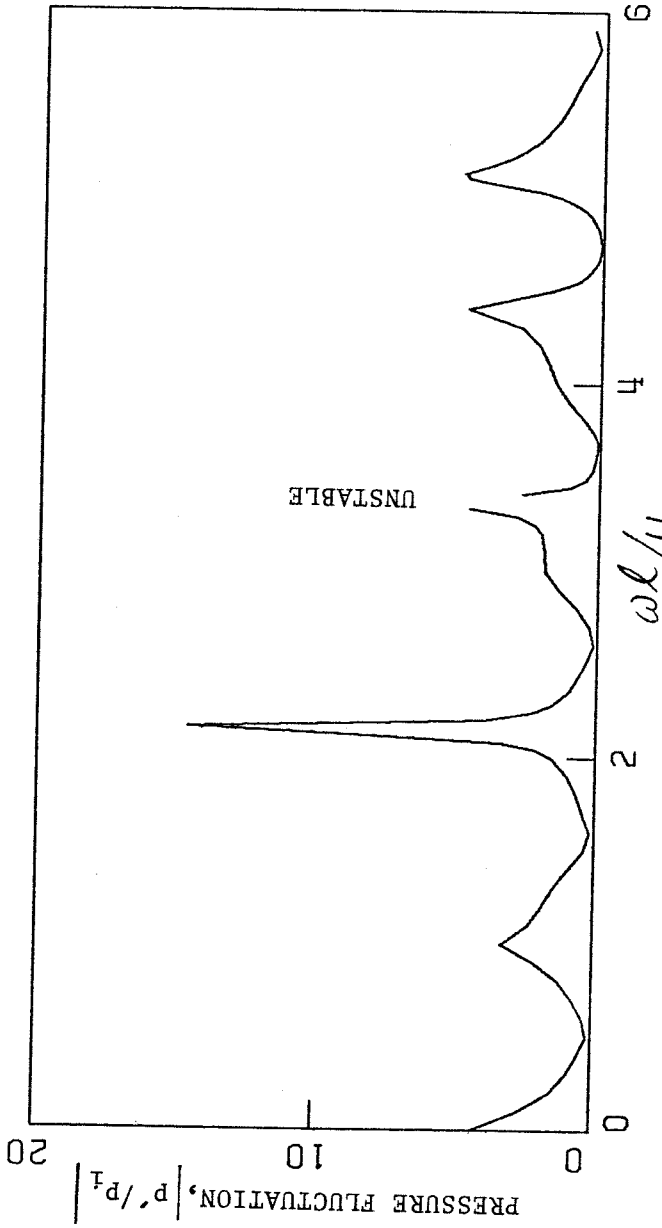

Figure 5.17 Pressure Fluctuation Spectrum, α_T =0.57
End of Flame Zone

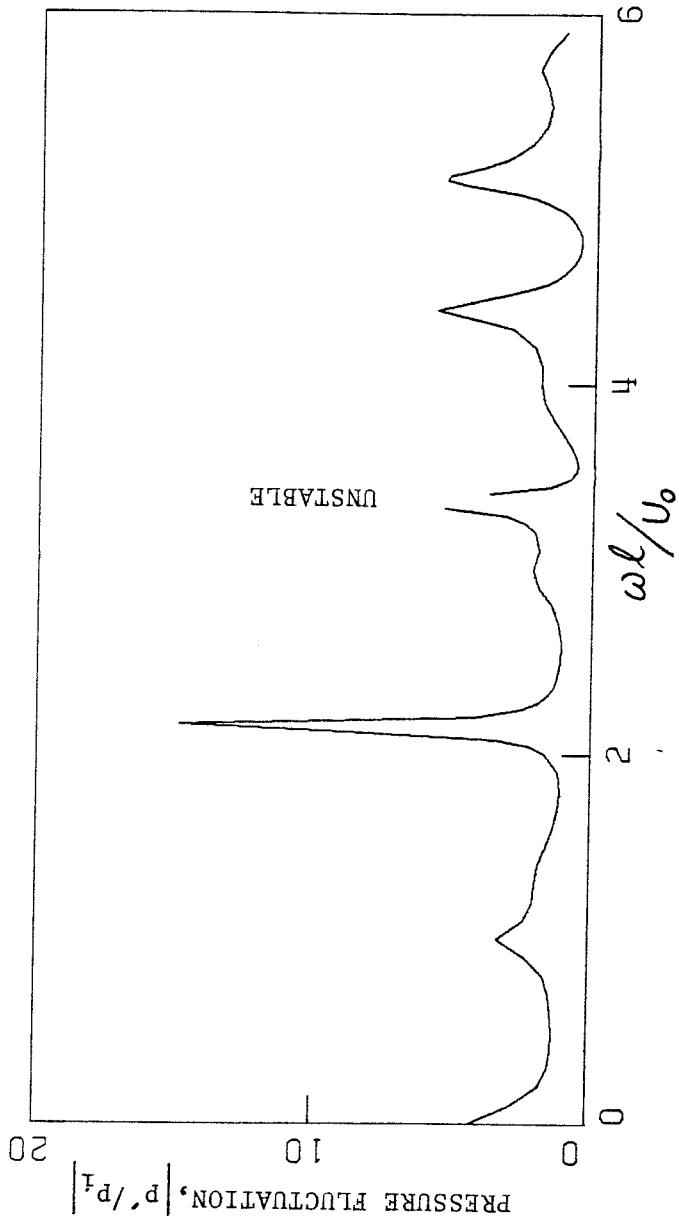

Figure 5.18 Pressure Fluctuation Spectrum, $\alpha_T = 0.57$
Nozzle Inlet

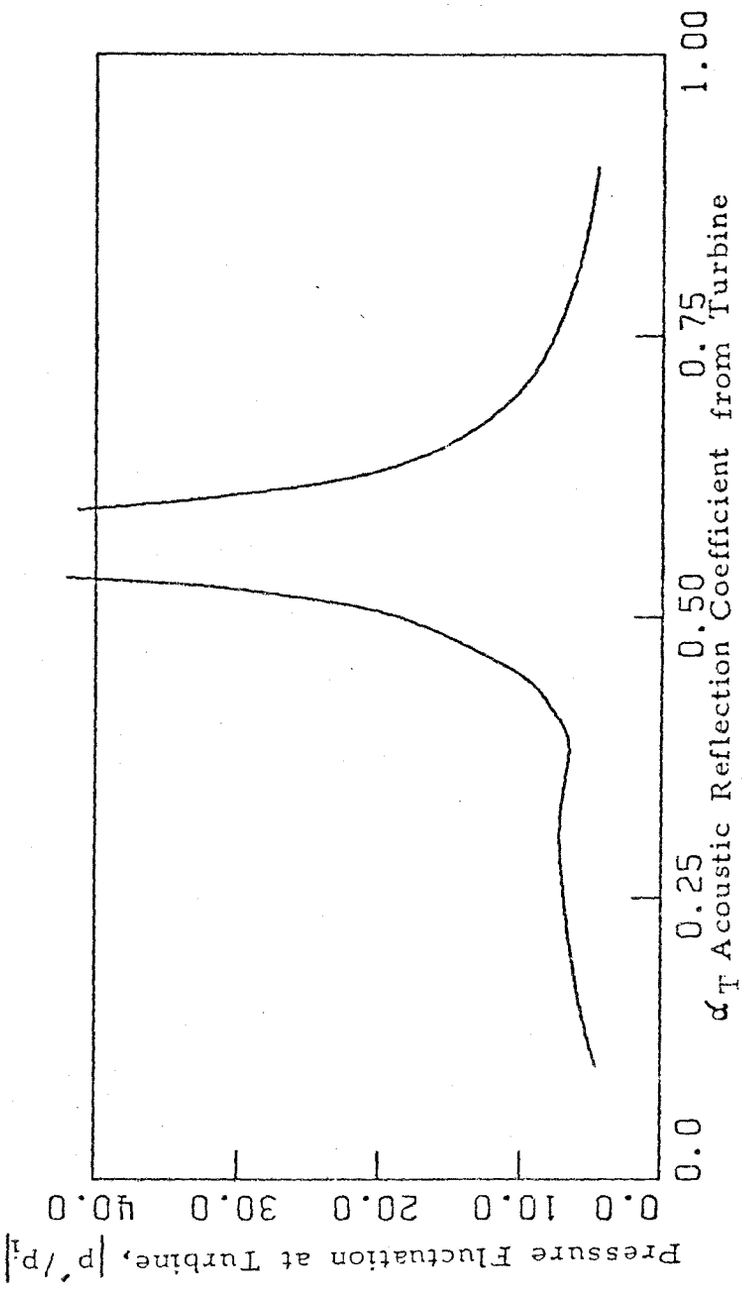

Figure 5.19 Pressure Fluctuation as a Function of Acoustic Reflection Coefficient at Turbine Discharge. $L_1/\ell = 5.54$, Corresponding to Maximum Amplitude from Figure 5.10